FERTILITY CHIP

a point-of-care semen analyser

Loes Segerink
4 November 2011

The research described in this thesis was carried out at the BIOS Lab on a Chip group of the MESA+ Institute for Nanotechnology of the University of Twente, Enschede, the Netherlands. It was carried out in close cooperation with the Medisch Spectrum Twente, Enschede, the Netherlands. This research was financially supported by the Dutch Technology Foundation STW, which is an applied division of NWO, and the Technology Program of Ministry of the Economic Affairs, Agriculture and Innovation (project number 07994).

Members of the committee:

Chairman	prof. dr. ir. A.J. Mouthaan	University of Twente
Promotor	prof. dr. ir. A. van den Berg	University of Twente
Assistant promotor	dr.ir. A.J. Sprenkels	University of Twente
Referent	dr. G.J.E. Oosterhuis	Medisch Spectrum Twente
Members	prof. dr. J.G.E. Gardeniers	University of Twente
	prof. dr. I. Vermes	University of Twente
	prof. dr. ir. J.M.J. den Toonder	Eindhoven University of Technology
	prof. dr. G.L. Kovács	University Pécs
	prof. dr. L.J. Kricka	University of Pennsylvania

Title: Fertility chip, a point-of-care semen analyser
Author: Loes Segerink
ISBN: 978-90-365-3242-6
Publisher: Wöhrmann Print Service, Zutphen, the Netherlands
Cover design: Loes Segerink
The cover shows a schematic representation of a microchannel which consists of planar electrodes used for the detection of single spermatozoa. On the background a selection of the media attention for this project is shown (for details see appendix A.1).

FERTILITY CHIP

A POINT-OF-CARE SEMEN ANALYSER

PROEFSCHRIFT

ter verkrijging van
de graad van doctor aan de Universiteit Twente,
op gezag de rector magnificus,
prof.dr. H. Brinksma,
volgens besluit van College voor Promoties
in het openbaar te verdedigen
op vrijdag 4 november 2011 om 14:45 uur

door

Loes Irene Segerink
geboren op 25 mei 1984
te Oldenzaal

Dit proefschrift is goedgekeurd door:

Promotor	Prof. dr. ir. A. van den Berg
Assistent promotor	dr. ir. A.J. Sprenkels

Contents

chapter 1

Aim and thesis outline

The problem description and the goal of the STW project “Fertility-chip, point-of-care semen analyzer using a lab-on-a-chip” are described in this chapter. Furthermore the outline of this thesis is given.

1.1 Male fertility

About one out of six couples will visit the fertility department of the hospital since they have problems with getting pregnant [1-3]. In the Netherlands about 30 000 couples with fertility problems will go to the hospital annually [4]. Male subfertility or infertility is the main factor in about 30% of the cases [1, 2], while a combination of abnormalities for both the man and woman account for the same percentage [2]. Couples with fertility problems can be treated with assisted reproductive technologies, such as in vitro fertilization (IVF) or intracytoplasmic sperm injection (ICSI). Of all the children born in the Netherlands in 2006, 2.4% of them were fathered by a woman with help of one of these techniques [5].

Before a treatment decision can be made by the gynaecologist, the fertility of the man and woman needs to be investigated. In case of the male fertility, this implies a semen analysis to determine parameters such as the concentration and motility of spermatozoa in semen. This analysis is performed in the hospital laboratory by a technician and for this the man has to bring his semen in a special container to the hospital within one hour. Besides that this is embarrassing for the man, the analysis in the hospital is time consuming, subjective and needs quality control. Testing multiple times at home with a system that provides a reliable, objective semen analysis will be a better alternative for the current analysis.

At the moment several at home tests for assessing the semen quality are commercially available, such as the SpermCheck® [6, 7] and the FertilMARQ [8]. One of the first examples, the Fertell device, is currently not commercially available anymore [9, 10]. All these tests give only qualitative information about the concentration of (motile) spermatozoa instead of quantitative values necessary for treatment decisions. Additionally, microscopes are for semen analysis at home at the market [11]. Disadvantages of these devices are that the man has to subjectively interpret the results and the tests are not (completely) validated, so these home tests are not recommended for diagnostic purposes [12].

In this thesis a step has been made towards the development of a portable system for semen analysis that can be used at home. This system consists of a measurement box and disposable microfluidic chips on which the actual analysis is performed. With the system multiple analyses can be performed at home. After a certain time period, the man will go back to the hospital where the gynaecologist will read out and analyse the results. During this project we mainly focused on the development of a microfluidic chip that is able to quantitatively determine the concentration and motility of spermatozoa, since these parameters are of main importance in today's semen analysis. The work has been performed at BIOS, Lab on a Chip group, which is

part of the MESA+ Institute for Nanotechnology of the University of Twente and was carried out in close cooperation with the department Obstetrics and Gynaecology of Medisch Spectrum Twente in Enschede. This thesis describes the results of the project "Fertility-chip, point-of-care semen analyzer using a lab-on-a-chip" with project number 07994. The project was financed by the Dutch Technology Foundation STW, which is an applied division of NWO, and the Technology Program of the Ministry of Economic Affairs, Agriculture and Innovation.

1.2 Thesis outline

The aim of the PhD project is to develop a fertility chip for the analysis of semen at home. In chapter 2 the fluid of interest, the semen, is described in more detail. The available tests for the examination of the semen are also given, including the accepted gold standards and reference values. At the end of the chapter a review of microfluidic chips for spermatozoa applications is presented, which is not only restricted to the determination of semen parameters, but also on-chip purification and separation techniques are shown.

Chapter 3 gives background information about electrical impedance measurements in microfluidic devices. Microfluidic impedance cytometry and various electrode configurations are discussed as well as an equivalent circuit model for the microfluidic chip, such that the influence of the frequency and the chip dimensions on the measured impedance can be determined. Additionally, the dielectric properties of a single cell are described, followed by the determination of the influence of these properties on the measured impedance change by the use of two models. The use of microfluidic impedance cytometry for medical applications is discussed at the end of this chapter.

The development of a microfluidic chip for the determination of the spermatozoa concentration is described in chapter 4. The fabrication process of the microfluidic chip and the chip design for the electrical impedance measurements are given. The method used for the determination of the concentration of spermatozoa is described and a comparison between the experimental results and the values obtained with the conventional semen analysis is made.

Since the used electrode design for the spermatozoa concentration determination creates an inhomogeneous electrical field, an alternative electrode design consisting of parallel electrodes is given in chapter 5. The novel, easy fabrication process for parallel electrodes is shown and the results obtained with the new design are compared with the old configuration.

In chapter 6 the microfluidic chip used for the motility determination is presented. This chip consists of two parts: a separation part and a detection part. For the description of the behaviour of the spermatozoa in the separation part, a model has been proposed. Furthermore experiments were performed and compared with the actual motility of the spermatozoa and the theoretical model.

The preceding experimental chapters all describe the use of electrical impedance measurements for the detection of spermatozoa. However, other techniques can also be used, such as flow cytometry, in which fluorescent dyes are used for highly selective labelling of cells. To investigate this, the development of a compact fluorescence detection system for microfluidic chips is described in chapter 7.

In the last chapter first the results of this thesis are summarized, followed by recommendations regarding the further development and validation of the fertility chip.

1.3 References

1. Hull, M.G.R., et al., *Population study of causes, treatment, and outcome of infertility.* British Medical Journal, 1985. **291**: p. 1693-1697.
2. NVOG. *Richtlijnen voortplantingsgeneeskunde - Orienterend Fertiliteitsonderzoek (OFO) (2.0)*. (2004) [cited 4 July 2011]; Available from: http://www.nvog.nl/.
3. Beurskens, M.P.J.C., J.W.M. Maas, and J.L.H. Evers, *Subfertiliteit in Zuid-Limburg: berekening van incidentie en van beroep op specialistische zorg.* Nederlands tijdschrift der Geneeskunde, 1995. **139**(5): p. 235-238.
4. NVOG. *Landelijke netwerkrichtlijn Subfertiliteit*. (2010) [cited 4 July 2011]; Available from: http://www.nvog.nl/.
5. de Mouzon, J., et al., *Assisted reproductive technology in Europe, 2006: results generated from European registers by ESHRE.* Human Reproduction, 2010. **25**(8): p. 1851-1862.
6. Coppola, M.A., et al., *SpermCheck® Fertility, an immunodiagnostic home test that detects normozoospermia and severe oligozoospermia.* Human Reproduction 2010. **25**(4): p. 853-861.
7. Contravac. *Advancing male reproductive health care*. (2011) [cited 4 July 2011]; Available from: http://www.contravac.com/.
8. Embryotech. *FertilMARQ*. (2011) [cited 4 July 2011]; Available from: http://www.embryotech.com/.
9. Kokopelli. *Fertell - home male and female fertility test*. (2011) [cited 4 July 2011]; Available from: http://www.fertilityformen.com/.
10. Björndahl, L., et al., *Development of a novel home sperm test.* Human Reproduction 2006. **21**(1): p. 145-149.

11. Kokopelli. *Microscopes for semen analysis*. (2011) [cited 4 July 2011]; Available from: http://www.fertilityformen.com/.
12. Brezina, P.R., E. Haberl, and E. Wallach, *At home testing: optimizing management for the infertility physician.* Fertility and Sterility, 2011. **95**(6): p. 1867-1878.

chapter 2

Semen, male fertility and microfluidics

Semen analysis is a first step in the investigation of the male fertility and it gives a description of the semen and its contents. The gold standards for the determination of semen parameters are manual assessments, making it subjective and labour intensive. The expensive computer assisted semen analysis systems partly solve this, but quality control and one or more hospital visits for the man are still needed. Recently, the enormous developments of lab on chip systems offer several advantages not only for the assessment of semen but also for research on the functioning of spermatozoa.

2.1 Semen

Semen is a mixture of spermatozoa and seminal fluid. The testes and epididymis secrete the spermatozoa, that are mixed with fluids from the prostate, seminal vesicles and bulbourethral glands [1, 2]. Most of the volume of semen is generated by the seminal vesicles [3].

2.1.1 Spermatozoon

A normal human spermatozoon consists of a head, a midpiece and a tail (see figure 2-1). The head consists of an acrosomal cap and is several micrometers long. In table 2-1 a summary of several dimensions of a normal human spermatozoon is given. The shape of the head is a flattened ellipsoid. Most of the dimensions mentioned in table 2-1 are measured from Papanicolauo-stained preparations and are 6-15% smaller than the dimensions of living spermatozoa [4, 5]. Katz and co-workers have shown that spermatozoa with a normal head morphology move significantly faster compared to spermatozoa with a deviating head [6].

The swimming speed of a spermatozoon is linearly dependent on the length of the tail and the beat frequency of the tail. The viscosity of the fluid also indirectly influences the speed, because it effects the beat characteristics [7]. During swimming about 60% of the spermatozoa rotate with small and rapid oscillations in a counter clockwise direction as seen from the anterior end of the head [8]. In table 2-2 some typical swimming characteristics of a spermatozoon are given. The beat amplitude and the beat wavelength have also been investigated and found to be 4.76 ± 0.27 µm and 12.05 ± 0.40 µm respectively [6]. According to Baltz and co-workers, the waveform behaves like a helix with an elliptical cross section with amplitudes of 6.4 µm and 1.3 µm [9]. They also determined the pulling force of a motile spermatozoon as 200 pN [9].

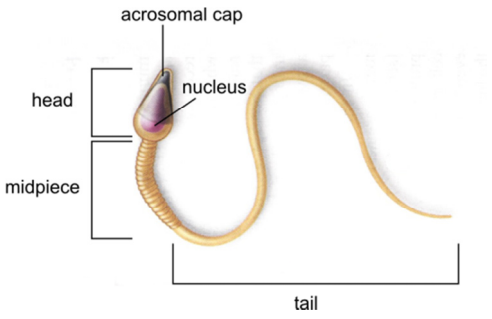

figure 2-1 Schematic picture of a spermatozoon (modified from [10]).

table 2-1 Dimensions of a normal human spermatozoon. A range indicates the 95% confidence interval (PAP = Papanicolaou staining , none = no staining).

Dimensions of a normal human spermatozoon			
	Value	**Staining**	**References**
Head			
Length [µm]	3-5	PAP	Katz et al. (1982) [6]
	3.7 - 4.7	PAP	WHO (2010) [2]
	4-5	PAP	WHO (1999) [1]
	3.8 - 4.8	PAP	Maree (2010) [5]
	4.3 - 5.3	none	Maree(2010) [5]
Width [µm]	2-3	PAP	Katz et al. (1982) [6]
	2.5 - 3.2	PAP	WHO (2010) [2]
	2.5 - 3.5	PAP	WHO (1999) [1]
	2.3 - 3.0	PAP	Maree (2010) [5]
	2.4 - 3.3	none	Maree(2010) [5]
Midpiece			
Length [µm]	~ 1.5 times head	PAP	WHO (1999) [1]
	3.3 - 5.2	PAP	WHO (2010) [2]
Width [µm]	< 1	PAP	WHO (1999) [1]
	0.5 - 0.7	PAP	WHO (2010) [2]
Tail			
Length [µm]	~ 45	PAP	WHO (1999) [1], WHO (2010) [2]
Width [µm]	< midpiece	PAP	WHO (1999) [1]
	0.5	?	Dresdner et al. (1981) [7]

table 2-2 A summary of the swimming characteristics of a spermatozoon.

Swimming characteristics of a spermatozoon			
	Value	**Remark**	**Reference**
Swimming velocity [µm·s^{-1}]	51 ± 2	straight line velocity	Katz et al. (1982) [6]
	43	straight line velocity	Dresdner et al. (1981) [7]
	~ 50	straight line velocity	Harvey (1960) [11]
Beat frequency [Hz]	15.2 ± 0.7		Katz et al. (1982) [6]
	14		Dresdner et al. (1981) [7]
	22		Baltz et al. (1988) [9]
	<29.4	hyperactive	Mortimer et al. (1997) [12]
	>29.4	non-hyperactive	Mortimer et al. (1997) [12]
Flagellar beat angle [°]	96 - 242	hyperactive	Mortimer et al. (1997) [12]
	55 - 87	non-hyperactive	Mortimer et al. (1997) [12]
Rotation frequency head [Hz]	9.33 ± 4.85		Ishijima et al. (1992) [8]

Several swimming behaviours of spermatozoa can be observed. One is the swimming of concentrated semen in wave motion, meaning that the spermatozoa move not in random directions but in waves [13]. Also spermatozoa are oriented in the flow, like elongated particles tend to do [13]. Furthermore spermatozoa accumulate near boundaries; most motile spermatozoa are located within 100 µm of a wall [14]. Another behaviour is that spermatozoa are oriented against the flow and swim upstream, a phenomenon called positive rheotaxis [15, 16]. Bretherton and Rothschild observed that the orientation of dead spermatozoa in a horizontal tube is downstream at the top of the tube and upstream at the bottom half of the tube. They explained this by the local velocity gradient due to the flow and the slightly lower position of the head of the spermatozoon in the channel [15]. For viable human spermatozoa only positive rheotaxis was observed both at the bottom and at the top of the tube [15]. Roberts explained this by the migration of spermatozoa to the lower part of a horizontal tube as a result of the equilibrium between flow orienting and gravitational forces, where a velocity gradient exists that creates this orientation [17]. Later, it was observed that the effect of gravity is relatively weak and that the rheotaxis phenomenon arises due to spermatozoa accumulation near walls and a local velocity gradient of 3.5 s^{-1} at this position [14]. In flow, the spermatozoa swim also in more straighten trajectories than in stagnant fluid [16].

2.1.2 Sperm-egg interactions

Fertilization of an oocyte by a spermatozoon is believed to be the result of twelve events that are sequentially dependent (see figure 2-2) [18]. In short, the first barrier of the actual fertilization consists of the penetration of the cervical mucus by the spermatozoa. After that the spermatozoa is transported to the uterus and oviduct, where the spermatozoa are probably stored some time [19]. At this storage site, in the Fallopian tube, a part of the spermatozoa becomes capacitated and hyperactivated. Capacitation is a process, enabling the spermatozoa to undergo the acrosome reaction after some structural and functional changes [18-21]. Capacitation is necessary for fertilizing an oocyte, so freshly ejaculated (and thus uncapacitated) spermatozoa are not able to fertilize an oocyte [22, 23]. The capacitated cells swim through the cumulus matrix, bind to the zona pellucida and penetrate it with hyperactivated motility after the release of the contents of the acrosome (the acrosome reaction). Subsequently a spermatozoon binds and fuses with the oocyte and activates the oocyte such that only one spermatozoon can fuse with it. The final event in the fertilization process is the fusion of both pronuclei [18].

Guiding mechanisms

The spermatozoon has to travel a long way before it arrives at the oocyte and only a small fraction arrives at the fertilization site [24]. Therefore the idea exists that spermatozoa are guided by several mechanisms (see figure 2-2). An important mechanism is chemotaxis; the reaction of motile cells to move to or away from a gradient of a chemical substance by changing the direction of travel [25, 26]. Spermatozoa show chemotactic and chemokinetic (change of swimming velocity due to a chemical substance) behaviour when placed in a gradient of follicular fluid [25], secretion of the oocyte and the surrounding cumulus cells [27]. Olfactory receptors located on the spermatozoon are involved in the chemotaxis [28] and only capacitated spermatozoa exhibit chemotactic behaviour, meaning that only 2-12% of the spermatozoa in semen have chemotactic responsiveness [29, 30]. This population is continuously replaced within the cell population over time [29].

Another guiding mechanism is thermotaxis. Bahat and co-workers showed that human spermatozoa respond on temperature gradients by changing their direction. Like for chemotaxis, only capacitated cells respond to temperature differences. For rabbits and pigs, it has already been shown that a temperature difference exists during ovulation [31, 32]. If thermotaxis exists during fertilization is still unknown.

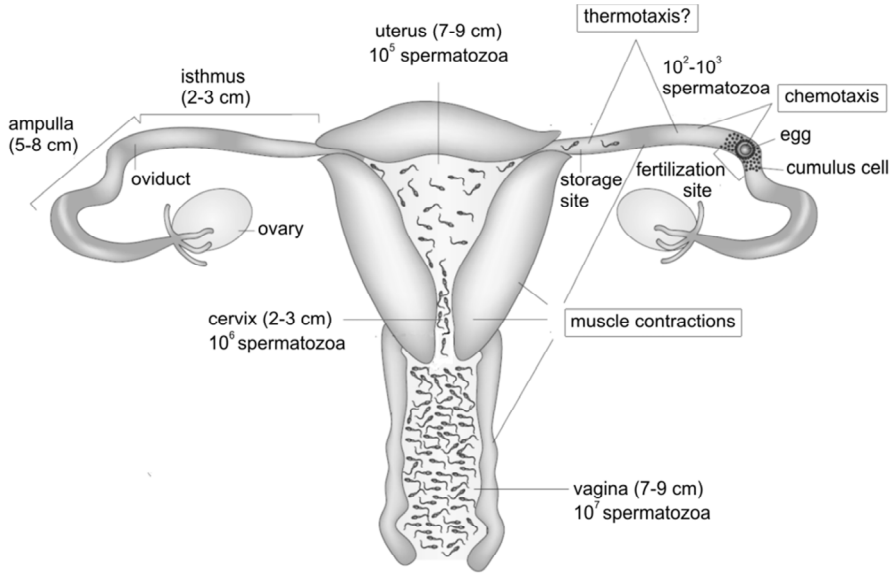

figure 2-2 The possible guiding mechanisms in the female genital tract. There are no publications about the existence of a temperature difference between the fertilization site and storage site, so it is not known if thermotaxis exists during the fertilization. In parentheses the lengths of the structures are given (adapted from [33, 34]).

2.2 Examination of semen

Currently when a couple remains involuntary childless after unprotected sexual intercourse for more than a year, it will be referred to the fertility division of a hospital. To obtain general information about the male fertility, a semen analysis is performed. During a semen analysis, a description of the semen and its contents are made. However, the ability of fertilizing an oocyte is not assessed with a semen analysis; for that purpose a sperm function test has to be performed [35].

2.2.1 Semen analysis

For a semen analysis, the man has to collect his semen in a special container. Preferably this is done at the hospital, but at several hospitals the man also has the possibility to do this at home and bring the sample within one hour to the hospital laboratory [2]. Before analysis, the semen has to be liquefied and usually this is achieved within 15 minutes. Immediately after that, the volume of the semen is measured, followed by assessment of the concentration, motility and morphology [2].

table 2-3 The reference values of semen parameters as given by the WHO in 1999 and their revised values of 2010 (adapted from [1, 2]).

Reference values of the semen parameters		
	WHO 1999	**WHO 2010**
Traditional parameters		
Volume [mL]	≥2.0	≥1.5
Concentration [mL^{-1}]	$\geq 20 \cdot 10^6$	$\geq 15 \cdot 10^6$
Total sperm number	$\geq 40 \cdot 10^6$	$\geq 39 \cdot 10^6$
Progressive motile spermatozoa [%]	≥25	≥32
Total motile spermatozoa [%]	≥50	≥40
Morphology [%]	≥15	≥4
Additional parameters		
Vitality [%]	≥50	≥58
pH	≥7.2	≥7.2
Leukocyte concentration [mL^{-1}]	$<1 \cdot 10^6$	$<1 \cdot 10^6$
MAR test [%]	<50	<50
Immunobead test [%]	<50	<50

Sometimes additional examinations are done, such as measuring the pH, the vitality of the spermatozoa and the amount of antibodies on the spermatozoon using the immunobead test or the mixed antiglobulin reaction (MAR) [2]. In table 2-3 the reference values of these tests are shown for the criteria proposed by the World Health Organization (WHO) in 1999 and the revised values of 2010 based on recent results of Cooper and co-workers [36]. These WHO values are not strict values that tell whether a man can father a child or not. Moreover, the results of a semen analysis are important for giving a prognosis that an on-going pregnancy may occur [36-38].

Besides the reference values, the WHO gives guidelines about the way semen has to be examined in the laboratory. According to the WHO the best method to determine the volume is by weighing the sample in the container. Knowing the mass of an empty container and assuming a 1 $g \cdot mL^{-1}$ density, the semen volume can be calculated [2]. A haemocytometer is used as a gold standard to determine the spermatozoa concentration [1, 2]. For the assessment of the motility, spermatozoa need to be

classified as progressive, non-progressive or immotile by a clinical technician using a microscope. Morphological assessment is done with a fixated, stained smear of semen and the percentage of normal forms is determined possibly in combination with classification of the abnormal forms. Hence the gold standards for these traditional parameters are time consuming, need manual assessments and for reliable results a quality control is essential [39]. For the determination of the concentration, motility and morphology at least 200 spermatozoa need to be assessed in duplicate, according to the guidelines of WHO [1, 2]. Since the semen quality of men varies over time, at least three semen samples should be examined to get reliable information about the male fertility [40].

The semen analysis is used as a diagnostic tool and helps the gynaecologist to choose the most suitable treatment like intrauterine insemination (IUI), IVF or ICSI. There is no general consensus about which parameter is the best predictor for each treatment. For example, the percentage of progressive motile spermatozoa is related to the pregnancy rate for subfertile couples, while this was not found for concentration and morphology [41]. On the contrary for a general population it was shown that concentration, total sperm count and morphology are important values for prediction of pregnancy [42, 43]. Another study showed that the percentage of normal morphological spermatozoa is positively correlated with IVF and pregnancy outcome [44]. In all literature it is generally accepted that none of the traditional parameters is the absolute predictor of fertility [44-46].

Based on the semen analysis results, the semen can be described according to specific nomenclature [1, 2]. In table 2-4 some of the descriptions and their meanings are given. The prefixes can also be sequentially combined to one word that describes the semen quality. For instance oligoasthenozoospermia means that the concentration of the spermatozoa is below $20 \cdot 10^6$ mL^{-1} and the percentage of progressively motile spermatozoa is lower than 32%. Grimes and Lopez argued that this nomenclature should be abandoned, since it leads to misinterpretations, is vague and unscientific [47]. However, in many studies these definitions are (still) used.

table 2-4 The nomenclature for semen quality as proposed by the WHO including their reference values (adapted from [2]).

Nomenclature for semen quality	
	Definition
Describing semen	
Aspermia	No semen.
Haemospermia	Presence of red blood cells in the semen.
Leukocytospermia	Presence of leucocytes in the semen.
Describing spermatozoa	
Asthenozoospermia	Percentage of progressively motile spermatozoa below 32%.
Azoospermia	No spermatozoa in the semen.
Necrozoospermia	Low percentage of live and high percentage of immotile spermatozoa in the semen.
Normozoospermia	Spermatozoa concentration (or total sperm number) equal or above $15 \cdot 10^6$ mL^{-1} (or $39 \cdot 10^6$), percentages of progressive motile spermatozoa and morphologically normal spermatozoa equal or above 32% and 4% respectively.
Oligoozoospermia	Spermatozoa concentration (or total sperm number) equal or below $15 \cdot 10^6$ mL^{-1} (or $39 \cdot 10^6$).
Teratozoospermia	Percentage of morphologically normal spermatozoa below 4%.

Computer assisted semen analysis

To avoid the subjective character of manual semen analysis and to obtain more information about the motility, computer assisted semen analysis (CASA) systems have been developed. According to the WHO guidelines a CASA system can be used to determine various semen parameters but a quality control is needed to guarantee a reliable operation of the system [2]. With a CASA system more motility parameters can be determined, like the straight line velocity (VSL), amplitude of lateral head displacement (ALH) and curvilinear velocity (VCL) (see figure 2-3). Besides the three traditional parameters assessed with CASA, the VSL, ALH and VCL are related to

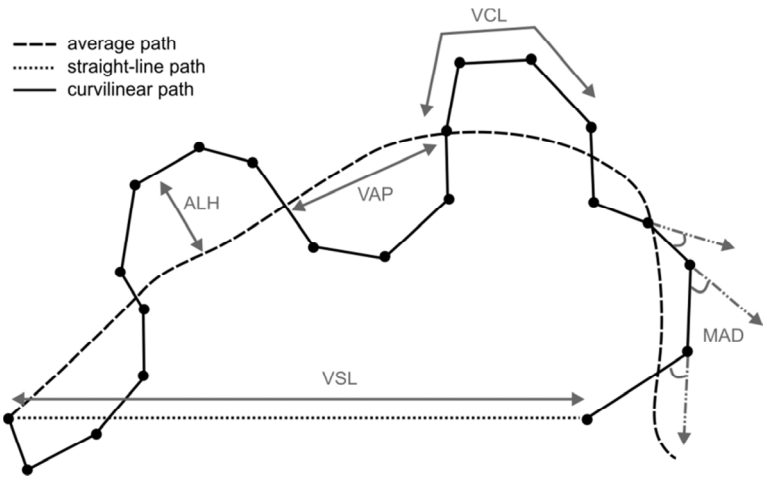

figure 2-3 Schematic drawing of some motility parameters determined with a CASA system. ALH = amplitude of lateral head displacement [µm]; VAP = average path velocity [µm·s^{-1}]; VCL = curvilinear velocity [µm·s^{-1}]; MAD = mean angular displacement [°]; and VSL = straight line velocity [µm·s^{-1}] (adapted from [2]).

fertilization rates for IVF [48]. Furthermore, the morphological results and the VSL obtained with CASA are better predictors of the pregnancy rate for subfertile couples compared to the values obtained from manual assessment [41]. For couples from a general population, it was shown that the motile concentration determined by the VCL and concentration is the only independent predictor for pregnancy rate [49]. However, in accordance with the manual analysis there is no general consensus which parameter is the best predictor.

For the analysis with CASA, the semen is put into a 20 µm deep chamber using capillary flow. This chamber is shallower than the haemocytometer used for manual assessment of the concentration (100 µm). The distribution of spermatozoa in a capillary loaded chamber is influenced by the Segre-Silverberg effect. During filling of the chamber there is a Poiseuille flow resulting in velocity gradients perpendicular to the flow. Due to these gradients the spermatozoon experiences a force, driving it to stable planes located at a certain distance from the wall. This phenomenon is called the Segre-Silverberg effect [50, 51] and depends on the viscosity of the sample, the surface tension, the depth of the chamber and the size of the particles or cells [51]. For the 100 µm deep haemocytometer this effect is negligible, but for the 20 µm deep chamber used with CASA systems it cannot be ignored. The amount of spermatozoa near the meniscus is higher, since the spermatozoa migrate to a plane with a velocity

larger than the average flow velocity. At the trailing part of the flow, which is examined during the assessment, the concentration is reduced. Theoretical calculations estimate that the measured concentration in the 20 μm deep chamber is 77% of the true concentration measured with a haemocytometer [50], which agrees well with the experimental value found (85%) [51].

2.2.2 Sperm function tests

Semen analysis is often the first step performed to investigate the semen quality. Good semen analysis results do not always implicate that the spermatozoa are functioning properly. To investigate the ability of spermatozoa to fertilize an oocyte, sperm function tests have been developed [18, 45, 52]. Several sperm function tests exist today, which can be divided in tests that investigate the functioning of the spermatozoa directly by interaction assays and indirectly by biochemical assays [53].

Interaction assays

The penetration of the cervical mucus is the first obstacle spermatozoa encounter which can be tested with a so-called postcoital test. With this in-vivo test the number, the behaviour and the survival rate of spermatozoa are determined in cervical mucus several hours after intercourse. Besides this in-vivo test also in-vitro tests exist, in which it is determined whether spermatozoa are able to penetrate cervical mucus on a slide or in a capillary [2, 35, 52]. Instead of cervical mucus, also hyaluronate polymers can be used [54].

Another step in the fertilization process is the binding of the spermatozoon to the zona pellucida of the oocyte. This can be tested with human oocytes or with the hemizona assays, where the binding of spermatozoa to the zona pellucida is observed [2, 18, 35, 52]. After binding to the oocyte, the spermatozoon has to acrosome react. This can be investigated by inducing an acrosome reaction using for instance human oocytes [55] or ionophore A3187 [2, 35, 52], followed by investigation of the acrosomal cap that is fluorescently labelled. The acrosome reaction is normally followed by the penetration of the spermatozoon into the oocyte. To test this ability, the zona-free hamster oocyte penetration assay is used [2, 18, 35, 52].

Biochemical assays

The functioning of the spermatozoon is affected by oxidative stress. A low level of antioxidants in the seminal plasma or an increased reactive oxygen species (ROS) production by leucocytes and/or spermatozoa result in oxidative stress due to high levels of ROS. Oxidative stress can damage the membrane and the DNA of the

spermatozoon, reduce its motility, lower the number of spermatozoa by a higher rate of apoptosis induced by DNA damage and thus impairing the sperm function [56]. Oxidative stress is related with infertility of men who have normal semen analysis results [57]. Chemiluminescence arrays have been developed to test the ROS level in washed semen [2, 52, 56]. In addition another chemiluminescence array can be used to measure the total antioxidant capacity (TAC) of the seminal plasma. Combining the ROS and TAC results leads to the ROS-TAC score, and lower values of this score are predictive for infertility [57].

High ROS levels can cause DNA damage like deteriorating the DNA condensation. The two most used methods for DNA integrity testing are the sperm chromatine structure array (SCSA) and the deoxynucleotidyl transferase-mediated dUTP nick end labelling (TUNEL). Both methods make use of fluorescence stains that label intact and fragmented DNA (SCSA) or strand breaks (TUNEL) and can be assessed using flow cytometry. A low DNA fragmentation index (<30%) determined with SCSA is related to significant larger pregnancy rates for IUI, while for IVF and ICSI no relation was observed [58]. Combination of the results of several studies revealed that the DNA integrity cannot be used as predictor for pregnancy in clinics, although a small but significant predictive value for pregnancy rate for IVF and ICSI was shown for both methods [59].

2.3 Spermatozoa on chip

At the end of the 17th century Anthoni van Leeuwenhoek discovered “little animaliculi” in semen, when he put it under his self-made microscope (see figure 2-4) [60]. Today laboratory technicians still look at spermatozoa in the semen through a microscope, as a first step in the treatment of an involuntary childless couple. For this analysis the man has to collect his semen in a special container and has to bring it within one hour to the laboratory of the hospital. In addition to the fact that it is often felt embarrassing by the man, the analysis is time consuming, subjective and labour

figure 2-4 A drawing of the ‘little animaliculi” in semen as observed by Anthoni van Leeuwenhoek (modified from [60]).

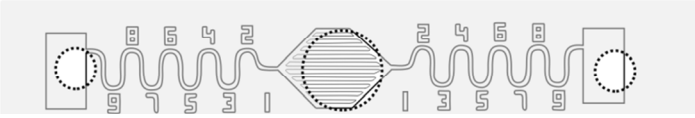

figure 2-5 The two channel design for motility assessment. The dashed circles indicate the inlet (middle) and two outlets. (adapted from [61]).

intensive in case of manual assessment. CASA systems partly solve these disadvantages, but comprehensive quality control is still needed and is expensive.

During the last two decades an enormous development in the field of lab on chip devices has been reported. These lab on chip systems are not only used for chemical applications, like capillary electrophoresis [62], but also as platforms for cell based research. Li and Harrison were one of the first researchers who use a microfluidic chip for erythrocyte cell lysis [63]. Advantages of using microfluidic systems for cell biology applications are the possibility of integrating processes on one chip, working in dimensions comparable to cell size, fast response times and low sample and reagent volumes [64, 65]. The use of lab on chip systems for assessing the semen quality or function can solve the problems encountered with current technologies in the hospital laboratories.

2.3.1 Semen analysis

Motility

The first experiments with spermatozoa on-chip have been reported by Kricka already in 1993 [66]. Several silicon/glass chips containing straight or branched microchannels (depth: 20 μm, width: 40-80 μm) have been developed and motile spermatozoa were able to swim into these channels. Several sperm functions could be analysed after visual inspection using a microscope. Kricka and co-workers improved the chips for motility assessment by constructing 40 μm deep branching channels in silicon with a scale bar next to it. Semen consisting of spermatozoa with normal motility reaches a larger distance than semen samples containing less and poor motile spermatozoa [67]. In a later version of these chips, two or four curved microchannels were made in a glass substrate (see figure 2-5). The results obtained with these chips showed a correlation in the time needed for the first spermatozoon to swim to the end of the channel and the motility scores of the spermatozoa [61].

Concentration

The concentration of spermatozoa in semen is another characteristic that is assessed in a semen analysis. Among others the immunodiagnostic method SpermCheck® [68-

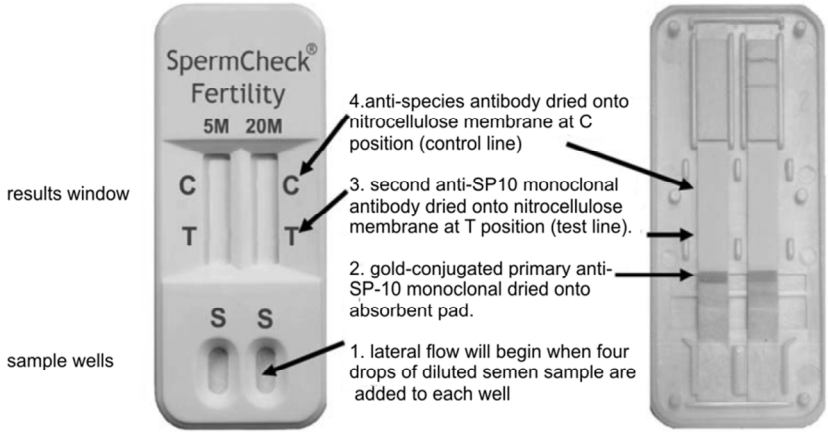

figure 2-6 Schematic working principle of the SpermCheck® device (adapted from [69]).

70] is one of best known examples today (see figure 2-6). In this system the spermatozoa are first lysed in a bottle and a small amount of the lysed cells are placed on a nitrocellulose strip [69, 70]. Via capillary action these lysed cells are mixed with conjugated gold monoclonal antibodies that bind specifically to the acrosomal protein SP-10. The gold-antibody-SP10 complexes migrate along the strip and are captured at an antibody strip that colours red at a certain concentration of SP-10. Since the amount of SP-10 is linearly related to the concentration of spermatozoa [68], the concentration can be qualified. This method was used to test the semen after vasectomy [70] as well as to classify the concentration above or below commonly used threshold values of $5 \cdot 10^6$ mL^{-1} and $20 \cdot 10^6$ mL^{-1} [69].

In another example the concentration of spermatozoa is determined using electrical impedance measurements. The chip consists of a microchannel with a planar electrode pair that allows detection of the passage of a spermatozoon. By the addition of a known concentration of beads, it was possible to determine the concentration of spermatozoa in a semen sample [71].

Besides the immunodiagnostic and electrical approaches, Su and co-workers have reported a holographic on-chip imaging platform [72]. In this concept the diluted semen is put into a commercially available glass counting chamber with a depth of 20 µm and this chamber was loaded into the system. In a period of 10 seconds, about 20 holographic images are made. From digital subtraction and summation of the holographic images information about the concentration of motile and immotile spermatozoa could be derived respectively [72].

Concentration of motile spermatozoa

All before mentioned systems assess the motility or the concentration of spermatozoa. Both parameters can be combined to one parameter: the concentration of motile spermatozoa. Björndahl and co-workers developed a home testing device that determines whether the motile spermatozoa concentration is above or below a certain value [73]. The semen is put into a chamber and only the motile spermatozoa are able to penetrate the hyaluronic acid. These motile spermatozoa are labelled with an anti-CD59 antibody and if a red line appears on the nitrocellulose strip, it indicates that the motile spermatozoa concentration is larger than $10{\cdot}10^6$ mL^{-1} [73]. The same reference value is used in another microfluidic device, consisting of two prefilled chambers connected via a microchannel (cross section 52 μm^2). First the semen is fluorescently labelled and after insertion in the chamber, the labelled motile spermatozoa travel to the other chamber, where 50 minutes after insertion the fluorescence is classified as below or above the threshold using a microfluorometer [74].

Yet another method to determine the motile spermatozoa concentration makes use of specific flow patterns in combination with electrical impedance measurements. The polydimethylsiloxane (PDMS) chip separates motile spermatozoa from the semen by using the tendency of motile spermatozoa to swim upstream. Only the cells that overcome the counter flow are detected with a Coulter counter system [75, 76]. Semen of good quality differs from poor quality semen, since the total number of detected spermatozoa over a time interval of 12 minutes was larger [76]. In a later version of this device the setup was more compact and stand-alone [77].

2.3.2 Purification and selection for IVF and ICSI

Separation of good spermatozoa from the semen is essential for IVF and ICSI treatments. Simple washing, direct swim-up and discontinuous density gradients are commonly used to obtain spermatozoa with good motility and morphology [2]. These techniques are time consuming and centrifugation steps are needed which can impair sperm function [78]. Therefore microfluidic devices have been developed for this purpose.

Separation based on swimming

The chip designed by Kricka and co-workers has been used to assess the motility of spermatozoa, but was also able to separate motile spermatozoa from the semen sample [66]. Another example of a chip that separates spermatozoa based on their motility uses a 50 μm deep, 4 mm wide channel in combination with diffraction

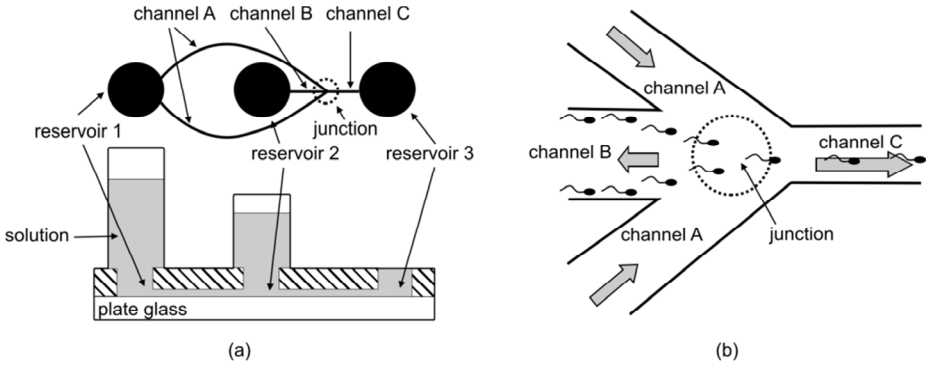

figure 2-7 Separation of motile spermatozoa based on the ability that motile cells can swim against the flow. (a) Schematic drawing of chip design. The semen sample is placed in reservoir 2. (b) Motile spermatozoa are able to swim against flow in channel B and are collected in channel C (adapted from [81]).

imaging using a CCD camera. With this device, the motility parameters of the spermatozoa could be determined during the sorting, resulting in additional information [79]. The migrating of motile spermatozoa away from the inlet was also used in the development of a microchamber by Lih and co-workers [80]. This microchamber, with dimensions in the millimetre range, was used to concentrate motile spermatozoa in side wells as selection tool for IVF [80]. The separation mechanism of another microfluidic chip is based on the observation that spermatozoa are oriented and able to swim against the liquid flow (see figure 2-7). By adjusting the fluid flow rates in different microchannels using hydrostatic pressure a counter flow was created in the PDMS chip. After 20 minutes, it was shown that the motility increased from 20% to 80% after separation [81]. Combination of the swimming ability of spermatozoa and their chemotactic response is also used for the development for an on-chip selection tool for IVF procedures. The first part of the chip consists of an optimized selection tool for the separation of motile spermatozoa, followed by a diffusion chamber connected with two outlets. So, with this chip the motility as well as the chemotactic response of the cells are simultaneously screened [82].

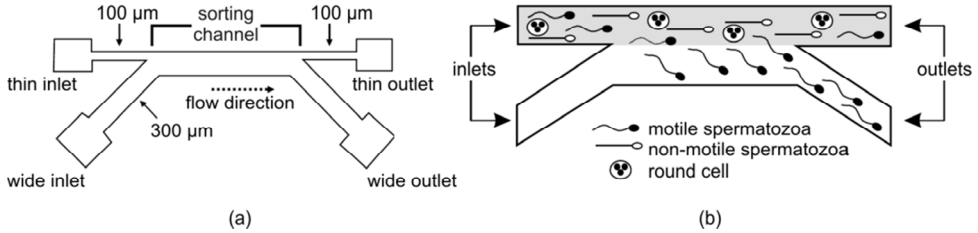

figure 2-8 The MISS device. (a) A schematic drawing of the channel design. The depth of the channel is 50 µm and the width of the sorting channel is 500 µm. (b) Operating principle of the MISS device. Motile spermatozoa are able to cross the laminar flow, while non-motile cells are not (adapted from [83]).

Microscale integrated sperm sorter

The flow in a microchannel is different from fluid flows normally seen in daily life. Due to the velocity of the fluid, the dimensions of the channel and certain fluid properties the flow in a microchannel is laminar instead of turbulent. Specific characteristics of laminar flow are that mixing only occurs due to diffusion and the flow is in streamlines and predictable [84-86]. The microscale integrated sperm sorter (MISS) uses the laminar flow for the separation of motile spermatozoa, since only motile spermatozoa are able to cross streamlines (see figure 2-8) [87]. The first version of a MISS has been made of PDMS and has two inlet and two outlet channels (both having two widths, 100 and 300 µm) that combine to a 5 mm long sorting channel which has a width and depth of 500 µm and 50 µm respectively. Flow originates from a gravity-driven pump system such that the residence time in the sorting channel is about 20 seconds. The washed semen sample is placed in one inlet and a buffer in the other one. About 40% of the motile spermatozoa in the inlet were able to cross the flow and the purity at this outlet was almost 100% [87]. Additionally an unprocessed semen sample was tested with the MISS. This unwashed sample could not be placed in the thin outlet (width: 100 µm) as was done with the washed sample, because then clogging occurred. However, the separation was still successful when the sample was put into the wider inlet channel [83]. The separation with MISS yields spermatozoa populations with higher DNA integrity and larger mean motility compared to other semen processing techniques such as centrifugation and swim-up [88].

Hyakutake and co-workers did some numerical simulations of the MISS, to predict the separation efficiency for motile spermatozoa [89]. The average velocity in the

sorting channel appeared to be the main predictor for separation efficiency; lowering the mean flow velocity increases the efficiency. In addition a decrease in the width of the channel with spermatozoa leads to an increase in the number of separated spermatozoa [89]. Besides numerical simulations other studies describe experiments to investigate the motile spermatozoa recovery with the MISS device. High motile spermatozoa recovery was achieved, when the sample was put into the curve straight channel instead of the horizontal channel [90, 91], such that the spermatozoa arrive at the sorting channel under an angle.

The material of the MISS device was originally untreated PDMS which has been adapted by others. To extend the hydrophilic nature of the device up to 56 days, the PDMS microchannels were coated with PEG-MA [92]. Instead of PDMS, Shibata and co-workers fabricated a device of quartz that has been used for ICSI purposes. The fertilization rate with this device was 46.9% (n=49) [93].

The MISS device has also been used for the separation of hyperactivated boar sperm subpopulations by adding bicarbonate to the samples [94]. The use of the chemo-attractant hyaluronic acid in a microfluidic chip (with a 3 cm long sorting channel) improves the progressive motility and nuclear maturity of gradient processed spermatozoa [95]. To prevent polyspermic penetration in porcine IVF, a slightly modified MISS device, with a larger outlet chamber containing holes for oocyte capture, has been developed. Compared to transient and standard drop IVF methods, the ratio of monospermic penetrated oocytes to the total number of oocytes examined was larger [96].

Selection based on electrophoresis and dielectrophoresis

Using microtechnology an optoelectronic tweezers device has been developed, that is part of a bigger set-up consisting of among other things a laser, microscope and function generator [97]. With the laser an electrical field gradient is created on the optoelectronic tweezers device and viable spermatozoa experience a positive dielectrophoretic force, while dead cells experience no or a negative dielectrophoretic force. Even non motile spermatozoa that are viable can be selected by this setup, such that it can be used as a selection tool for ICSI procedures [97].

Another approach makes use of electrophoretic separation of spermatozoa from semen based on size and electronegative charge. In this device, spermatozoa are attracted via electrophoresis to the other side of a membrane, while other larger cells that are present in semen are blocked by the membrane. Results showed that the separated sample has less DNA damage and an improved percentage of normal morphology [98]. The electrophoretic separation device was also clinically used to improve the semen quality of a specific case that has high levels of DNA damage. The

separated semen was used for ICSI and resulted after two cycles in the birth of a healthy child [99].

2.3.3 Other applications

Besides on-chip methods for semen analysis and spermatozoa selection, other microfluidic chips have been developed for applications with spermatozoa. These are summarized in this paragraph.

Spermatozoa behaviour

Microfluidic devices can also be used to study the behaviour of spermatozoa in enforced circumstances. For instance a PDMS IVF device is used to investigate the behaviour of spermatozoa in a flow and how the spermatozoon-oocyte interaction occurs [100]. It was shown that spermatozoa swam in the same direction as the flow when the velocity was larger than 17 $\mu m \cdot s^{-1}$ and preferred to migrate along the walls resulting in a low spermatozoon-oocyte attachment. At lower flow rates, the spermatozoa swam in different directions, such that attachment with the oocyte occurred almost immediately [100].

Characterization of the behaviour of a spermatozoon is also possible after trapping. Fuhr and co-workers developed chips containing microelectrodes. With four or eight electrodes slow or immotile spermatozoa were especially trapped with negative dielectrophoresis (DEP) for minutes in a field funnel or field cage respectively. A different chip design with interdigitated electrodes was able to trap fast swimming spermatozoa [101].

The chemotaxis of spermatozoa is part of the fundamental research in reproductive science. To improve the temporal and spatial stability of existing sperm chemotaxis arrays, a microfluidic device was developed that assesses the chemotactic behaviour of spermatozoa [102]. The PDMS device has three input channels, three output channels and one main channel (width: 100 μm, depth: 20 μm). Due to the channel geometry, a gradient in the chemical concentration of the carrying liquid can be formed and the behaviour of the cells can be evaluated [102].

Sexual assault evidence

For identifying the perpetrator of sexual assaults the DNA containing components of a swab, the spermatozoa of the men and epithelial cells of the woman, need to be separated. To make this procedure faster a glass-glass chip has been developed that has one straight 50 μm deep channel [103]. After a settling time in the inlet, a flow is

introduced in the channel and only spermatozoa are mobilized because the epithelial cells adsorb better to glass and have a shorter settling time.

Acoustic trapping on chip is another method that has been used for this type of DNA separation on chip [104]. The chip has a piezo transducer on the bottom of the channel (depth: 191.4 μm) and the spermatozoa are trapped in single pressure nodes. By using hydrodynamic focusing and laminar flow valving in combination with the acoustic trapping, separation of female and male DNA was demonstrated [104].

2.4 Conclusion

The gold standards for assessing the traditional parameters determined with a semen analysis are manual methods, meaning that it is subjective and quality control is essential. There are correlations between the traditional parameters and the pregnancy chance, but there is still no general consensus about which parameter is the best predictor. In recent years, there is an enormous increase in the development of lab on chips for applications involving spermatozoa. These lab on chips are not only restricted to the determination of some semen parameters, but also used for the separation and selection of spermatozoa for assisted reproductive technology and forensics as well as more fundamental research. Although several home testing devices that determine the semen quality already exist, these provide no quantitative data that is necessary for medical treatment decisions. With the development of a microfluidic chip that objectively measures the concentration and motility of spermatozoa in semen, multiple measurements can easily be performed without the need for a laboratory facility. This will not only improve the conventional semen analysis, but also results in a more patient-friendly analysis.

2.5 References

1. WHO, *WHO Laboratory manual for the examination of human semen and sperm-cervical mucus interaction*. 4th ed. 1999, Cambridge: Cambridge University Press.
2. WHO, *WHO laboratory manual for the examination and processing of human semen*. 5th ed. 2010, Geneva.
3. Rothman, S.A. and A.A. Reese, *Semen analysis: the test techs love to hate*, in *Medical Laboratory Observer*. 2007, Medical Laboratory Observer. p. 18-27.
4. Katz, D.F., et al., *Morphometric analysis of spermatozoa in the assessment of human male fertility.* Journal of Andrology, 1986. **7**(4): p. 203-210.

5. Maree, L., et al., *Morphometric dimensions of the human sperm head depend on the staining method used.* Human Reproduction, 2010. **25**(6): p. 1369-1382.
6. Katz, D.F., L. Diel, and J.W. Overstreet, *Differences in the movement of morphologically normal and abnormal human seminal spermatozoa.* Biology of Reproduction, 1982. **26**: p. 566-570.
7. Dresdner, R.D. and D.F. Katz, *Relationships of mammalian sperm motility and morphology to hydrodynamic aspects of cell function.* Biology of Reproduction, 1981. **25**(5): p. 920-930.
8. Ishijima, S., et al., *Rotational movement of a spermatozoon around its long axis.* Journal of Experimental Biology, 1992. **163**: p. 15-31.
9. Baltz, J.M., D.F. Katz, and R.A. Cone, *Mechanics of sperm-egg interaction at the zona pellucida.* Journal of Biophysics, 1988. **54**: p. 643-654.
10. Marieb, E.N. and K. Hoehn, *The reproductive system*, in *Human anatomy & physiology*. 2010, Pearson Benjamin Cummings: San Fransisco, USA.
11. Harvey, C., *The speed of human spermatozoa and the effect on it of various diluents, with some preliminary observations on clinical material.* Journal of Reproduction & Fertility, 1960. **1**(1): p. 84-95.
12. Mortimer, S.T., et al., *Quantitative observations of flagellar motility of capacitating human spermatozoa.* Human Reproduction, 1997. **12**(5): p. 1006-1012.
13. Walton, A., *Flow orientation as a possible explanation of 'wave-motion' and 'rheotaxis' of spermatozoa.* Journal of Experimental Biology, 1952. **29**: p. 520-531.
14. Winet, H., G.S. Bernstein, and J. Head, *Observations on the response of human spermatozoa to gravity, boundaries and fluid shear.* Journal of Reproduction & Fertility, 1984. **70**: p. 511-523.
15. Bretherton, F.P. and F.R.S. Lord Rothschild, *Rheotaxis of spermatozoa.* Proceedings of the Royal Society of London. Series B, Biological Sciences, 1961. **153**(953): p. 490-502.
16. Sarkar, S., *Human sperm swimming in flow.* Differentiation, 1984. **27**(1-3): p. 126-132.
17. Roberts, A.M., *Motion of spermatozoa in fluid streams.* Nature, 1970. **228**: p. 375-376.
18. Muller, C.H., *Rationale, interpretation, validation, and uses of sperm function tests.* Journal of Andrology, 2000. **21**(1): p. 10-30.
19. Suarez, S.S. and A.A. Pacey, *Sperm transport in the femal reproductive tract.* Human Reproduction Update, 2006. **12**(1): p. 23-37.
20. Mortimer, S.T., *A critical review of the physiological importance and analysis of sperm movement in mammals*.* Human Reproduction Update, 1997. **3**(5): p. 403-439.
21. De Jonge, C., *Biological basis for human capacitation.* Human Reproduction Update, 2005. **11**(3): p. 205-214.
22. Austin, C.R., *The 'Capacitation' of the Mammalian Sperm.* Nature, 1952. **170**(4321): p. 326.

23. Chang, M.C., *Fertilizing capacity of spermatozoa deposited into the Fallopian tube.* Nature, 1951. **168**(4277): p. 697-698.
24. Williams, M., et al., *Sperm numbers and distribution within the human Fallopian tube around ovulation.* Human Reproduction 1993. **8**(12): p. 2019-2026.
25. Ralt, D., et al., *Chemotaxis and chemokinesis of human spermatozoa to follicular factors.* Biology of Reproduction, 1994. **50**(4): p. 774-785.
26. Eisenbach, M., *Mammalian sperm chemotaxis and its association with capacitation.* Developmental Genetics, 1999. **25**: p. 87-94.
27. Sun, F., et al., *Human sperm chemotaxis: both the oocyte and its surrounding cumulus cells secrete sperm chemoattractants.* Human Reproduction, 2005. **20**(3): p. 761-767.
28. Spehr, M., et al., *Identification of a testicular odorant receptor mediating human sperm chemotaxis.* Science, 2003. **299**: p. 2054-2058.
29. Cohen-Dayag, A., et al., *Sequential acquisition of chemotactic responsiveness by human spermatozoa.* Biology of Reproduction, 1994. **50**(4): p. 786-790.
30. Cohen-Dayag, A., et al., *Sperm capacitation in humans is transient and correlates with chemotactic responsivesness to follicular factors.* Proceedings of the National Academy of Sciences, 1995. **92**: p. 11039-11043.
31. Bahat, A. and M. Eisenbach, *Sperm thermotaxis.* Molecular and Cellular Endocrinology, 2006. **252**: p. 115-119.
32. Bahat, A., et al., *Thermotaxis of mammalian sperm cells: a potential navigation mechanism in the femal genital tract.* Nature Medicine, 2003. **9**(2): p. 149-150.
33. Eisenbach, M. and L.C. Giojalas, *Sperm guidance in mammals - an unpaved road to the egg.* Nature Reviews Molecular Cell Biology, 2006. **7**: p. 276-285.
34. Kaupp, U.B., N.D. Kashikar, and I. Weyand, *Mechanisms of sperm chemotaxis.* Annual Review of Physiology, 2008. **70**: p. 93-117.
35. Matson, P.L., *Clinical value of tests for assessing male infertility.* Baillière's Clinical Obstetrics and Gynaecology, 1997. **11**(4): p. 641-654.
36. Cooper, T.G., et al., *World Health Organization reference values for human semen characteristics.* Human Reproduction Update, 2010. **16**(3): p. 231-245.
37. Steeg van der, J.W., et al., *Role of semen analysis in subfertile couples.* Fertility and Sterility, 2011. **95**(3): p. 1013-1019.
38. Vreeburg, J.T.M., *Semenanalyse, nut en onnut.* Nederlands Tijdschrift voor Klinische Chemie, 2001. **26**: p. 277-282.
39. Keel, B.A., *How reliable are results from the semen analysis?* Fertility and Sterility, 2004. **82**(1): p. 41-44.
40. Keel, B.A., *Within- and between-subject variation in semen parameters in infertile men and normal semen donors.* Fertility and Sterility, 2006. **85**(1): p. 128-134.
41. Garrett, C., et al., *Automated semen analysis: 'zona pellucida preferred' sperm morphometry and straight-line velocity are related to pregnancy rate in subfertile couples.* Human Reproduction, 2003. **18**(8): p. 1643-1649.

42. Bonde, J.P.E., et al., *Relation between semen quality and fertility: a population-based study of 430 first-pregnancy planners.* Lancet, 1998. **352**(9135): p. 1172-1177.
43. Zinaman, M.J., et al., *Semen quality and human fertility: a prospective study with healthy couples.* Journal of Andrology, 2000. **21**(1): p. 145-153.
44. Coetzee, K., T.F. Krüger, and C.J. Lombard, *Predictive value of normal sperm morphology: a structured literature review.* Human Reproduction Update, 1998. **4**(1): p. 73-82.
45. Lewis, S.E.M., *Is sperm evaluation useful in predicting human fertility?* Reproduction, 2007. **134**: p. 31-40.
46. Guzick, D.S., et al., *Sperm morphology, motility, and concentration in fertile and infertile men.* New England Journal of Medicine, 2001. **345**(19): p. 1388-1393.
47. Grimes, D.A. and L.M. Lopes, *"Oligozoospermia", "azoospermia", and other semen-analysis terminology: the need for better science.* Fertility and Sterility, 2007. **88**(6): p. 1491-1494.
48. Hirano, Y., et al., *Relationships between sperm motility characteristics assessed by the computer-aided sperm analysis (CASA) and fertilization rates in vitro.* Journal of Assisted Reproduction and Genetics, 2001. **18**(4): p. 213-218.
49. Larsen, L., et al., *Computer-assisted semen analysis parameters as predictors for fertility of men from the general population.* Human Reproduction, 2000. **15**(7): p. 1562-1567.
50. Douglas-Hamilton, D.H., et al., *Particle distribution in low-volume capillary-loaded chambers.* Journal of Andrology, 2005. **26**(1): p. 107-114.
51. Douglas-Hamilton, D.H., et al., *Capillary-loaded particle fluid dynamics: effect on estimation of sperm concentration.* Journal of Andrology, 2005. **26**(1): p. 115-122.
52. Aitken, R.J., *Sperm function tests and fertility.* International Journal of Andrology, 2006. **29**: p. 69-75.
53. Oehninger, S., et al., *Sperm function assays and their predictive value for fertilization outcome in IVF therapy: a meta-analysis.* Human Reproduction Update, 2000. **6**(2): p. 160-168.
54. Tang, S., C. Garrett, and H.W.G. Baker, *Comparison of human cervical mucus and artificial sperm penetration media.* Human Reproduction, 1999. **14**(11): p. 2812-2817.
55. Liu, D.Y. and H.W.G. Baker, *Disordered zona pellucida-induced acrosome reaction and failure of in vitro fertilization in patients with unexplained infertility.* Fertility and Sterility, 2003. **79**(1): p. 74-80.
56. Agarwal, A., R.A. Saleh, and M.A. Bedaiwy, *Role of reactive oxygen species in the pathophysiology of human reproduction.* Fertility and Sterility, 2003. **79**(4): p. 829-843.
57. Pasqualotto, F.F., et al., *Oxidative stress in normospermic men undergoing infertility evaluation.* Journal of Andrology, 2001. **22**(2): p. 316-322.
58. Bungum, M., et al., *Sperm DNA integrity assessment in prediction of assisted reproduction technology outcome.* Human Reproduction, 2007. **22**(1): p. 174-179.

59. Collins, J.A., K.T. Barnhart, and P.N. Schleger, *Do sperm DNA integrity tests predict pregnancy with in vitro fertilization?* Fertility and Sterility, 2007. **89**(4): p. 823-831.
60. Leeuwenhoek van, A., *Observationes D. Anthonii Lewenhoeck, de Natis e Semine Genitali Animalculis.* Philosophical Transactions (1665-1678), 1678. **12**: p. 1040-1046.
61. Kricka, L.J., et al., *Micromachined analytical devices: microchips for semen testing.* Journal of Pharmaceutical and Biomedical Analysis, 1997. **15**(9-10): p. 1443-1447.
62. Manz, A., et al., *Planar chips technology for miniaturization and integration of separation techniques into monitoring systems - capillary electrophoresis on a chip.* Journal of Chromatography, 1992. **593**(1-2): p. 253-258.
63. Li, P.C.H. and D.J. Harrison, *Transport, manipulation, and reaction of biological cells on-chip using electrokinetic effects.* Analytical Chemistry, 1997. **69**(8): p. 1564-1568.
64. Andersson, H. and A. van den Berg, *Microfluidic devices for cellomics: a review.* Sensors and Actuators B-Chemical, 2003. **92**(3): p. 315-325.
65. Kricka, L.J. and P. Wilding, *Micromachining: A new direction for clinical analyzers.* Pure and Applied Chemistry, 1996. **68**(10): p. 1831-1836.
66. Kricka, L.J., et al., *Applications of a microfabricated device for evaluating sperm function.* Clinical Chemistry, 1993. **39**(9): p. 1944-1947.
67. Kricka, L.J., et al., *Sperm testing with microfabricated glass-capped silicon microchannels.* Clinical Chemistry, 1994. **40**(9): p. 1823-1824.
68. Herr, J.C., et al., *Progress in developing an immunochromatographic device for sperm detection.* Clinical Immunology Newsletter, 1999. **19**(4-5): p. 52-58.
69. Coppola, M.A., et al., *SpermCheck® Fertility, an immunodiagnostic home test that detects normozoospermia and severe oligozoospermia.* Human Reproduction 2010. **25**(4): p. 853-861.
70. Klotz, K.L., et al., *Clinical and consumer trial performance of a sensitive immunodiagnostic home test that qualitatively detects low concentrations of sperm following vasectomy.* The Journal of Urology, 2008. **180**(6): p. 2569-2576.
71. Segerink, L.I., et al., *On-chip determination of spermatozoa concentration using electrical impedance measurements.* Lab on a Chip, 2010. **10**: p. 1018-1024.
72. Su, T.-W., et al., *Compact and light-weight automated semen analysis platform using lensfree on-chip microscopy.* Analytical Chemistry, 2010. **82**(19): p. 8307-8312.
73. Björndahl, L., et al., *Development of a novel home sperm test.* Human Reproduction 2006. **21**(1): p. 145-149.
74. McCormack, M.C., S. McCallum, and B. Behr, *A novel microfluidic device for male subfertility screening.* Journal of Urology, 2006. **175**: p. 2223-2227.
75. Chen, Y.-A., et al., *Simultaneous and label-free evaluation of sperm quality and sortin in a microfluidic device*. in *Microtas* 2009. Jeju Island, South Korea.
76. Chen, Y.A., et al., *Analysis of sperm concentration and motility in a microfluidic device.* Microfluidics and Nanofluidics, 2011. **10**(1): p. 59-67.

77. Chen, Y.-A., et al., *Analysis of sperm quality in a microfluidic device*. in *Microtas*. 2010. Groningen, the Netherlands.
78. Aitken, R.J. and J.S. Clarkson, *Significance of reactive oxygen species and antioxidants in defining the efficacy of sperm preparation techniques.* Journal of Andrology, 1988. **9**(6): p. 367-376.
79. Zhang, X., et al. (2011) *Lensless imaging for simultaneous microfluidic sperm monitoring and sorting*. Lab on a Chip, DOI: 10.1039/C1LC20236G.
80. Lih, C.H., et al., *Development of a microchamber which spontaneously selects high-quality sperm for use in in vitro fertilization or micromanipulation.* Journal of Assisted Reproduction and Genetics, 1996. **13**(8): p. 657-662.
81. Seo, D., et al., *Development of sorting, aligning, and orienting motile sperm using microfluidic device operated by hydrostatic pressure.* Microfluidics and Nanofluidics, 2007. **3**: p. 561-570.
82. Xie, L., et al., *Integration of sperm motility and chemotaxis screening with a microchannel-based device.* Clinical Chemistry, 2010. **56**(8): p. 1270-1278.
83. Schuster, T.G., et al., *Isolation of motile spermatozoa from semen samples using microfluidics.* Reproductive BioMedicine Online, 2003. **7**(1): p. 75-81.
84. Suh, R.S., et al., *Rethinking gamete/embryo isolation and culture with microfluidics.* Human Reproduction Update, 2003. **9**(5): p. 451-461.
85. Beebe, D.J., et al., *Microfluidic technology for assisted reproduction.* Theriogenology, 2002. **57**(1): p. 125-135.
86. Brody, J.P., et al., *Biotechnology at low Reynolds numbers.* Biophysical Journal, 1996. **71**(6): p. 3430-3441.
87. Cho, B.S., et al., *Passively driven integrated microfluidic system for separation of motile sperm.* Analytical Chemistry, 2003. **75**: p. 1671-1675.
88. Schulte, R.T., et al., *Microfluidic sperm sorting device provides a novel method for selecting motile sperm with higher DNA integrity.* Fertility and Sterility, 2007. **88**(Suppl. 1): p. S76.
89. Hyakutake, T., et al., *Application of a numerical simulation to improve the separation efficiency of a sperm sorter* Biomedical Microdevices, 2009. **11**(1): p. 25-33.
90. Huang, H.Y., et al., *Improved quantity and quality of recovered motile spermatozoa with modified microfluidic system device with curve-straight channel.* Reproductive Sciences, 2010. **17**(3): p. 931.
91. Wu, T.-L., et al., *High efficient sperm motility sorting based on encoutered surve-straight micro streaming flow*. in *Microtas*. 2008. San Diego, USA.
92. Wu, J.M., et al., *A surface-modified sperm sorting device with long-term stability.* Biomedical Microdevices, 2006. **8**: p. 99-107.
93. Shibata, D., et al., *Analysis of the sperm motility and fertilization rates after the separation by microfluidic sperm sorter made of quartz.* Fertility and Sterility, 2007. **88**(Suppl. 1): p. S110.
94. Holt, W., et al., *Microfluidic sorting of boar spermatozoa*. in *16th International congress on animal reproduction* 2008. Budapest, Hungary.
95. Karakoc Sokmensuer, L., et al., *A microfluidic chemotaxis system to select motile and mature sperm.* Fertility and Sterility, 2004. **82**(Suppl. 2): p. S327.

96. Sano, H., et al., *Application of a microfluidic sperm sorter to the in-vitro fertilization of porcine oocytes reduced the incidence op polyspermic penetration.* Theriogenology, 2010. **74**: p. 863-870.
97. Ohta, A.T., et al., *Motile and non-motile sperm diagnostic manipulation using optoelectronic tweezers.* Lab on a Chip, 2010. **10**(23): p. 3213-3217.
98. Ainsworth, C., B. Nixon, and R.J. Aitken, *Development of a novel electrophoretic system for the isolation of human spermatozoa.* Human Reproduction, 2005. **20**(8): p. 2261-2270.
99. Ainsworth, C., et al., *First recorded pregnancy and normal birth after ICSI using electrophoretically isolated spermatozoa.* Human Reproduction, 2007. **22**(1): p. 197-200.
100. Lopez-Garcia, M.D.C., et al., *Sperm motion in a microfluidic fertilization device.* Biomedical Microdevices, 2008. **10**(5): p. 709-718.
101. Fuhr, G., et al., *High-frequency electric field trapping of individual human spermatozoa.* Human Reproduction, 1998. **13**(1): p. 136-141.
102. Koyama, S., et al., *Chemotaxis assays of mouse sperm on microfluidic devices.* Analytical Chemistry 2006. **78**(10): p. 3354-3359.
103. Horsman, K.M., et al., *Separation of Sperm and Epithelial Cells in a Microfabricated Device: Potential Application to Forensic Analysis of Sexual Assault Evidence.* Analytical Chemistry, 2004. **77**(3): p. 742-749.
104. Norris, J.V., et al., *Acoustic Differential Extraction for Forensic Analysis of Sexual Assault Evidence.* Analytical Chemistry, 2009. **81**(15): p. 6089-6095.

chapter 3

Electrical impedance measurements

Microfluidic impedance cytometry can be used to assess the dielectric properties of single cells passing an integrated electrode pair in a microchannel. Since the dielectric properties of cells are frequency dependent, information about several cell characteristics can be obtained with electrical impedance measurements at different frequencies, which is often called impedance spectroscopy. However, at low measurement frequencies the electrical double layer capacitance present at the electrode-liquid interface mainly determines the measured impedance, while at high frequencies the influence of the parasitic capacitance is dominant, thereby limiting the impedance measurement of the cell to the intermediate frequencies. Due to the advantages of using microfluidic impedance cytometry, considerable effort has been put into making it applicable for diagnostic purposes.

3.1 Microfluidic impedance cytometry

The detection and counting of single cells in biological fluid is important for diagnostic purposes. Instead of using complex, large systems for the counting, the tendency is towards chip-based microfluidic diagnostic devices, since these tend to be low-cost, use only a small amount of sample and are small in size making on-site analysis possible [1]. Most of the used techniques with microfluidic chips are optical or electrical [2, 3]. In optical techniques the value of a blocked, scattered or fluorescent signal is measured, while with electrical measurements the impedance of the suspension is the parameter to be analysed [3]. The electrical impedance measurement has the advantage that it can be performed in a non-invasive, label-free way and can be easily integrated in a microfluidic system. Therefore the focus in this chapter is on microfluidic impedance cytometry, which is a technique to measure the dielectric properties of single particles or cells in a microchannel when they pass the integrated electrodes.

Coulter was the first who developed a system for counting single cells in suspension using impedance measurements [4, 5]. In a Coulter counter the DC impedance between two chambers filled with the fluid is measured through a small tube or aperture and when a cell flows through the aperture, the impedance changes. Assuming a infinite long tube and a small diameter of the particle d compared to the tube diameter D_t, the resistance change ΔR caused by a particle in the tube is [6]:

$$\Delta R = {}^{4\rho_{el} d^3}\Big/_{\pi D_t^4} \cdot F\left({}^{d^3}\Big/_{D_t^3}\right) \qquad [\Omega] \qquad (3.1a)$$

$$F\left({}^{d^3}\Big/_{D_t^3}\right) = 1 + 1.26\,{}^{d^3}\Big/_{D_t^3} + 1.1\,{}^{d^6}\Big/_{D_t^6} \qquad (3.1b)$$

with ρ_{el} the resistivity of the electrolyte and $F(d^3/D_t^3)$ a correction term. In theory particles down to 25 nm could be detected with this setup [6]. Reducing the size of the conventional Coulter counter to a chip format by integrating the electrodes in a microchannel, results in a microfluidic resistive pulse sensor. With such a system viruses suspended in blood and nanoparticles could be detected and their sizes determined at high throughput [7]. Another resistive pulse sensor design was able to detect simultaneously the impedance changes at four apertures in parallel in one channel [8]. Furthermore the resistive pulse sensor has been used in combination

with a fluorescence detector, making it possible to distinguish between fluorescently labelled and unlabelled white blood cells [9].

Instead of measuring the DC impedance of single cells, additional characteristics of single cells can be obtained using AC signals. Hoffman and co-workers developed a system with integrated electrodes in the channel which was able to measure at two frequencies simultaneously [10, 11]. With such configuration different cells having about the same size could be discriminated based on their contents [12, 13].

3.1.1 Electrode configuration

The electrical impedance measurements in a microfluidic chip can be done with several electrode configurations. These configurations vary in the number of electrodes used and the position of the electrodes with respect to each other and the microchannel (see figure 3-1).

The number of electrode pairs in the microchannel chip can be varied. For a differential measurement two electrode pairs into two successive channel parts are needed. This configuration has several advantages, such as enabling to measure the cell characteristics with respect to the background electrolyte, reducing the drift in the signal and giving the possibility to determine the particle velocity and the vertical position in the microchannel [13, 14]. A disadvantage of the differential measurement is that due to the multiple electrode pairs the measurement volume increases, such that measurements can only be performed at low particle or cell concentrations, avoiding the risk of detecting multiple particles or cells simultaneously.

Another variation in the electrode configuration is the position of the electrodes with respect to each other. Planar electrode configurations, where the electrodes are at the same side of the channel, are the easiest to fabricate. However, the impedance change that is caused by a particle in the measurement volume is lower compared to a parallel electrode configuration in case of corresponding dimensions [13, 15]. Furthermore the position of the particle in the microchannel influences the measured impedance change due to the non-homogeneous electrical field [13, 15, 16]. In case of a parallel electrode configuration, the measured impedance signal is hardly influenced by the position of the particle in the channel [17], except very close to the electrodes [18], where the simulated and experimentally observed impedance changes are larger due to a locally stronger electrical field [18]. Increasing the width of the electrode, also reduces the field non-uniformity [19]. However, the fabrication of a parallel electrode configuration is more complicated than a planar one, due to difficulties in alignment of both electrodes and more complicated electrical connections to the outer world.

Parallel electrodes are easier fabricated when using a floating electrode [21] (see chapter 5) or liquid electrodes [14]. For the floating electrode, two parallel electrode pairs are fabricated with a process comparable to the fabrication process of planar electrodes [21]. In the liquid electrode configuration relative large electrodes are placed in lateral chambers which are in contact with the main channel via narrow channels. The result is a homogenous electrical field across the main channel. Due to the large electrode area, the influence of the electrical double layer is limited to lower frequencies, making cell detection at 100 Hz possible [14].

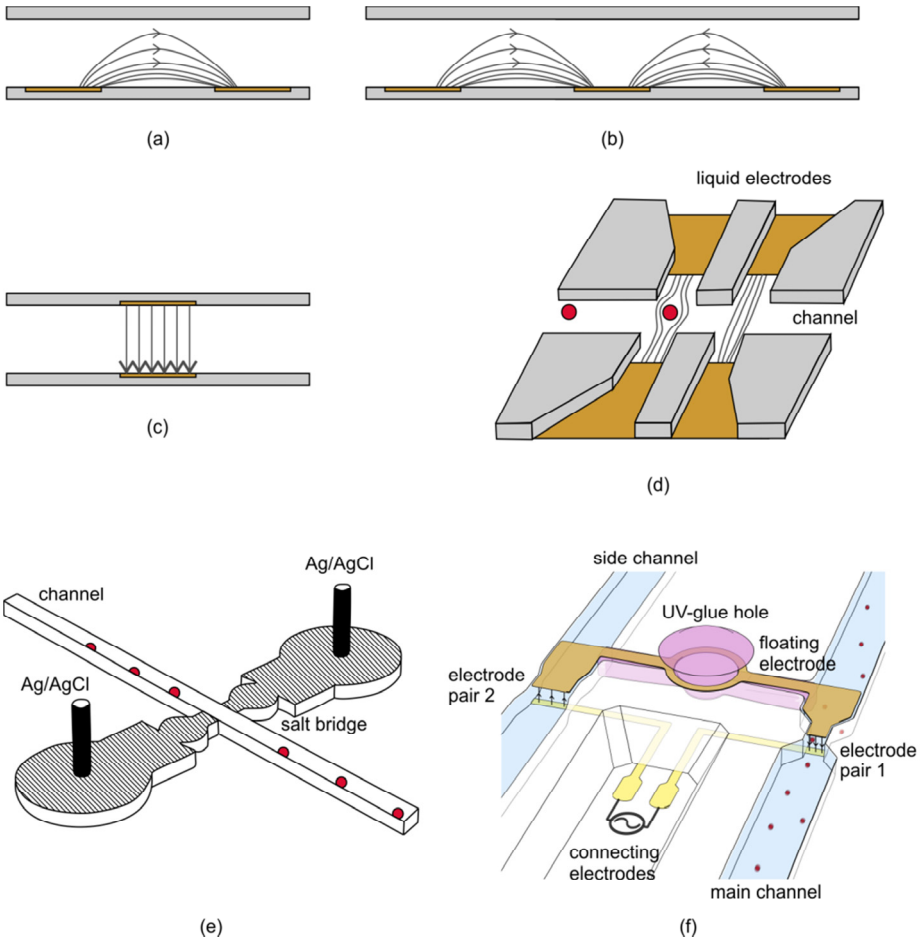

figure 3-1 The difference in electrode configurations for microfluidic impedance cytometry. Difference between (a) a single measurement and (b) a differential measurement with planar electrodes. Differences in the position of the electrodes with (c) a parallel electrode configuration; (d) liquid electrodes (modified from [14]); (e) the polyelectrolyte salt bridge based electrodes (modified from [20]) and (f) the parallel electrode configuration using a floating electrode [21].

A disadvantage of using integrated metal micro-electrodes is the influence of the electrical double layer on the measurements especially at low frequencies. To overcome this, polyelectrolyte salt bridge based electrodes can be used for the detection of cells with DC voltages [20]. These electrodes are integrated in side channels perpendicular to the main channel, creating a homogeneous electrical field in the main channel and connected via an Ag/AgCl electrode to the outer world. Additionally, in this configuration there is no direct contact between the metal electrodes and the fluid to be investigated, preventing sticking of cells to the metal electrodes and damage of the cells due to the electrical field [22].

3.1.2 Focusing

For some electrode configurations the position of the particle or cell relative to the measurement electrodes influences the measured impedance change. This effect can be reduced by focusing the particles or cells at a specific position in the microfluidic channel by means of either hydrodynamic or electrokinetic focusing methods (see figure 3-2) [2].

With hydrodynamic focusing non-conducting [23-26] or conducting [27] sheath fluids compress the conducting fluid flow with the particles to a certain position. The fluid flow can be compressed only in the horizontal direction [24, 25], but also in horizontal and vertical direction [23, 26, 27]. For example in case of a planar electrode configuration, the sheath flow positions the fluid flow against the wall of the microchannel with the electrodes. By increasing the flow rate of the sheath flow, the height of the fluid flow can be reduced, leading to a smaller measurement volume and thereby improving the sensitivity such that a broad range of sizes can be detected without increasing the risk of blocking [23, 26, 27]. Also hydrodynamic focusing for a parallel electrode configuration in a 200 µm wide microchannel was shown. Clogging is prevented due to the wide channel, but still sensitive measurements could be performed since the sample was hydrodynamic focused [24].

Dielectrophoretic forces can also be used for particle or cell alignment in a microchannel. This electrokinetic method uses integrated electrodes that generate electrical field gradients in the microfluidic channel from which the particles or cells are repelled, since they experience negative DEP in a conductive medium at frequencies up to $\sim 10^6$ Hz [2, 28-31]. Note that at low frequencies, negative DEP occur, but also electrophoretic and electro-osmotic effects which should be prevented [32]. To achieve the alignment, electrodes are positioned at the top and bottom of the microchannel in a funnel structure. Compared to the hydrodynamic focusing, only particles or cells suspended in the fluid are focused and not the fluid itself [28-30].

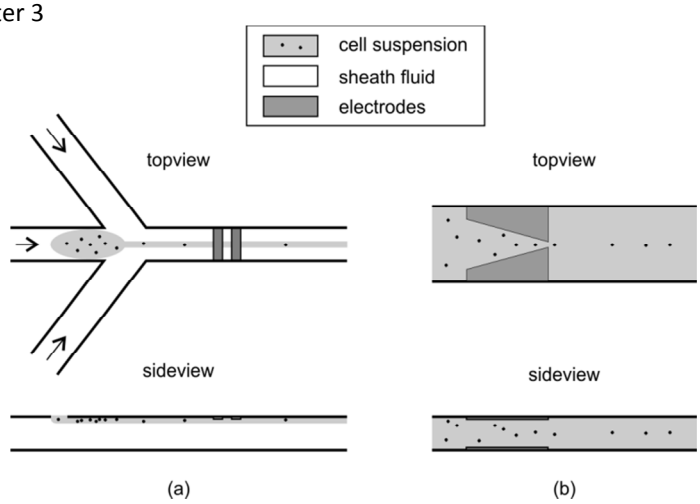

figure 3-2 Examples of two focusing techniques for cells in a microfluidic chip: (a) 3D hydrodynamic focusing and (b) electrokinetic focusing using a funnel structure (modified from [2, 23]).

A combination of both focusing techniques can also be used. Lin and co-workers developed a microfluidic chip where focusing in the horizontal plane was achieved by hydrodynamic focusing, while electrodes on the bottom and top of the channel caused the particles to align in the vertical direction by dielectrophoretic forces [33].

3.2 Equivalent circuit model of the chip

A microfluidic chip that can be used for electrical impedance measurements contains at least two electrodes. A typical example of such chip is given in figure 3-3(a) with its equivalent circuit model, consisting of two double layer capacitances (C_{DL}), the electrolyte resistance (R_{el}), the parasitic capacitance (C_{par}) and the lead resistance (R_{lead}). The frequency response of the equivalent circuit model is shown in figure 3-3(b) and clearly the influence of the different components can be seen.

The replacement impedance Z(jω) for the equivalent circuit model can be expressed as:

$$Z(j\omega) = R_{lead} + {}^{X}/_{j\omega C_{par} X + 1} \qquad [\Omega] \qquad (3.2a)$$

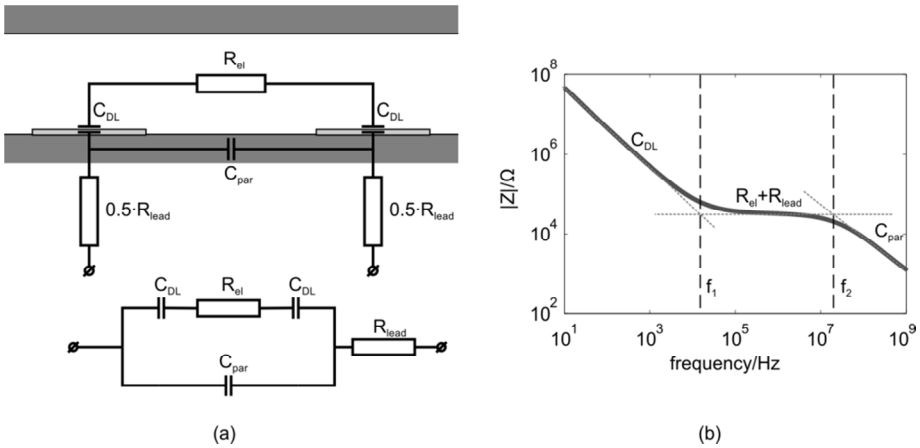

figure 3-3 (a) An equivalent circuit model of the microfluidic chip without a cell in the microchannel; (b) Typical frequency response of the real electrical impedance of the equivalent circuit model (adapted from [34]).

$$X = R_{el} + {}^{2}/_{j\omega C_{DL}} \qquad [\Omega] \qquad (3.2b)$$

with ω the angular frequency and j= $\sqrt{-1}$. When a particle or cell enters the measurement volume, it may cause a change in the effective electrolyte resistance. For the optimal measurement of this change, it is important to choose the measurement frequency of the setup in the resistive plateau. This means that the measurement frequency is above f_1 and below f_2, as indicated in figure 3-3(b). Langereis estimated these frequencies by assuming that $C_{DL} \cdot R_{el} \cdot C_{par} \cdot R_{lead} << 1$ as [35]:

$$f_1 \approx {}^{1}/_{\pi R_{el} C_{DL}} \qquad [Hz] \qquad (3.3)$$

$$f_2 \approx {}^{1}/_{2\pi R_{el} C_{par}} \qquad [Hz] \qquad (3.4).$$

The value of these frequencies can be adapted to optimize the measurement accuracy. For instance changing the electrode dimensions (C_{DL}) or using a background electrolyte with different conductivity (R_{el}) influences directly the position of the resistive plateau in the bode plot [36].

3.2.1 Double layer capacitance

The interface between the electrodes and the solution can be described with C_{DL} (see figure 3-4). The effect of the double layer is clearly visible at low frequencies in the typical frequency response. The C_{DL} can be best modelled by Gouy-Chapman theory with Stern's modification:

$$1/C_d = 1/C_H + 1/C_D \qquad [m^2 \cdot F^{-1}] \qquad (3.5)$$

where C_H is the influence of the Helmholtz layer which is also called the Stern layer and C_D is the capacitance caused by the diffuse layer as proposed by Gouy and Chapman [37]. These two capacitances per unit area can be calculated using the following equations:

$$C_H = \varepsilon\varepsilon_0 / x_{OHZ} \qquad [F \cdot m^{-2}] \qquad (3.6)$$

$$C_D = \sqrt{\left(2z^2e^2\varepsilon\varepsilon_0 n^0 / kT\right)}\, cosh\left(ze\varphi_{OHZ} / 2kT\right) \qquad [F \cdot m^{-2}] \qquad (3.7)$$

with ε the dielectric constant of the solution, ε_0 the permittivity of free space ($8.86 \cdot 10^{-12}$ $F \cdot m^{-1}$), x_{OHZ} the position of the outer Helmholtz plane (the transition of Helmholtz layer to diffuse layer), φ_{OHZ} is the potential at x_{OHZ} with respect to the bulk solution, z the magnitude of the charge on the ions, e the charge of the electron ($1.60 \cdot 10^{-19}$ C), n^0 is the number concentration of each ion in the bulk, k the Boltzmann constant ($1.38 \cdot 10^{-23}$ $J \cdot K^{-1}$) and T the absolute temperature [37].

Since the C_d is expressed in $F \cdot m^{-2}$ the C_{DL} can be determined by multiplying C_d with the surface area of the electrode (A):

$$C_{DL} = A \cdot C_d = w \cdot L \cdot C_d \qquad [F] \qquad (3.8)$$

where w is the width of the electrode and L the length of the electrode [35, 38]. For solutions with high electronic strength, the C_d is largely determined by C_H which is approximately 10 - 20 $\mu F \cdot cm^{-2}$ [35, 39].

The model of the electrical double layer assumes a smooth electrode surface, which is not always true. To model the inhomogeneity of the surface, the constant phase element (CPE) is used:

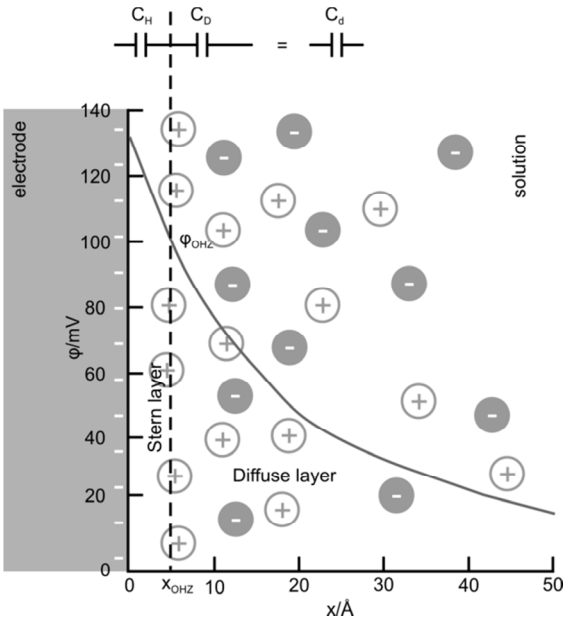

figure 3-4 Schematic view of the double layer. The potential profile indicates the profile through the solution side of the double layer according to the Gouy-Chapman theory with Stern's modification. The outer Helmholtz plane is indicated with the vertical dashed line (adapted from [37]).

$$Z_{CPE} = {}^{1}/_{Q_a(j\omega)^a} \qquad [\Omega \cdot s^{-a}] \qquad (3.9)$$

with Q_a and a the parameters of the CPE (for a=1, Q_a=C_{DL}) [39]. Normally for an electrode electrolyte interface a is between 0.8 and 1 [39].

3.2.2 Electrolyte resistance

The electrolyte resistance mainly determines the frequency response at frequencies between f_1 and f_2 and can be calculated using the following equation:

$$R_{el} = K_{cell} \cdot \rho_{el} \qquad [\Omega] \qquad (3.10)$$

with K_{cell} the cell constant [35, 38, 40]. The cell constant is dependent on the geometry of the electrodes. For two parallel electrodes the cell constant is:

$$K_{cell} = \alpha \cdot {}^{s}/_{A} \qquad [m^{-1}] \qquad (3.11)$$

with α the correction term for the spreading of current field lines and s the distance between the electrodes [38]. For interdigitated planar electrodes in contact with a semi-infinite medium on top, the cell constant can be expressed as:

$$K_{cell} = {}^{2}/_{(N-1)L} \cdot {}^{K(p)}\Big/_{K(\sqrt{1-p^2})} \qquad [\mathrm{m^{-1}}] \qquad (3.12a)$$

$$K(p) = \int_0^1 {}^{1}\Big/_{\sqrt{(1-t^2)(1-p^2t^2)}}\, dt \qquad (3.12b)$$

with N the number of fingers and K(p) the complete elliptic integral of the first kind [35, 38, 40]. For two planar electrodes (N=2), p can be estimated by:

$$p = {}^{s}/_{s+2w} \qquad (3.13)$$

while for more than two electrodes p has to be calculated with:

$$p = \cos({}^{\pi}/_{2} \cdot {}^{w}/_{s+w}) \qquad (3.14)$$

with s the interelectrode distance and w the width of the electrode [35, 36, 40]. For the calculation of the cell constant as indicated in 3.11, a semi-infinite medium on top of the electrodes is assumed. For a microchannel with integrated electrodes there is no semi-infinite medium on top of the electrodes, but this is restricted to the channel depth. Linderholm and co-workers have derived a more accurate cell constant for planar electrodes in a microchannel (for more information see [41]).

3.2.3 Parasitic capacitance and lead resistance

The capacitive coupling between both electrodes is represented by C_{par}. This capacitance determines the frequency response at high frequencies and can be calculated according:

$$C_{par} = {}^{\varepsilon\varepsilon_0}/_{K_{cell}} \qquad [\mathrm{F}] \qquad (3.15)$$

where K_{cell} is the cell constant [35, 40]. Furthermore the wiring both on chip as off chip also contributes to the C_{par}.

R_{lead} is the resistance of the wiring on-chip and off-chip and can be calculated with the following formula:

$$R_{lead} = {\rho_{wire} L_{wire}}/{A_{wire}} \quad [\Omega] \quad (3.16)$$

with ρ_{wire} is the specific resistivity of the material of the wiring, L_{wire} the length of the wires and A_{wire} the cross sectional area of the wire. On-chip the cross sectional area of the wire is much smaller than off-chip, such that the resistance of the wiring on-chip mainly determines the lead resistance.

3.3 Modelling the cell

3.3.1 Dielectric properties

The dielectric properties of tissues are described by permittivity ε and conductivity σ, which are the charge and current densities in response to an electrical field [42]. These values are related to each other:

$$\varepsilon^* = \varepsilon - {j\sigma}/{\omega\varepsilon_0} \quad (3.17)$$

$$\sigma^* = \sigma + j\omega\varepsilon\varepsilon_0 \quad [S \cdot m^{-1}] \quad (3.18)$$

with σ^* and ε^* the complex conductivity and permittivity respectively [42]. The complex impedance of the material z^* can be determined with the following equation [42]:

$$z^* = {1}/{\sigma^*} = {\sigma - j\omega\varepsilon\varepsilon_0}/{\sigma^2 + (\omega\varepsilon\varepsilon_0)^2} \quad [\Omega \cdot m] \quad (3.19).$$

Applying an electric field to a tissue, results in charge displacements in the tissue, such that relaxation occurs. The charge displacement can be fast or slow, resulting in a frequency dependency of the tissue on the applied electrical field [42]. There are three relaxation mechanisms that influence the dielectric properties of tissues and each mechanism has its own time constant. The first relaxation mechanism has to do with ionic diffusion in the electrical double layer and this effect is typically seen at frequencies between 10 - 10^5 Hz. The second one is the interfacial polarization or the Maxwell-Wagner effect. If a tissue is heterogeneous, several interfaces exist and these

are charged, influencing the dielectric properties of the tissue mainly at frequencies between 10^5 - 10^7 Hz. The last relaxation mechanism is caused by the partial orientation of permanent dipoles. This mechanism is known as dipolar orientation and is seen at frequencies around 10^9-10^{11} Hz [42]. Due to these relaxation mechanisms, dispersion regions can be found in the permittivity and conductivity. In figure 3-5 the dispersion regions in the permittivity as function of the frequency are shown. The α-dispersion around a frequency of 10^2 Hz is caused by the ionic diffusion effects, the β-dispersion visible at 10^5 Hz results from the Maxwell-Wagner effect and the γ-dispersion seen around 10^9 Hz arises from the dipolar orientation of water [5, 42]. Sometimes a fourth dispersion region can be observed between 10^8-10^9 Hz, the δ-dispersion, which is caused by a combination of the relaxation mechanisms. The decrease in permittivity with frequency is associated with an increase in conductivity. For the conductivity at frequencies below $5{\cdot}10^5$-$1{\cdot}10^6$ the cell in suspension acts as an insulator [13, 14, 42, 43]. Above the beta relaxation frequency (> 10^6 Hz) the cell membrane permits a current to flow through it and the cells do not behave as insulators anymore, resulting in an increase in the conductivity [13, 14, 42, 43]. Impedance simulations of a 10 µm cell showed that changing its size has an influence on the impedance at all frequencies. Changing the membrane capacitance or the cytoplasm conductivity influences the impedance only at frequencies around 10^6 and 10^7 Hz respectively [17].

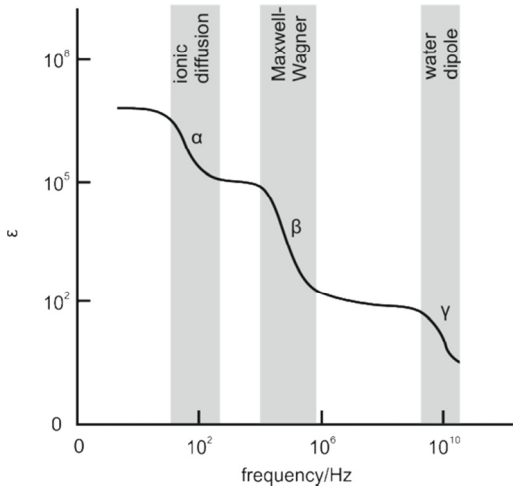

figure 3-5 The dielectric dispersion regions in the permittivity (modified from [42]).

3.3.2 Maxwell-Wagner Theory

The Maxwell-Wagner effect can be modelled such that the dielectric properties of a suspension at a specific frequency can be determined. The first model that describes the dielectric properties of a cell suspension applied to a DC electrical field was developed by Maxwell [44]. This model was extended for an AC electrical field, resulting in the Maxwell-Wagner theory that is only applicable for volume fractions Φ lower than 10%. Assuming a homogeneous electrical field and a homogeneous spherical cell, the equivalent complex conductivity of the suspension can be determined with this model [42, 44]:

$$\sigma_{eq}^{*}-\sigma_{el}^{*} \Big/ \sigma_{eq}^{*}+2\sigma_{el}^{*} = \Phi \, \sigma_{p}^{*}-\sigma_{el}^{*} \Big/ \sigma_{p}^{*}+2\sigma_{el}^{*} \tag{3.20a}$$

or rewritten in an equivalent complex dielectric permittivity of the suspension ε_{eq}^{*} [45, 46]:

$$\varepsilon_{eq}^{*} = \varepsilon_{el}^{*} \, 1 + 2\Phi f_{CM}^{*} \Big/ 1 - \Phi f_{CM}^{*} \tag{3.20b}$$

$$f_{CM}^{*} = \varepsilon_{p}^{*} - \varepsilon_{el}^{*} \Big/ \varepsilon_{p}^{*} + 2\varepsilon_{el}^{*} \tag{3.20c}$$

with ε_{p}^{*} and ε_{el}^{*} the complex permittivity of the particle and electrolyte respectively and f_{CM}^{*} the Clausius-Mossoti factor (see figure 3-6 II and III). In case that the

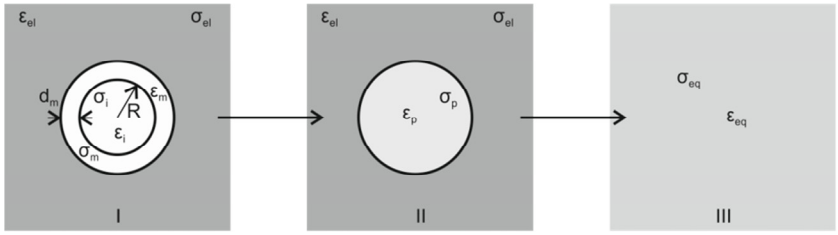

figure 3-6 A schematic representation of the Maxwell-Wagner theory in combination with the single-shell model. In the left image (I) the single-shell particle in medium is shown, representing the suspended cell. Using eqn. 3.21 the single-shell particle can be written as a homogeneous particle (see II). With the Maxwell-Wagner theory (eqn. 3.20) the equivalent dielectric properties can be determined as shown in the right image (III).

thickness of the cell membrane d_m is much smaller than the inner radius of the cell r, the ε_p^* of a cell can be determined with the single-shell cell model [45, 46]:

$$\varepsilon_p^* = {\gamma^3 + 2F}\Big/{\gamma^3 - F} \tag{3.21a}$$

$$\gamma = {r + d_m}\Big/{r} \tag{3.21b}$$

$$F = {\varepsilon_i^* - \varepsilon_m^*}\Big/{\varepsilon_i^* + 2\varepsilon_m^*} \tag{3.21c}$$

with ε_i^* and ε_m^* the complex permittivity of the cytoplasm of the cell and membrane respectively (see figure 3-6 I and II). One assumption in the Maxwell-Wagner Theory is that the particle is spherical. For non-spherical particles a shape factor γ_s is introduced, leading to [42, 47]:

$${\sigma_{eq}^* - \sigma_{el}^*}\Big/{\sigma_{eq}^* + \gamma_s\sigma_{el}^*} = \Phi\,{\sigma_p^* - \sigma_{el}^*}\Big/{\sigma_p^* + \gamma_s\sigma_{el}^*} \tag{3.22}.$$

Another assumption is that the theory is only valid for low volume fractions. Bruggeman [48] and Hanai [49] extended the theory for higher cell concentrations [42], resulting in the following expression:

$$(1 - \Phi) = \left({\varepsilon_{eq}^* - \varepsilon_p^*}\Big/{\varepsilon_{el}^* - \varepsilon_p^*}\right)\left({\varepsilon_{el}^*}\Big/{\varepsilon_{eq}^*}\right)^{1/3} \tag{3.23}.$$

In figure 3-6 the Maxwell-Wagner Theory in combination with the single-shell model are schematically shown. Taking in account the inhomogeneous electrical field, the electrical impedance of the suspension $Z_{eq,MWT}$ can be calculated with the following equation:

$$Z_{eq,MWT} = {K_{cell}}\Big/{j\omega\varepsilon_{eq}^*\varepsilon_0} \quad [\Omega] \tag{3.24}$$

with K_{cell} the cell constant of the electrode configuration [50].

3.3.3 Equivalent circuit model of a cell

The frequency behaviour of single cells in an electrical impedance measurement can also be modelled with an equivalent circuit model [14, 42, 51] and a simplified version is shown in figure 3-7. In this model the membrane resistance R_m and the capacitance of the cytoplasm C_i are ignored. The membrane capacitance $C_{m,0}$ and conductance $G_{m,0}$ can be calculated from the dielectric properties [42]:

$$C_{m,0} = {\varepsilon_m \varepsilon_0}/{d_m} \qquad [\text{F}\cdot\text{m}^{-2}] \qquad (3.25)$$

$$G_{m,0} = {\sigma_m}/{d_m} \qquad [\text{S}\cdot\text{m}^{-2}] \qquad (3.26).$$

Sun and co-workers rewrote the Maxwell-Wagner theory in combination with the single-shelled model as follow [45, 52]:

$$\varepsilon^*_{eq}\varepsilon_0 = \varepsilon_\infty + {\Delta\varepsilon_1}/{1 + j\omega\tau_1} + {\Delta\varepsilon_2}/{1 + j\omega\tau_2} + {\sigma_0}/{j\omega} [\text{F}\cdot\text{m}^{-1}] \qquad (3.27)$$

with ε_∞ the permittivity at infinite frequency, τ_1, τ_2 relaxation constants of the cell membrane and the polarization of the cytoplasm with the medium respectively, $\Delta\varepsilon_1$, $\Delta\varepsilon_2$ the magnitude of the dielectric dispersions with time constants τ_1 and τ_2 respectively and σ_0 the limiting low frequency conductivity. The time constants for the cell model are for low volume fractions [45]:

$$\tau_1 = rC_{m,0} \left(\frac{1}{\sigma_i} + \frac{1}{2\sigma_{el}}\right) \Big/ 1 + rG_{m,0}\left(\frac{1}{\sigma_i} + \frac{1}{2\sigma_{el}}\right) \qquad [\text{s}] \qquad (3.28)$$

$$\tau_2 = {\varepsilon_i\varepsilon_0 + 2\varepsilon_m\varepsilon_0}/{\sigma_i + 2\sigma_m} \qquad [\text{s}] \qquad (3.29)$$

with σ_i and σ_{el} the conductivity of the cytoplasm of the cell and the electrolyte respectively. The equivalent impedance of the simplified equivalent circuit model of the cell suspended in a medium $Z_{eq,ECM}$ as shown in figure 3-7 can be described as [50]:

$$Z_{eq,ECM} = {R_{el}(1 + j\omega R_i C_m)}/{Y} \qquad [\Omega] \qquad (3.30a)$$

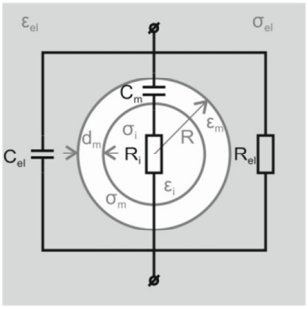

figure 3-7 Simplified equivalent circuit model of a cell.

$$Y = j\omega R_{el} C_m + (1 + j\omega R_{el} C_{el})(1 + j\omega R_i C_m) \tag{3.30b}$$

with R_i the resistance of the cytoplasm of the cell and C_m the capacitance of the cell membrane. In conclusion the following relations for the individual electrical components apply [42, 50, 52]:

$$C_m = {}^{9\Phi r C_{m,0}}\Big/_{4K_{cell}} \quad [\mathrm{F}] \tag{3.31}$$

$$R_i = {}^{4K_{cell}\left({}^{1}\Big/_{2\sigma_{el}} + {}^{1}\Big/_{\sigma_i}\right)}\Big/_{9\Phi} \quad [\Omega] \tag{3.32}$$

$$C_{el} = \left({}^{\varepsilon_{el}\varepsilon_0}\Big/_{K_{cell}}\right)\left(1 - 3\Phi\left({}^{\varepsilon_{el} - \varepsilon_i}\Big/_{2\varepsilon_{el} + \varepsilon_i}\right)\right) \quad [\mathrm{F}] \tag{3.33}$$

$$R_{el} = {}^{K_{cell}}\Big/_{\sigma_{el}\left(1 - {}^{3\Phi}\Big/_{2}\right)} \quad [\Omega] \tag{3.34}.$$

3.4 Applications

A variety of applications exist for microfluidic flow cytometry, among them for instance measuring the differentiation of cells, the induction of apoptosis or cell growth [43], but also blood analysis and the detection of infected cells. In this paragraph some of these applications will be discussed into more detail.

For some applications, not only the measured impedance change is used to obtain information about the cell characteristic, but also a variable that is related to impedance changes called opacity. Opacity is independent of cell size and position in the microchannel [17] and can be expressed as follows [11]:

$$opacity = {|Z_{high}|}/{|Z_{low}|} \tag{3.35}$$

with $|Z_{high}|$ and $|Z_{low}|$ the impedances at high and low frequency respectively.

3.4.1 Blood count

Blood analysis is widely used as a diagnostic test for a variety of diseases. An important example of blood analysis is the blood count, whereby the concentrations of erythrocytes and (types of) leukocytes are determined. Microfluidic impedance cytometers have been successfully used to count blood cells. For example a PDMS device with platinum black electrodes was used to detect erythrocytes in 1000-fold diluted whole blood and leukocytes in leukocytes rich plasma [53]. With the polyelectrolyte salt bridge electrode configuration it was possible to classify the size of erythrocytes and leukocytes based on the detected peak height [20] and perform a blood count using 800-fold diluted whole blood, which is a better result compared to existing clinical systems [22].

The leukocyte population of blood consists of different cell types: lymphocytes, monocytes and granulocytes. In a 3-part differential count the percentages of these three cell types are determined. With a chemically pre-treated whole blood sample, thereby lysing the erythrocytes and changing the membrane properties of monocytes, the 3-part differential count could be performed on-chip by measuring the electrical impedance at two frequencies (503 kHz and 1.7 MHz) (see figure 3-8). The result of this differential count was in good agreement with measurements performed at the hospital [54]. In this example preparation of the blood sample outside the chip was still needed. To overcome this disadvantage, a microfluidic system has been developed that contains a sample preparation and a detection part. This microfluidic system provides not only the results of a 3-part differential count, but it is extended with platelets and erythrocytes counts [55].

The count of T-lymphocytes expressing CD4 is used as marker for HIV infection; if this value is below a certain threshold treatment is recommended. By introducing a sample containing CD4+ lymphoblasts in a microfluidic chip with integrated planar electrodes, the concentrations of the live and dead lymphoblasts could be determined using electrical impedance measurements, which closely match the results obtained

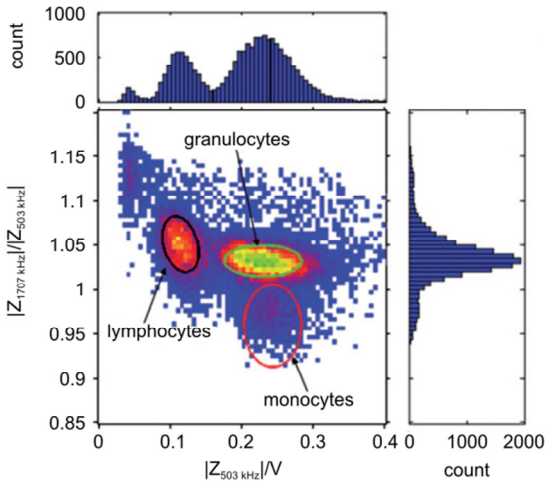

figure 3-8 The result of a 3-part differential leukocyte count using a microfluidic impedance cytometer. The ellipses show the leukocyte subpopulations, from which the relative populations were calculated (adapted from [54]).

with a conventional flow cytometer [27]. However, a cell line of precursor lymphocytes was used in these experiments and not a real leukocyte sample containing more cell types. A different design of a microfluidic chip containing two electrical impedance detection regions with planar electrodes and a capture chamber in between has been used to measure the amount of CD4+ T-lymphocytes in a leukocyte population. CD4+ T-lymphocytes bind to antibodies in the capture chamber and by using a differential counting technique, the CD4+ T-lymphocytes count could be determined [56]. Another method to determine the percentage and number of T-lymphocytes expressing CD4 in a leukocyte population with a microflow impedance cytometer uses so called 'impedance labelling', whereby the CD4 expressing cells are labelled with polystyrene beads. The attachment of polystyrene beads to the cells changes the impedance measured at two frequencies (500 kHz and 10 MHz), allowing discrimination between CD4 expressing T-lymphocytes and other lymphocytes, monocytes and granulocytes [57].

3.4.2 Infection of cells

Infection of cells changes the characteristics of the cell, which can also be measured with electrical impedance measurements in a microfluidic chip. Parasitized

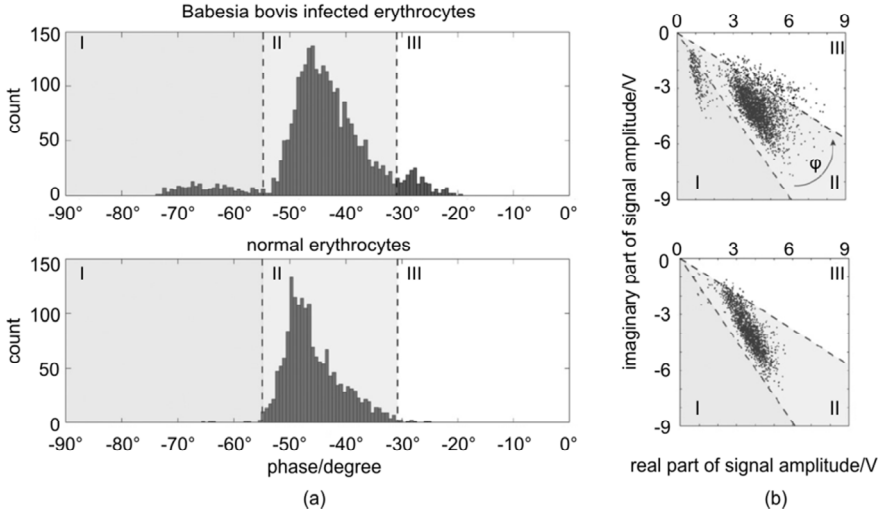

figure 3-9 Differences between infected and uninfected erythrocytes. (a) Histograms of the cell counts for infected (above) and normal (below) erythrocytes. (b) Scatter diagram of the real and imaginary part of the measured signal at 8.7 MHz. The population of erythrocytes are divided in ghost cells (I), normal cells (II) and infected cells (III). Note the change in phase for infected cells (adapted from [58]).

erythrocytes with Babesia bovis could be discriminated from healthy erythrocytes, by measuring the real and imaginary components of the impedance signal at 8.7 MHz using a microfluidic chip with a liquid electrode configuration (see figure 3-9) [14, 58].

Not only infection changes the cell properties, but also fixation processes. Normal and fixed erythrocytes could be distinguished from each other based on their respective opacity [31]. Additionally impedance differences between normal and ghost erythrocytes can be noticed [13, 31, 58]. Ghost erythrocytes have similar membrane properties as normal erythrocytes, only the cytoplasmic properties are different [31].

3.4.3 Cell division

Monitoring cell division is another application for microfluidic impedance cytometry. In a population yeast cells, the subpopulation of dividing yeast showed a different impedance response at 8 MHz compared to cells that do not divide at that moment [43]. One of the things that changes during cell division is the amount of DNA in the cell. By looking at the capacitance changes at 1 kHz, Sohn and co-workers were able to

determine the DNA content of single cells flowing through a microchannel. Not only cells in different phases of division could be distinguished, but also the DNA content between cells of different species (yeast, mouse, rat and human) [59].

3.4.4 Combination with other techniques

One of the advantages of using microfluidics is the possibility to easily integrate multiple functionalities in a single microfluidic system. Two examples where another technique is integrated in a microflow impedance cytometer are DEP elevation in the microchannel and the use of fluorescence detection.

The impedance detection of single cells is often measured at frequencies below 10^7 Hz. However, Ferrier and co-workers showed that the passage of a single yeast cell over an interdigitated electrode pair could be measured at 1.6 GHz by detecting change in capacitance. Additionally the change in elevation caused by DEP could be measured simultaneously with this microfluidic chip [60].

Fluorescence detection can be integrated in the microflow impedance cytometer. For instance the measured electrical impedance signal in a microchannel is used as trigger for the capture of the fluorescence signal from single fluorescent beads flowing in the microchannel [61]. Another example is the integration of a fluorescence detection component to the polyelectrolyte salt bridge electrode configuration. This leads to a portable microfluidic cytometer, making both electrical as well as optical detection of fluorescent and non-fluorescent cells possible [62].

3.5 Conclusion

The measurement of the properties of a single cell in a label-free, non-invasive way can be established by using microfluidic impedance cytometry. With this technique, information about the cell size, membrane properties and the cell contents can be obtained. This provides the possibility to distinguish between different cell types and even between the same cells with different properties due to for instance infection. The frequency behaviour of a microfluidic impedance cytometer is not only determined by single cells suspended in background electrolyte, but also depends on the design of the microfluidic chip. Due to the small electrodes, the electrical double layer at the electrode-liquid interface has a distinct influence on the impedance at low frequencies. At high frequencies, the parasitic capacitance caused by the capacitive coupling of the electrodes mainly influences the signal. For the detection of cells, the measurements should be preferably performed at intermediate frequencies. Models can be used to determine the influences of the microfluidic chip design and cell

properties on the frequency behaviour. Recently, microfluidic impedance cytometers have been developed for the detection and characterization of (different types of) cells suspended in fluid. Since these microfluidic devices tend to be fast, accurate and only need small sample and reagent volumes, it is a promising technique to be used in the future as alternative for the diagnostic tests of today.

3.6 References

1. Cheung, K.C., et al., *Microfluidic impedance-based flow cytometry.* Cytometry Part A, 2010. **77A**(7): p. 648-666.
2. Morgan, H., D. Holmes, and N.G. Green, *High speed simultaneous single particle impedance and fluorescence analysis on a chip.* Current Applied Physics, 2006. **6**(3): p. 367-370.
3. Zhang, H., et al., *Methods for counting particles in microfluidic applications* Microfluidics and Nanofluidics, 2009. **7**: p. 739-749.
4. Coulter, W.H., *High speed automatic blood cell counter and cell size analyzer.* Proceedings of the National Electronic Conference 1956. **12**: p. 1034-1040.
5. Sun, T. and H. Morgan, *Single-cell microfluidic impedance cytometry: a review* Microfluidics and Nanofluidics, 2010. **8**(4): p. 423-443.
6. Deblois, R.W. and C.P. Bean, *Counting and sizing of submicron particles by resistive pulse technique.* Review of Scientific Instruments, 1970. **41**(7): p. 909-&.
7. Fraikin, J.L., et al., *A high-throughput label-free nanoparticle analyser.* Nature Nanotechnology, 2011. **6**(5): p. 308-313.
8. Zhe, J., et al., *A micromachined high throughput Coulter counter for bioparticle detection and counting.* Journal of Micromechanics and Microengineering, 2007. **17**(2): p. 304-313.
9. Wu, X.D., et al., *Simultaneous particle counting and detecting on a chip.* Lab on a Chip, 2008. **8**(11): p. 1943-1949.
10. Hoffman, R.A. and W.B. Britt, *Flow-system measurement of cell impedance properties.* Journal of Histochemistry & Cytochemistry, 1979. **27**(1): p. 234-240.
11. Hoffman, R.A., T.S. Johnson, and W.B. Britt, *Flow cytometric electronic direct-current volume and radiofrequency impedance measurements of single cells and particles.* Cytometry, 1981. **1**(6): p. 377-384.
12. Ayliffe, H.E., A.B. Frazie, and R.D. Rabbitt, *Electrical impedance spectroscopy using microchannels with integrated metal electrodes.* IEEE Journal of Microelectromechanical Systems, 1999. **8**(1): p. 50-57.
13. Gawad, S., L. Schild, and P. Renaud, *Micromachined impedance spectroscopy flow cytometer for cell analysis and particle sizing.* Lab on a Chip, 2001. **1**: p. 76-82.

14. Valero, A., T. Braschler, and P. Renaud, *A unified approach to dielectric single cell analysis: impedance and dielectrophoretic force spectroscopy.* Lab on a Chip, 2010. **10**(17): p. 2216-2225.
15. Sun, T., et al., *Analytical electric field and sensitivity analysis for two microfluidic impedance cytometer designs.* IET Nanobiotechnology, 2007. **1**(5): p. 69-79.
16. Wood, D.K., et al., *High-bandwidth radio frequency Coulter counter.* Applied Physics Letters, 2005. **87**(18): p. 184106-3.
17. Gawad, S., et al., *Dielectric spectroscopy in a micromachined flow cytometer: theoretical and practical considerations.* Lab on a Chip, 2004. **4**: p. 241-251.
18. Spencer, D. and H. Morgan, *Positional dependence of particles in microfluidic impedance cytometry.* Lab on a Chip, 2011. **11**: p. 1234-1239.
19. Wood, D.K., M.V. Requa, and A.N. Cleland, *Microfabricated high-throughput electronic particle detector.* Review of Scientific Instruments, 2007. **78**(10): p. 104301.
20. Chun, T.D. Chung, and H.C. Kim, *Cytometry and velocimetry on a microfluidic chip using polyelectrolytic salt bridges.* Analytical Chemistry, 2005. **77**(8): p. 2490-2495.
21. Segerink, L.I., et al., *A new floating electrode structure for generating homogeneous electrical fields in microfluidic channels.* Lab on a Chip, 2011. **11**(12): p. 1995-2001.
22. Kim, K.B., et al., *Red blood cell quantification microfluidic chip using polyelectrolytic gel electrodes.* Electrophoresis, 2009. **30**(9): p. 1464-1469.
23. Rodriguez-Trujillo, R., et al., *High-speed particle detection in a micro-Coulter counter with two-dimensional adjustable aperture.* Biosensors & Bioelectronics, 2008. **24**(2): p. 290-296.
24. Bernabini, C., D. Holmes, and H. Morgan, *Micro-impedance cytometry for detection and analysis of micron-sized particles and bacteria.* Lab on a Chip, 2010.
25. Rodriguez-Trujillo, R., et al., *Low cost micro-Coulter counter with hydrodynamic focusing.* Microfluidics and Nanofluidics, 2007. **3**(2): p. 171-176.
26. Nieuwenhuis, J.H., et al., *Integrated Coulter counter based on 2-dimensional liquid aperture control.* Sensors and Actuators B-Chemical, 2004. **102**(1): p. 44-50.
27. Watkins, N., et al., *A robust electrical microcytometer with 3-dimensional hydrofocusing.* Lab on a Chip, 2009. **9**(22): p. 3177-3184.
28. Fiedler, S., et al., *Dielectrophoretic sorting of particles and cells in a microsystem.* Analytical Chemistry, 1998. **70**(9): p. 1909-1915.
29. Müller, T., et al., *A 3-D microelectrode system for handling and caging single cells and particles.* Biosensors and Bioelectronics, 1999. **14**(3): p. 247-256.
30. Holmes, D., H. Morgan, and N.G. Green, *High throughput particle analysis: combining dielectrophoretic particle focussing with confocal optical detection.* Biosensors and Bioelectronics, 2006. **21**(8): p. 1621-1630.

31. Cheung, K., S. Gawad, and P. Renaud, *Impedance spectroscopy flow cytometry: on-chip label-free cell differentiation.* Cytometry part A, 2005. **65A**: p. 124-132.
32. Flores-Rodriguez, N. and G.H. Markx, *Flow-through devices for the ac electrokinetic construction of microstructured materials* Journal of Micromechanics and Microengineering, 2006. **16**.
33. Lin, C.H., et al., *Vertical focusing device utilizing dielectrophoretic force and its application on microflow cytometer.* Journal of Microelectromechanical Systems, 2004. **13**(6): p. 923-932.
34. Segerink, L.I., et al., *On-chip determination of spermatozoa concentration using electrical impedance measurements.* Lab on a Chip, 2010. **10**: p. 1018-1024.
35. Langereis, G.R., *An integrated sensor system for monitoring washing processes*, PhD thesis, 1999, University of Twente
36. Hong, J., et al., *AC frequency characteristics of coplanar impedance sensors as design parameters.* Lab on a Chip, 2005. **5**(3): p. 270-279.
37. Bard, A.J. and L.R. Faulkner, *Electrochemical methods: fundamentals and applications*. 2nd ed. 2001, New York: John Wiley & Sons, Inc.
38. Jacobs, P., A. Varlan, and W. Sansen, *Design optimisation of planar electrolytic conductivity sensors.* Medical and Biological Engineering and Computing, 1995. **33**: p. 802-810.
39. Zoltowski, P., *On the electrical capacitance of interfaces exhibiting constant phase element behaviour.* Journal of Electroanalytical Chemistry, 1998. **443**(1): p. 149-154.
40. Olthuis, W., W. Streekstra, and P. Bergveld, *Theoretical and experimental determination of cell constants of planar-interdigitated electrolyte conductivity sensors.* Sensors and Actuators B, 1995. **24-25**: p. 252-256.
41. Linderholm, P. and P. Renaud, *Comment on "AC frequency characteristics of coplanar impedance sensors as design parameters" by Jongin Hong, Dae Sung Yoon, Sung Kwan Kim, Tae Song KOm, Sanghyo Kim, Eugene Y. Pak and Kwangsoo No, Lab Chip, 2005, 5, 270.* Lab on a Chip, 2005. **5**: p. 1416-1417.
42. Foster, K.R. and H.P. Schwann, *Dielectric properties of tissues and biological materials: a critical review.* Critical Reviews in Biomedical Engineering, 1989. **17**(1): p. 25-104.
43. Schade-Kampmann, G., et al., *On-chip non-invasive and label-free cell discrimination by impedance spectroscopy.* Cell Proliferation, 2008. **41**(5): p. 830-840.
44. Maxwell, J., *A treatise on electricity and magnetism*. Vol. 1. 1873, Oxford: Clarendon Press.
45. Sun, T., et al., *Dielectric spectroscopy of single cells: time domain analysis using Maxwell's mixture equation.* Journal of Physics D: Applied Physics, 2007. **40**: p. 1-8.
46. Asami, K., *Characterization of biological cells by dielectric spectroscopy.* Journal of Non-Crystalline Solids 2002. **305**: p. 268-277.

47. Fricke, H., *A mathematical treatment of the electric conductivity and capacity of disperxe systems. I. The electric conductivity of a suspension of homogeneous spheroids.* Phycials Review, 1924. **24**: p. 575-587.
48. Bruggeman, D.A.G., *Berechnung verschiedener physikalischer Konstanten von heterogenen Substanzen. I. Dielektrizitätskonstanten und Leitfähigkeiten der Mischkörper aus isotropen Substanzen.* Annalen der Physik, 1935. **24**: p. 636-664.
49. Hanai, T., *Electrical properties of emulsions*, in *Emulsion science*, P. Sherman, Editor. 1968, Academic press: London and New York.
50. Morgan, H., et al., *Single cell dielectric spectroscopy.* Journal of Physics D: Applied Physics, 2007. **40**: p. 61-70.
51. Gimsa, J. and D. Wachner, *A unified resistor-capacitor model for impedance, dielectrophoresis, electrorotation, and induced transmembrane potential.* Biophysical Journal, 1998. **75**(2): p. 1107-1116.
52. Sun, T., C. Bernabini, and H. Morgan, *Single-colloidal particle impedance spectroscopy: Complete equivalent circuit analysis of polyelectrolyte microcapsules.* Langmuir, 2010. **26**(6): p. 3821-3828.
53. Zheng, S., M. Liu, and Y.-C. Tai, *Micro coulter counters with platinum black electroplated electrodes for human blood cell sensing.* Biomedical Microdevices, 2008. **10**: p. 221-231.
54. Holmes, D., et al., *Leukocyte analysis and differentiation using high speed microfluidic single cell impedance cytometry.* Lab on a Chip, 2009. **9**: p. 2881-2889.
55. Berkel van, C., et al., *Integrated systems for rapid point of care (PoC) blood cell analysis* Lab on a Chip, 2011. **11**(7): p. 1249-1255
56. Watkins, N.N., et al., *A microfabricated electrical differential counter for the selective enumeration of CD4+T lymphocytes.* Lab on a Chip, 2011. **11**(8): p. 1437-1447.
57. Holmes, D. and H. Morgan, *Single cell impedance cytometry for identification and counting of CD4 T-Cells in human blood using impedance labels.* Analytical Chemistry, 2010. **82**(4): p. 1455-1461.
58. Kuttel, C., et al., *Label-free detection of Babesia bovis infected red blood cells using impedance spectroscopy on a microfabricated flow cytometer.* Acta Tropica, 2007. **102**(1): p. 63-68.
59. Sohn, L.L., et al., *Capacitance cytometry: Measuring biological cells one by one.* Proceedings of the National Academy of Sciences of the United States of America, 2000. **97**(20): p. 10687-10690.
60. Ferrier, G.A., et al., *A microwave interferometric system for simultaneous actuation and detection of single biological cells.* Lab on a Chip, 2009. **9**(23): p. 3406-3412.
61. Holmes, D., et al., *Bead-based immunoassays using a micro-chip flow cytometer.* Lab on a Chip, 2007. **7**: p. 1048-1056.
62. Joo, S., et al., *A portable microfluidic flow cytometer based on simultaneous detection of impedance and fluorescence.* Biosensors and Bioelectronics, 2010. **25**(6): p. 1509-1515.

chapter 4

On-chip concentration determination*

For the determination of the concentration of spermatozoa in semen, a microfluidic glass-glass chip is used, consisting of a microchannel with a planar electrode pair that allows the detection of spermatozoa using electrical impedance measurements. The change in electrical impedance is related to the size of cells passing the electrodes allowing to distinguish between spermatozoa, HL-60 cells and polystyrene beads suspended in washing medium. By adding a known concentration of polystyrene beads to a boar semen sample, the spermatozoa concentrations of seven mixtures have been measured and show a good correlation with the actual concentration (R^2-value = 0.97).

* Modified from: L.I. Segerink, A.J. Sprenkels, P.M. ter Braak, I. Vermes and A. van den Berg. *On-chip determination of spermatozoa concentration using electrical impedance measurements.* Lab on a Chip, 2010. **10**: p. 1018-1024.

4.1 Introduction

A first step in the treatment of a couple with an unfulfilled desire to have children is the assessment of the semen quality. One of the parameters assessed with a semen analysis is the spermatozoa concentration, whereby the generally accepted lower limit for fertile men is $20 \cdot 10^6$ mL^{-1} [1]. Recently, the reference values have been changed by the WHO and this value is now $15 \cdot 10^6$ mL^{-1} [2]. Visual counting the spermatozoa in the semen by putting the semen into a counting chamber is the gold standard for this determination. This labour intensive method is in larger hospitals replaced by a CASA system. The results of the manual tests are often subjective and can hardly be compared between different laboratories [3], while the CASA system is expensive and needs comprehensive quality control. In addition, only reliable results are obtained after analysis of at least three consecutive samples [4]. To overcome the above mentioned problems of the current procedure, we present here a microfluidic chip that can be used by the man himself at convenient moments at home.

In general, glass-based microfluidic chips are very well suited to analyse cells [5, 6] and for disposable diagnostic systems for medical purposes [7]. In this chapter we will focus on the detection of spermatozoa and the determination of spermatozoa concentration on-chip using electrical impedance measurements. In order to determine the concentration of cells in suspensions electrical impedance measurements on-chip have already been reported [8, 9], however for a reliable result the volume fraction of the cells in the suspension needs to be high [10]. Since the volume fraction of spermatozoa is low (0.1% for $20 \cdot 10^6$ mL^{-1}), the cells need to be analysed in a small measurement volume, also known as single cell analysis. One of the earliest reported single cell impedance measurements were performed by Coulter about 50 years ago [11]. Later, Brotherton and Barnard used a so-called Coulter counter to estimate the human spermatozoa concentration, but it was only applicable for concentrations above $5 \cdot 10^6$ mL^{-1}[12].

The need for analysing smaller sample volumes and cost reduction resulted in the development of a microfabricated version of the Coulter counter. Previous studies showed that with two electrode pairs in a microchannel it is possible to discriminate among bead sizes, different cells and various phytoplankton, if the differential impedance variation between the two pairs was measured at two frequencies [13-16]. Systems with top-bottom electrodes, measuring at only a single frequency, were also able to distinguish between bead sizes, even at a higher throughput [17]. However, in none of these approaches concentrations larger than $2 \cdot 10^6$ mL^{-1} were used [13, 15, 17] and none of the reported systems was able to determine the concentration of the specimens in the carrying fluid.

In some of the approaches micro-Coulter counters were used in combination with fluorescent detection [15, 16]. This miniaturized flow cytometer requires fluorescence labelling of the sample and thus additional pre-processing steps. With a classical flow cytometer, several semen parameters can be determined among which the spermatozoa concentration [18, 19]. By measuring the ratio of spermatozoa to added fluorospheres of a known concentration, the spermatozoa concentration can be calculated. In this chapter we describe a comparable method to determine the concentration of spermatozoa by using electrical impedance measurements. For a reliable result a significant difference in electrical impedance signal for the added beads and spermatozoa is required, but also for spermatozoa and other cells, like leukocytes, present in semen. Without differentiation between leukocytes and spermatozoa, it gives rise to an overestimated concentration of spermatozoa, since it interferes with the count of spermatozoa. Furthermore, a high leukocyte concentration ($> 1 \cdot 10^6$ mL^{-1}) is an indication of infection and poor sperm quality [1] and it is useful to obtain this additional information as well.

In this chapter a microfluidic chip is described which is used for the calculation of the concentration of spermatozoa using electrical impedance measurements without knowing the actual flow speed. The electrical impedance is measured between two planar electrodes at a single frequency, enabling differentiation between polystyrene beads, spermatozoa and leukaemia white blood cells (HL-60). First a theoretical description of the measurement cell is given, followed by a description of the chip design, the measurement setup and the various samples that have been used. Next the measurement results are described and discussed into detail. Finally some conclusions are given.

4.2 Theory

In figure 4-1(a) a simplified equivalent circuit model for the microfluidic device is given, consisting of two double layer capacitances (C_{DL}), an electrolyte resistance (R_{el}), a parasitic capacitance (C_{par}) and the total lead resistance (R_{lead}). A typical bode plot of the equivalent circuit model is shown in figure 4-1(b). The interface phenomena at the electrodes can be simplified with a double layer capacitance, that influences the spectrum signal mainly at low frequencies [14, 16] as can be seen in the bode plot. For intermediate frequencies, a plateau is observed in the bode plot predominantly caused by the electrolyte resistance [14] and for a smaller part by the lead resistance. The drop at high frequencies arises from the parasitic capacitance of the system, mainly caused by direct coupling between the two electrodes [20].

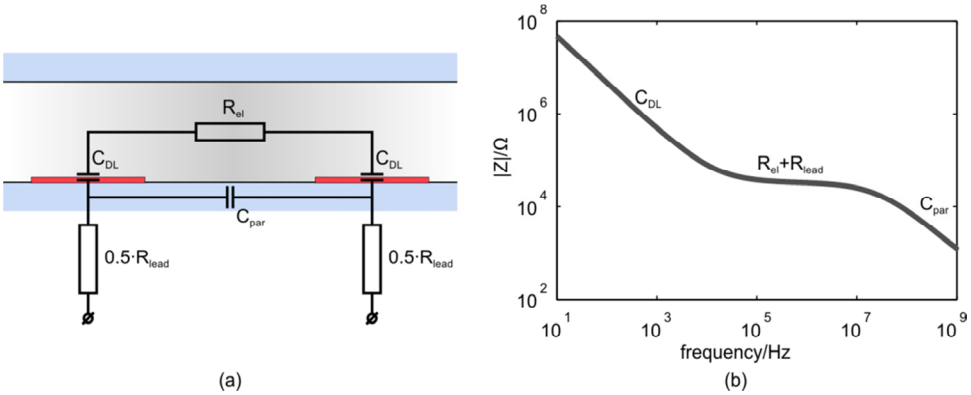

figure 4-1 (a) The simplified equivalent circuit model of the microfluidic device without a particle or cell in the channel. The interface between the two planar electrodes and the electrolyte is represented by the double layer capacitance (C_{DL}). R_{el} is the electrolyte resistance, R_{lead} the lead resistance and C_{par} is the parasitic capacitance. (b) Typical frequency response of the real electrical impedance of the equivalent circuit model.

When a cell or particle enters the volume between the two electrodes, parts of the equivalent circuit model change. Such a particle or cell can also be represented with an equivalent circuit model consisting of linear elements, containing capacitances representing the cell membrane and a resistance corresponding to the cytoplasmatic conductivity [16, 21]. At frequencies below 1 - 3 MHz [10, 13], cells and particles can be represented solely by the membrane capacitance such that they behave like isolating spheres, resulting in a change in the effective electrolyte resistance as a particle or cell enters the measurement volume. This change is dependent on the cell size [13, 22]. Besides spermatozoa, semen contains also other cells, like leukocytes and macrophages [23]. These cells are larger than spermatozoa; consequently a larger change in the electrical impedance may be measured at the resistive plateau making differentiation in cell size possible.

If the differentiation between beads and spermatozoa is possible, it can be used to calculate the concentration of spermatozoa (c_s) by adding a known concentration of beads (c_b) to the sample. Therefore the values of the measured electrical impedance changes need to be classified as 'bead' and 'spermatozoon'. By counting the number of spermatozoa and beads in a sample, the concentration of spermatozoa can be calculated with the following expression:

$$c_s = {}^{N_s}/_{N_b} \cdot c_b \qquad [\mathrm{mL^{-1}}] \qquad (4\text{-}1)$$

with N_s and N_b are the number of counted spermatozoa and beads respectively.

4.3 Method

4.3.1. Chip design and fabrication

A schematic diagram of the measurement setup is shown in figure 4-2. The glass-glass chip consists of a microchannel that tapers to a channel width of 38 µm at the electrode area. The change in electrical impedance caused by a cell or particle passing the electrodes is related to the volume at the electrode area. For this reason the depth of the channel is 18 µm, such that the volume is as small as possible without the risk of clogging of cells or particles. At the electrode area, two 200 nm thick and 20 µm wide platinum electrodes cross the channel with an interelectrode distance of 30 µm. Since the chip has planar electrodes, the fabrication process is rather easy. The microfluidic chips were made of two 500 µm thick 100 mm Borofloat glass substrates and the fabrication process is schematically shown in figure 4-3. In glass layer 1, the microchannel was isotropically etched with HF using a chromium/gold (Cr/Au) mask and access holes were powder blasted from the backside. In glass layer 2 the

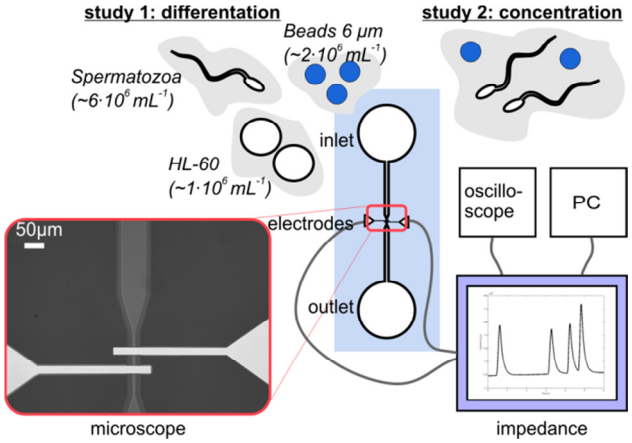

figure 4-2 A schematic picture of the measurement setup. The microfluidic chip is connected to the home-made impedance analyser, which is connected to a PC and an oscilloscope. Visual inspection of the setup is possible using an inverted microscope. Different samples are used for the two studies.

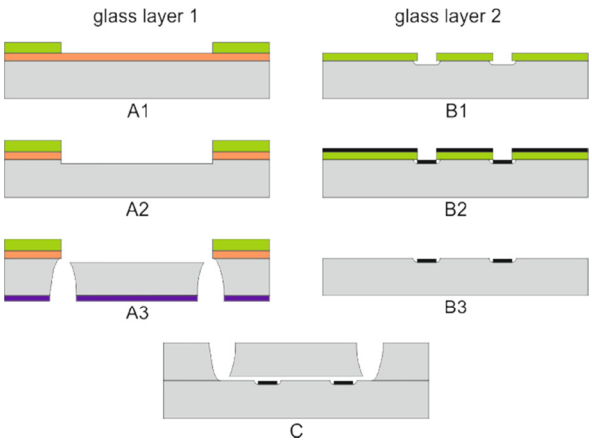

figure 4-3 Schematic diagram of the fabrication process. Glass layer 1 is firstly sputtered with Cr and Au, which is subsequently coated with a resist. After several photolithography steps (A1), the microchannel is formed by isotropically etching (A2). Access holes are powder blasted (A3). On glass layer 2 first a photolithography step is done defining the electrodes (B1). Subsequently Pt is sputtered (B2) and the electrodes are created by lift-off (B3). Bonding of the two glass wafers (C) finalizes the chip.

(embedded) electrodes were formed by lift-off technique. First a 200 nm recess was etched with BHF using a photoresist mask. Then a 15 nm thick tantalum (Ta) adhesion layer and 180 nm thick platinum (Pt) layer was sputtered. At last the photoresist was stripped in aceton in an ultrasonic bath, leaving the electrodes behind. Finally the two glass wafers were bonded together using fusion bonding and annealed at 625 °C before dicing them into separate chips.

To determine the frequency behaviour of the microfluidic chip filled with background electrolyte, a bode plot from 100 Hz to 40 MHz was made using a HP impedance/gainphase analyser type HP4194A, controlled by LabVIEW (7 Express, version 7.0, 2003, National Instruments). With this result, the optimal measurement frequency within the resistive plateau for the successive experiments was determined.

4.3.2 Measurement setup

All chips were measured in a chipholder that provides reliable electrical and fluidic connections to the chip. The samples were introduced by pipetting the sample in the

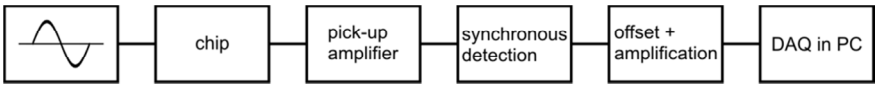

figure 4-4 A simplified electrical block diagram of the home-made impedance measurement system.

inlet and outlet. By adjusting the heights of the fluid columns in both the inlet and outlet, a fluid flow was generated and controlled in the microchannel. The chip with chipholder was mounted on an inverted microscope (Leica DM IRM, Leica Microsystems GmbH, Wetzlar, Germany) equipped with a computer controlled CCD camera, to make video images simultaneously with the electrical impedance measurements possible.

The electrical impedance signal was measured at 96 kHz with a home-made measurement system, with a sampling rate of 400 Hz and a detection limit (ΔR/R) below 0.005%. A simplified block diagram is given in figure 4-4. A sine wave signal of 96 kHz was created for the excitation of the sensor. A pick-up amplifier in the transimpedance mode converted the sensor current to a voltage, which was successively fed to a synchronous detector, a low-pass filter and an amplifier with an offset facility to suppress any possible DC bias and amplify the signal to increase the overall sensitivity. The final signal was fed to a PC for data capture and analysis using Matlab (R2007B, version 7.5.0.342, 2007, the Mathworks Inc). All detector electronics were contained in a small metal box in order to suppress noise. In the Matlab program all signals were converted to electrical impedance values, next the peaks in the signal were detected and finally their heights were calculated. The peak height is calculated as the maximum value minus the mean of the start and end point values of the peak (see figure 4-5(b)), such that any minor drift of the signal does not influence the analysis.

4.3.3 Samples

As background electrolyte Ferticult™ Flushing medium chemically balanced salt solution, HEPES buffered with 0.4% HSA, purchased from Fertipro NV (Beernem, Belgium) with a specific electrical conductivity of 1.4 $S \cdot m^{-1}$ was used. This medium is generally used in hospitals to keep the spermatozoa after the necessary pre-processing steps. Polybead Polystyrene Blue Dyed beads with a diameter of 6 μm were used, obtained from Polysciences Inc (Warrington, Pennsylvania, USA). Human

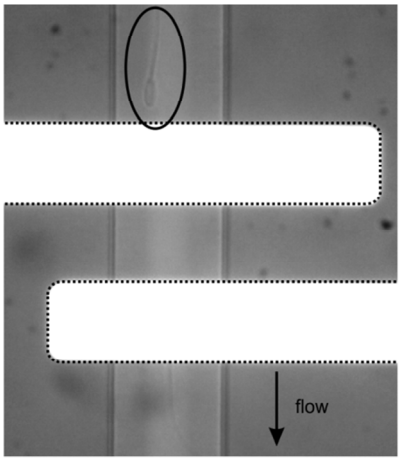

(a)

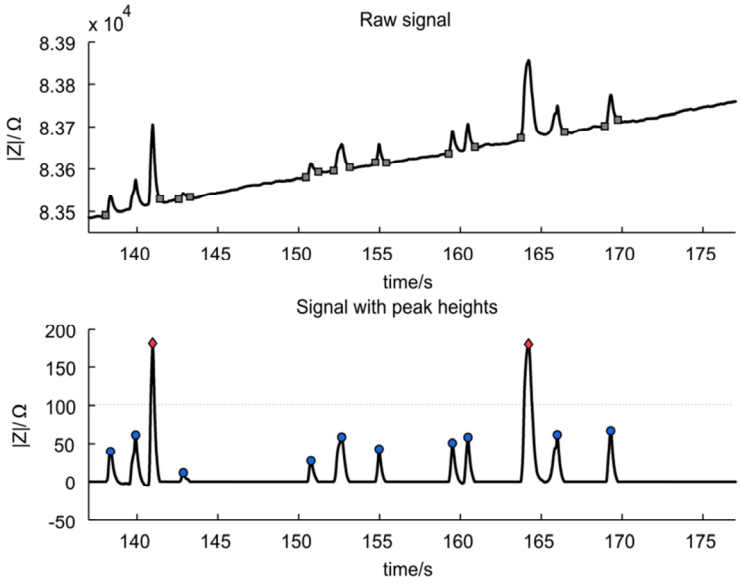

(b)

figure 4-5 (a) A microscopic image of a spermatozoon passing the electrode pair (white horizontal stripes). (b) The above image shows an example of a raw impedance signal of the measurement with a spermatozoa concentration of $3.8 \cdot 10^6$ mL^{-1}. The squares indicate the start and end of each peak and are used to calculate the peak heights. The image below shows the processed signal with the peak heights. For this measurement a threshold of 100 Ω was chosen such that two peaks are classified as 'beads' (red rhombus) and ten as 'spermatozoon' (blue circle).

promyelocytic leukaemia HL-60 cells of 10 - 15 µm were obtained from the German Collection of Microorganisms (Braunschweig, Germany) and were used as a substitute for the other cells present in semen. Equipment for tissue culture was obtained from Greiner Bio-One (Alphen a/d Rijn, the Netherlands). RPMI-1640 medium supplemented with 10% heat-inactivated Foetal Bovine Serum, 100 $IU \cdot mL^{-1}$ penicillin, 100 $\mu g \cdot mL^{-1}$ streptomycin, 2 mM L-glutamine and 0.4 $\mu g \cdot mL^{-1}$ fungizone was used for cell culture and both medium, supplements as antibiotics were purchased from Lonza Group Ltd (Basel, Switzerland). Cell cultures were sustained in a 5% CO_2 humidified atmosphere at 37 °C. Every 3 - 4 days the medium was refreshed and only exponentially growing cells were used for the experiments. From a local insemination centre of pigs, boar spermatozoa kept in Beltsville Thawning Solution (BTS) were obtained. This boar semen had some advantages with respect to human semen, since it can be stored for several days and it has a guaranteed good quality. Before the experiments, the semen was centrifuged at 600 g for 15 min. The supernatant was removed and the background electrolyte was added, replacing the BTS. Typically the head of a boar spermatozoon has a length and width of 8 and 4 µm respectively [24]. The head of a human spermatozoon is slightly smaller; about 5 – 6 µm and 2.5 - 3.5 µm in length and width respectively [25]. The volume of boar spermatozoa and human spermatozoa are between 20 - 29 μm^3 and 15 - 25 μm^3 respectively which is in correspondence with the difference in dimensions [26]. By comparison, the volume of polystyrene beads and HL-60 cells are 63 - 156 μm^3 and 524 - 1767 μm^3 respectively.

4.3.4 Study 1: differentiation

In the first experiment HL-60 cells, diluted in washing medium with a concentration of about $1 \cdot 10^6$ mL^{-1} were guided along the two electrodes and the electrical impedance change was measured. Subsequently the same experiment was done with boar spermatozoa (concentration of $6 \cdot 10^6$ mL^{-1}) and finally with 6 µm polystyrene beads (concentration of $2 \cdot 10^6$ mL^{-1}).

4.3.5 Study 2: concentration determination

In the second study seven mixtures of polystyrene beads and spermatozoa diluted in washing medium were made. The goal was to have a polystyrene bead concentration in every mixture of about $1 \cdot 10^6$ mL^{-1} and a spermatozoa concentration varying from $2 \cdot 10^6$ - $60 \cdot 10^6$ mL^{-1}. Before the concentration of spermatozoa with help of the bead concentration could be determined, the actual concentrations needed to be known. Therefore 20 µL of both solutions was put into a Bürker counting chamber. However, since spermatozoa are motile, it was difficult to count cells immediately using a

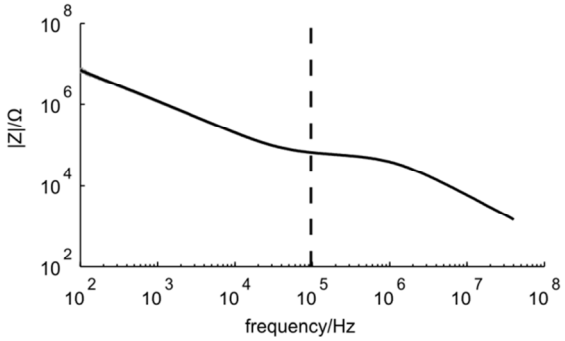

figure 4-6 The measured frequency behaviour of the microfluidic chip. The black line in the graph is the average of 50 measurements obtained with the impedance/gainphase analyser. The dashed line indicates the measurement frequency used during all subsequent experiments.

microscope. Therefore four images of different areas of the counting chamber were made and from these images both concentrations were calculated.

4.4 Results and discussion

The frequency behaviour of the microfluidic chip was investigated to ensure that the electrical impedance measurements were done at a frequency within the resistive plateau and below 1 MHz, since cells and beads behave like insulating particles [10, 13]. The averaged results of 50 impedance measurements of a chip filled with the background electrolyte for frequencies from 100 Hz to 40 MHz is shown in figure 4-6. Clearly, the influences of the double layer capacitance, electrolyte resistance and parasitic capacitance can be seen. Furthermore the measurement frequency of 96 kHz is in the resistive plateau and thus a good choice for detecting particles or cells passing the electrodes.

4.4.1 Study 1: differentiation

A cell or bead passing the electrodes causes a change in the electrical impedance signal as observed from the results of the synchronization of the video images with the measurement data. As expected this change is an increase in the measured impedance, since the cells and beads behave like insulating particles at the applied measurement frequency [10, 13]. In figure 4-5(a) a microscopic image of a spermatozoon passing the electrode pair is given. Three typical examples of the

processed impedance signals (the drift is removed) when a HL-60 cell, a spermatozoon or a bead passes the electrodes are shown in figure 4-7. The peak heights of 52 HL-60 cells, 33 spermatozoa and 47 polystyrene beads have been determined. The average electrical impedance change and standard deviation have been calculated as 1730 ± 620 Ω, 240 ± 60 Ω and 27 ± 13 Ω for HL-60 cells, polystyrene beads and spermatozoa respectively, resulting in the 95% confidence intervals shown in figure 4-8. The measured impedance changes are in correspondence with calculated changes for insulating particles with comparable dimensions as HL-60 cells, spermatozoa and 6 µm polystyrene beads in a measurement volume of 16.1 pL. Despite the wide distribution in peak heigth, the 95% confidence interval of the 6 µm beads lies well between the confidence limits of spermatozoa and HL-60 cells (dashed lines), as expected by their size. Since the confidence intervals do not overlap, it is possible to classify the cells and beads based on their respective calculated peak heights. The wide distribution can be decreased by using parallel electrodes instead of planar ones, which is investigated in chapter 5. There is a trade-off between the size difference of spermatozoa and polystyrene beads, but also between polystyrene beads and the other cells present in semen. Larger beads will improve the distinction between beads and spermatozoa, leading to less wrong classified peaks. However, if a semen sample contains leukocytes larger beads will deteriorate the distinction between beads and these cells.

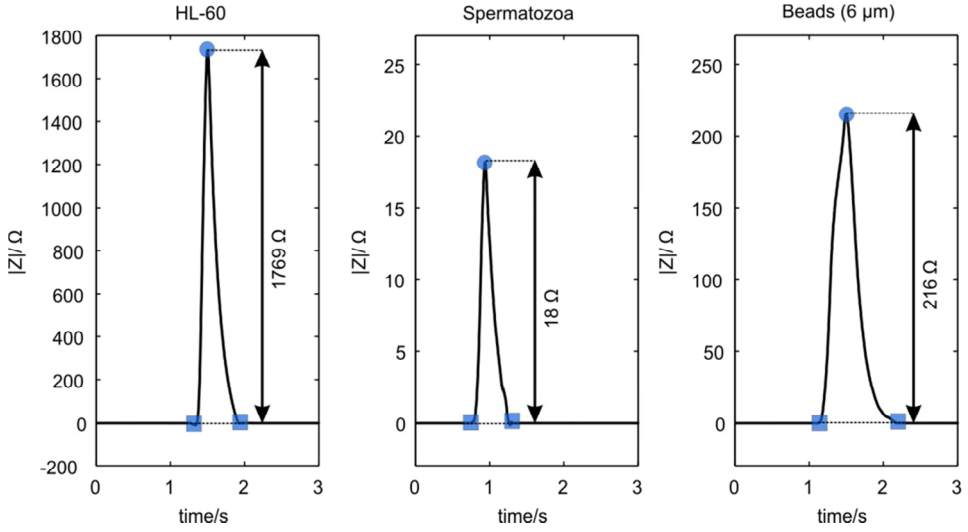

figure 4-7 Measured examples of the processed impedance signal |Z| showing the peak heights, when a HL-60 cell (left), a spermatozoon (middle) and a 6 µm polystyrene bead (right) passed the electrode pair.

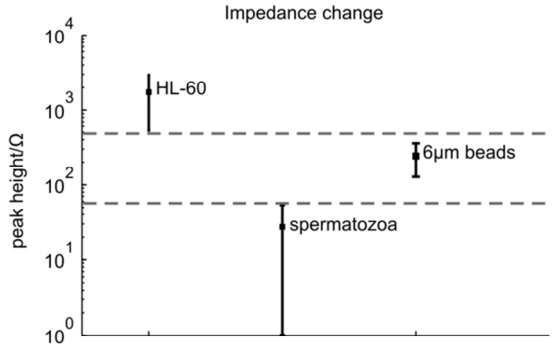

figure 4-8 The averaged peak heights from HL-60 cells, spermatozoa and 6 µm polystyrene beads passing the electrode pair. The dashed lines show the higher and lower points of the 95% confidence intervals of HL-60 cells and spermatozoa respectively.

4.4.2 Study 2: concentration determination

The concentrations of polystyrene beads and spermatozoa determined with the counting chamber ranged from $1.1 \cdot 10^6$ - $2.7 \cdot 10^6$ mL^{-1} and $2.1 \cdot 10^6$ - $61.4 \cdot 10^6$ mL^{-1} respectively. Assuming a random distribution of the cells and particles in the background electrolyte, the exact number of cells and particles in the volume follows a Poisson distribution [1]. The standard deviation of this distribution is the square root of the number of beads or cells counted. Using this, the 95% confidence intervals were calculated for the concentrations of spermatozoa in the seven mixtures. The occurrence of two cells or beads in the measurement volume can also be estimated with a Poisson distribution [17]. For a concentration of $27 \cdot 10^6$ mL^{-1} and a measurement volume of 16.1 pL, the probability of having two cells or beads in the measurement volume at the same time can be calculated to be lower than 6.1%. Therefore, we did not take this into account for the calculation of the spermatozoa concentration using the microfluidic chip. Nonetheless, we have done experiments with a spermatozoa concentration of $61.4 \cdot 10^6$ mL^{-1}. According to the Poisson distribution about 18% of the events counted should be two cells. However, during the measurements, this even has not been visually observed and the calculated spermatozoa concentration amounted to $59.3 \cdot 10^6$ mL^{-1}, which is in good agreement with the actual concentration. This can possibly be explained by a lower effective measurement volume than the calculated one as a result of the planar electrode configuration, resulting in a lower occurrence of two cells in the measurement

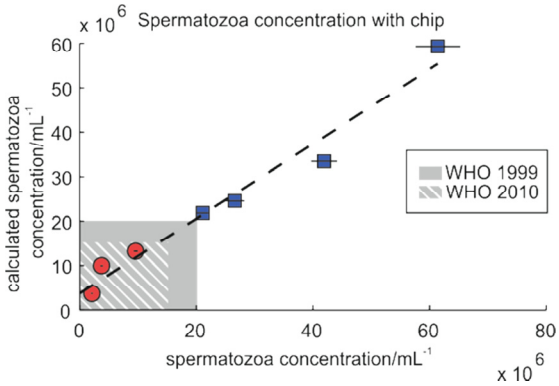

figure 4-9 The determination of the concentration using the microfluidic chip. The circles and squares are the seven mixtures analysed and the horizontal black lines are the 95% confidence intervals of the actual spermatozoa concentration. The expression of the dashed line is $y = 0.84x + 3.70 \cdot 10^6$ ($R^2 = 0.97$). The grey and striped grey areas show the subfertile regions according to WHO guidelines of 1999 and 2010 respectively.

volume. Additionally, the parabolic velocity profile can also have an effect, lowering the effective measurement volume. For every mixture, a threshold was chosen such that the sensitivity and specificity were the highest. Above the threshold, the peak is classified as bead and below as spermatozoon. The specificity and sensitivity for the seven mixtures was larger than 0.91 and 0.89 respectively. The flow rates during the measurements of the different mixtures ranges from 5 - 143 $pL \cdot s^{-1}$. The thresholds were slightly different for the seven mixtures, caused by differences in flow velocity: at higher flow velocities, the threshold was lower, which can be explained by the low pass filter in the measurement system. At higher flow velocities the length of stay in the measurement volume is shorter, resulting in more high frequency components in the signal. With a low pass filter, these high frequency components are suppressed, resulting in a lower calculated peak height.

In figure 4-9 the results of the determination of the concentration of spermatozoa using the known concentration of polystyrene beads are given. Clearly the estimation of a spermatozoa concentration of $42 \cdot 10^6$ mL^{-1} is underestimated. During this measurement some clogging of spermatozoa was observed, leading to false classified peaks, since the peak heights of clogged spermatozoa were comparable with the peak heights of beads. Increasing the bead concentration decreases the influence of false

detected beads. Another possible solution is to dilute the semen sample before the measurement. Since beads need to be added anyhow, this is easy and will decrease the chance of clogging.

In the seven experiments an average of 686 events in each experiment (spermatozoa + beads) were counted and classified for the calculation. There is a tendency in the amount of counted spermatozoa and counted events to the relative difference between both spermatozoa concentrations. The more counted events and spermatozoa, the better the estimation. The amount of counted beads does not show this relation, but a higher concentration of beads give better estimates of the concentration of spermatozoa (data not shown). Moreover, the determination of higher concentrations of spermatozoa with the microfluidic chip is better than for lower concentrations, in accordance with results obtained with the conventional flow cytometer [18].

Currently, during semen analysis at the hospital at least 200 spermatozoa are counted with the gold standard, leading to a percentage error of 7.1% [1], so for a concentration of $20 \cdot 10^6$ mL^{-1} the 95% confidence interval is $17 \cdot 10^6$ mL^{-1} - $23 \cdot 10^6$ mL^{-1}. To achieve the same confidence level in our experiments, the amount of beads that needs to be counted is calculated by taking the error propagation into account. For a spermatozoa and bead concentration of $20 \cdot 10^6$ mL^{-1} and $2 \cdot 10^6$ mL^{-1} respectively, at least 220 beads need to be counted in our chip. At bead concentrations comparable to the spermatozoa concentration, a minimum amount of events needs to be counted to obtain the same error, resulting in the lowest measurement time. With the conventional flow cytometry superimposable results for normal sperm concentrations were obtained when at least 10000 spermatozoa or 2000 fluorospheres were counted [18]. The number of events counted in our chip is lower, due to the recording of video images and visual inspection afterwards. However, the determination of the concentration agrees with the concentration determined with the counting chamber and increasing the counted events will improve it. During the experiments the throughput was relatively slow ($\sim$ 1.0 s^{-1}), due to visual inspection. Theoretically up to 200 particles per second can be measured with our home-made system. In case of a spermatozoa concentration of $20 \cdot 10^6$ mL^{-1} and a bead concentration of $2 \cdot 10^6$ mL^{-1} the measurement takes minimally 12 s which is faster than the gold standard or computer assisted semen analysis systems that still require visual inspection by the lab technician.

The determination of the concentration in our described experiments is independent of the flow velocity. However, during the measurements at lower flow rates, it was observed that beads and spermatozoa tend to stick in the microchannel.

This did not influence the calculation of the spermatozoa concentration in our case, but in future experiments this has to be avoided.

4.5 Conclusions

A microfluidic chip for the determination of spermatozoa concentration has been developed based upon electrical counting of spermatozoa related to the counting of beads added in a known concentration to the semen sample. With this internal calibration method, there is no need to accurately measure the fluid flow through the chip, making the measurement easier and more reliable. To our knowledge this is the first time that the concentration of spermatozoa is determined on chip by using electrical impedance measurements in combination with internal calibration. Determination of the concentration of other cells, such as HL-60 cells, in suspension is also possible; the only condition for reliable results is the necessity to be able to distinguish particles and cells by their change in impedance when passing the electrode pair. Future work will focus on using the developed chip to measure the spermatozoa and leucocytes concentration in human semen of fertile and subfertile men.

4.6 Acknowledgements

This research is supported by the Dutch Technology Foundation STW, which is an applied science division of NWO, and the Technology Programme of the Ministry of Economic Affairs, Agriculture and Innovation. The chip fabrication by Jan van Nieuwkasteele, Johan Bomer and Daniel Wijnperlé and the electronic support from Stefan Lenk are gratefully acknowledged. We thank “KI station Twenthe” for providing the boar semen samples.

4.7 References

1. WHO, *WHO Laboratory manual for the examination of human semen and sperm-cervical mucus interaction*. 4th ed. 1999, Cambridge: Cambridge University Press.
2. WHO, *WHO laboratory manual for the examination and processing of human semen*. 5th ed. 2010, Geneva.

3. Keel, B.A., et al., *Results of the American Association of Bioanalysts national proficiency testing programme in andrology.* Human Reproduction, 2000. **15**(3): p. 680-686.
4. Keel, B.A., *Within- and between-subject variation in semen parameters in infertile men and normal semen donors.* Fertility and Sterility, 2006. **85**(1): p. 128-134.
5. Valero, A., et al., *Apoptotic cell death dynamics of HL60 cells studied using a microfluidic cell trap device.* Lab on a Chip, 2005. **5**(1): p. 49-55.
6. Andersson, H. and A. van den Berg, *Where are the biologists? A series of mini-reviews covering new trends in fundamental and applied research, and potential applications of miniaturised technologies.* Lab on a Chip, 2006. **6**(4): p. 467-470.
7. Vrouwe, E.X., R. Luttge, and A. Berg van den, *Direct measurement of lithium in whole blood using microchip capillary electrophoresis with integrated conductivity detection.* Electrophoresis, 2004. **25**: p. 1660-1667.
8. Gheorghiu, E., *Measuring living cells using dielectric spectroscopy.* Bioelectrochemistry and Bioenergetics, 1996. **40**(2): p. 133-139.
9. Krommenhoek, E.E., et al., *Monitoring of yeast cell concentration using a micromachined impedance sensor.* Sensors and Actuators B: Chemical, 2006. **115**(1): p. 384-389.
10. Asami, K., *Characterization of biological cells by dielectric spectroscopy.* Journal of Non-Crystalline Solids 2002. **305**: p. 268-277.
11. Coulter, W.H., *High speed automatic blood cell counter and cell size analyzer.* Proceedings of the National Electronic Conference 1956. **12**: p. 1034-1040.
12. Brotherton, J. and G. Barnard, *Estimation of number, mean size and size distribution of human spermatozoa in oligospermia using a coulter counter.* Journal of Reproduction & Fertility, 1974. **40**: p. 341-357.
13. Gawad, S., L. Schild, and P. Renaud, *Micromachined impedance spectroscopy flow cytometer for cell analysis and particle sizing.* Lab on a Chip, 2001. **1**: p. 76-82.
14. Cheung, K., S. Gawad, and P. Renaud, *Impedance spectroscopy flow cytometry: on-chip label-free cell differentiation.* Cytometry part A, 2005. **65A**: p. 124-132.
15. Benazzi, G., et al., *Discrimination and analysis of phytoplankton using a microfluidic cytometer.* IET Nanobiotechnology, 2007. **1**(6): p. 94-101.
16. Holmes, D., et al., *Leukocyte analysis and differentiation using high speed microfluidic single cell impedance cytometry.* Lab on a Chip, 2009. **9**: p. 2881-2889.
17. Wood, D.K., M.V. Requa, and A.N. Cleland, *Microfabricated high-throughput electronic particle detector.* Review of Scientific Instruments, 2007. **78**(10): p. 104301.
18. Eustache, F., P. Jouannet, and J. Auger, *Evaluation of flow cytometric methods to measure human sperm concentration.* Journal of Andrology, 2001. **22**(4): p. 558-567.

19. Perticarari, S., et al., *A new multiparameter flow cytometric method for human semen analysis.* Human Reproduction, 2007. **22**(2): p. 485-494.
20. Langereis, G.R., *An integrated sensor system for monitoring washing processes*, PhD thesis, 1999, University of Twente
21. Morgan, H., et al., *Single cell dielectric spectroscopy.* Journal of Physics D: Applied Physics, 2007. **40**: p. 61-70.
22. Gawad, S., et al., *Dielectric spectroscopy in a micromachined flow cytometer: theoretical and practical considerations.* Lab on a Chip, 2004. **4**: p. 241-251.
23. Johanisson, E., et al., *Evaluation of `round cells' in semen analysis: a comparative study.* Human Reproduction Update, 2000. **6**(4): p. 404-412.
24. Gil, M.C., et al., *Morphometry of porcine spermatozoa and its functional significance in relation with the motility parameters in fresh semen.* Theriogenology, 2009. **71**(2): p. 254-263.
25. Obara, H., et al., *Prediction of unexpectedly poor fertilization and pregnancy outcome using the strict criteria for sperm morphology before and after sperm separation in IVF-ET.* International Journal of Andrology, 2001. **24**: p. 102-108.
26. Curry, M.R., et al., *Surface area and volume measurements for ram and human spermatozoa.* Biology of Reproduction, 1996. **55**: p. 1325-1332.

chapter 5

Parallel electrode configuration*

A new parallel electrode structure in a microfluidic channel is described that makes use of a floating electrode to get a homogeneous electrical field. Compared to existing parallel electrode structures, the new structure has an easier production process and there is no need for an electrical connection to both sides of the microfluidic chip. The results of electrical impedance changes caused by polystyrene beads passing the electrodes are compared with results in a similar planar electrode configuration. It is shown that in the new configuration the coefficient of variation of the impedance changes is lower compared to the planar configuration (0.39 versus 0.56) and less dependent on the position of the beads passage in the channel as a result of the homogeneous electrical field.

* Modified from L.I. Segerink, A.J. Sprenkels, J.G. Bomer, I. Vermes and A. van den Berg. *A new floating electrode structure for generating homogeneous electrical fields in microfluidic channels.* Lab on a Chip, 2011. **11**: p. 1995-2001.

5.1 Introduction

Electrical impedance measurements of single cells in microfluidic chips are used for a variety of applications, such as diagnostic purposes [1-3], drug screening [4, 5], cell characterization [6-8] and environmental issues [9]. The measurement of the electrical impedance is a label-free method that measures the dielectric properties of the cells or particles in the measurement volume.

Counting of single particles in suspension was firstly done with the use of a Coulter counter [10], measuring the DC resistance through an orifice. Based on this system, techniques have been developed that use AC signals to measure the electrical properties of cells [11]. Recently, systems for electrical impedance measurements have been miniaturized by integrating the electrodes in the walls of the microchannel [8], resulting in so-called microfluidic impedance cytometers [12, 13]. These microfluidic impedance cytometers have the same advantages as other lab on chip systems, like a small sample volume, reduction of costs and the possibility to integrate multiple processes. Furthermore it is possible to incorporate optical analysis in the system as well [3, 9].

Several electrode configurations are possible in a microfluidic impedance cytometer with a different number of electrodes. Some microfluidic impedance cytometers use a differential measurement between two electrode pairs into two successive channel parts [3, 9, 14-17], while other designs consist of only one electrode pair [2, 18]. A differential measurement has the advantage that the electrical impedance change caused by a passing cell is measured with respect to the surrounding electrolyte, such that the influence of environmental changes are reduced and that the speed of the cell can be determined [16]. However, to get reliable results, the cell concentration cannot be too high, since the probability of detecting multiple cells simultaneously increases.

Another important difference that can be made in the electrode configuration is the position of the electrodes with respect to each other. For instance the microfluidic cytometer can have a planar or a parallel electrode configuration. In a planar electrode configuration, two electrodes are positioned at the same side of the channel with an interelectrode distance of several tens of μm. The electrical field distribution between the planar electrodes is inhomogeneous. Due to this inhomogeneity, the position of the particle between the electrodes influences the amount of the electrical impedance change [13, 16, 17]. This can also explain the relatively large variation we found in the electrical impedance change for the cells passing planar electrodes as shown in chapter 4 [2]. Furthermore the relative electrode impedance change caused by a cell is less, compared to the changes measured with systems consisting of parallel

electrodes [16, 19]. Using a planar configuration in combination with hydrodynamic focusing reduces the position dependency and increases the sensitivity [17]. However, the complexity of the microfluidic chip containing such focusing system is substantially increased compared to our approach.

Systems with parallel (top-bottom) electrodes in a microchannel have already been reported [3, 14, 15, 18]. In these systems an additional layer of for instance PDMS [18] or polyimide [14] is incorporated between two glass substrates both containing the electrodes. The alignment of the electrodes is critical and connection with the electrodes has to be made at both sides of the microchannel, making the fabrication more elaborate than that of planar electrodes. Furthermore the sidewalls of the channel are formed by an additional layer, consisting of a different material. In another embodiment instead of a top-bottom electrode configuration liquid electrodes [1] at the sidewalls of the channel are used. However, according to simulations the relative electrical impedance change is less compared to the changes measured with top-bottom electrode configurations with comparable dimensions [1, 16, 19].

In this chapter we describe a new process for the fabrication of top-bottom electrodes that combines the ease of fabrication of planar electrodes with the higher sensitivity of the parallel configuration. In only one extra processing step, compared to the fabrication of planar electrodes, a floating electrode opposite of two planar electrodes in the channel is realized. The proposed system has a sensitivity comparable to other published top-bottom electrode systems, but a much easier fabrication process. With this new parallel electrode configuration, the electrical impedance changes of single polystyrene beads are measured and the results are compared with an existing planar configuration. First we describe the theory and concept of the new chip design. Next the newly developed production process is described, followed by electrical characterization of the microfluidic chip and detection of beads passing the electrode using electrical impedance measurements. Subsequently, the results of these measurements are discussed in detail and compared with results obtained with a planar electrode configuration. Finally some conclusions are given.

5.2 Theory

The concept of the floating electrode structure is shown in figure 5-1. It consists of three electrodes: two connecting electrodes on the upper side of the microfluidic channel and one floating electrode on the bottom of the channel. The floating

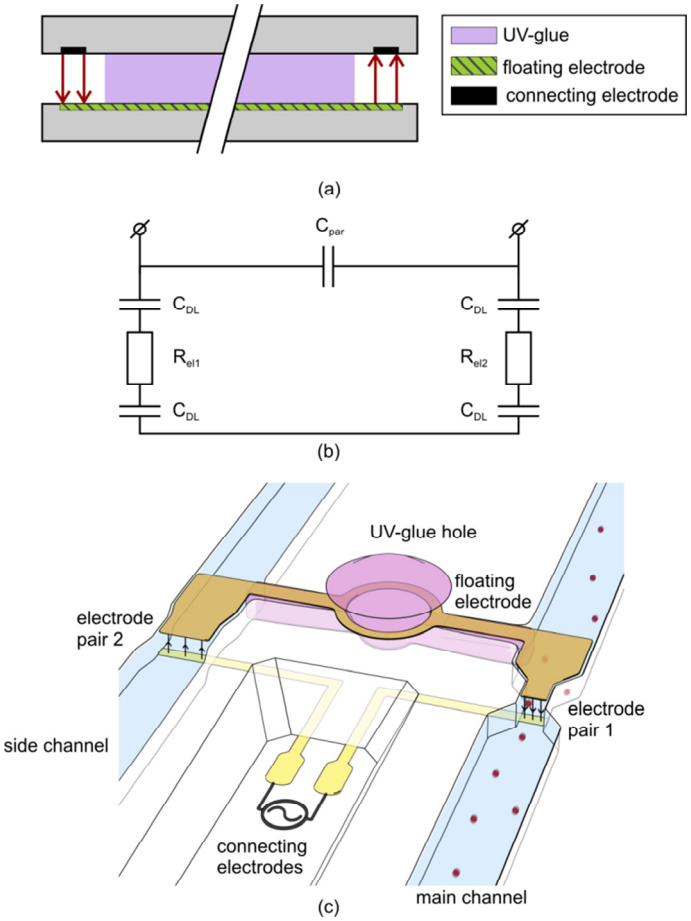

figure 5-1 (a) Schematic illustration of the floating electrode with (b) the simplified equivalent circuit model. C_{DL} is the double layer capacitance, C_{par} is the parasitic capacitance and R_{el1} and R_{el2} are the electrolyte resistances between electrode pair 1 and 2 respectively. (c) Simplified illustration of chip design type 2. The electrode area of electrode pair 2 of type 2 is 7 times the size of electrode pair of type 1 (not shown).

electrode merely functions as a lead between both connecting electrodes. Since AC signals are used to measure the electrical impedance, no charge built up can occur on the floating electrode. Advantages of this floating electrode structure are that electrical connections are only necessary on one side of the chip and the sidewalls of the microfluidic channels consist of the same material as the substrates. Furthermore

the production process does not involve difficult alignment steps as compared to reported processes for parallel electrodes [14, 18]. It uses the ease of fabrication of the planar electrodes with the addition of just one processing step.

The total electrical impedance that is measured between the two top electrodes is the sum of the electrical impedance between electrode pair 1 and electrode pair 2. When a suspension of particles is added, it is not clear whether a change in electrical impedance is caused by a particle passing electrode pair 1 or electrode pair 2. Furthermore a larger change in the electrical impedance can be caused by two or more small particles that simultaneously pass both electrodes pairs or by one larger particle that passes one electrode pair. Therefore it is necessary to detect only particles between electrode pair 1 and measure only the fluid between electrode pair 2. This can be achieved by the addition of a second channel as shown in figure 5-1(c). However, to prevent particles to enter electrode pair 2, the fluidic connection between both electrode pairs should be blocked. This blocking can easily be accomplished by introduction of a drop of UV curing glue in the UV-glue hole, as shown in figure 5-1(c).

The microfluidic chip can be modelled by a simplified equivalent circuit model (see figure 5-1(b)). At every electrode–electrolyte interface there is a double layer capacitance (C_{DL}). In our microfluidic chip, there are in total four double layer capacitances that are dominant at low frequencies in the bode plot [13, 20]. The electrolyte resistance (R_{el1} and R_{el2}), in our case the resistance of the fluid between both electrode pairs, plays a role at intermediate frequencies, resulting in a plateau in the bode plot [20]. The detection of particles can best be done with a measurement frequency at this resistive plateau well below 1 MHz [16, 21], since at these frequencies particles and cells behave like insulating spheres. In this case, a particle or cell causes a change in the electrical impedance, when passing along an electrode pair. For low volume fractions ($\Phi \ll 1$), this change can be described by a simplified form of the Maxwell Mixture equation [13, 22]:

$$\rho_{eq} = \rho_{el}\left(1 + {}^{3\Phi}/_{2}\right) \qquad [\Omega\cdot\mathrm{m}] \qquad (5\text{-}1)$$

with ρ_{eq} the equivalent resistivity of the electrolyte with a particle in it and ρ_{el} the resistivity of the background electrolyte. At frequencies well above those of the resistive plateau, the bode plot is mainly influenced by the parasitic capacitances (C_{par}) of the system [23].

5.3 Method

5.3.1 Chip design and fabrication

The schematic diagram of the fabrication is shown in figure 5-2. Compared to the fabrication of planar electrodes that was previously reported [2], this process contains only one additional step. The microfluidic chips were made of two 500 µm thick 100 mm Borofloat glass wafers. In the top wafer the microfluidic channels with floating electrodes were made. This wafer was covered with sputtered Cr (30 nm) and Au (150 nm) layers; the Cr layer acts as an adhesion layer for Au. This step was followed by a photolithography step and wet etching of the Au and Cr layers. Subsequently the microfluidic channel was isotropically etched in a 25% HF solution. In the next step the floating electrode was realized by placing a shadow mask on top of the photoresist, followed by sputtering of Ta as adhesion layer (20 nm) and Pt forming the floating electrode (140 nm). Next access holes were powderblasted from the back using a photopatternable foil. On the bottom wafer Pt electrodes were realized that form the connecting electrodes to the measurement setup. These were prepared by etching a recess with buffered HF, after a photolithography step. The

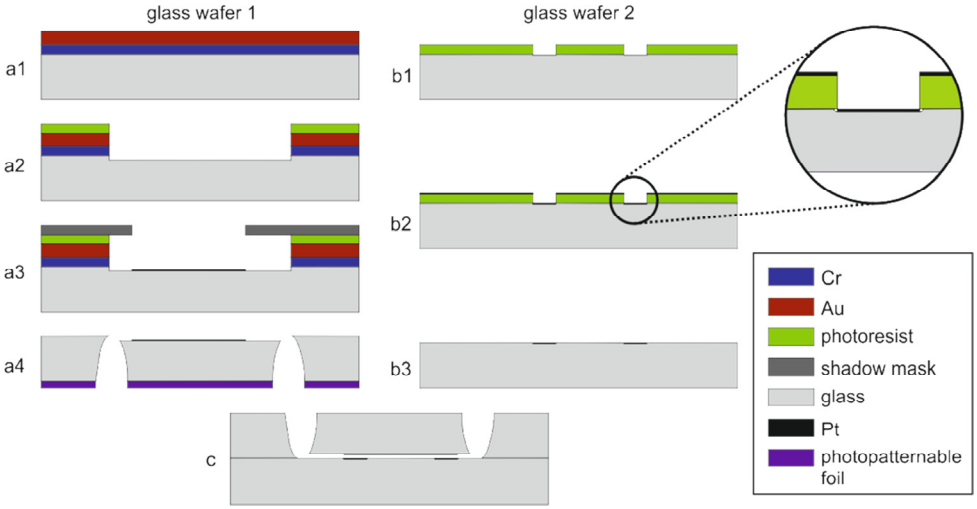

figure 5-2 Schematic diagram of the fabrication. Glass wafer 1 is firstly sputtered with Cr and Au layers (a1). By means of photolithography and etching, the microfluidic channel is formed (a2). Next a shadow mask is used for the sputtering of the floating electrode on the bottom of the channel (a3). After removing several layers, access holes are powder blasted from the back (a4). On glass wafer 2, the embedded connecting electrodes are formed using a lift-off technique (b1, b2 and b3). Finally both glass wafers are bonded together (c).

recess was filled with sputtered Pt with Ta as an adhesion layer. In the next step the photoresist was removed, leaving a glass surface with embedded electrodes, which was bonded to the channel side of the top glass wafer using fusion bonding (T = 625 °C). Finally both bonded wafers were diced into separate chips.

Two types of microfluidic chips have been designed, each having a microchannel with a depth of 18 μm. Due to the floating electrode configuration, the chip consists of two parallel electrode pairs. It is not desirable to have both electrode pairs in the same fluidic channel, since there is a probability that more than one particle is simultaneously detected between both electrode pairs disturbing the impedance measurement. Therefore the second electrode pair is separated from the first electrode pair by use of an additional microfluidic channel. The microchannel containing electrode pair 1 is filled with the suspension containing the particles, while the other channel only contains a background electrolyte. In this way the particles are only detected between electrode pair 1. In both chip designs, the microchannel tapers to a width of 42 μm at the electrode area of electrode pair 1, while at both electrode pairs the width of the active electrodes that span the microchannel is 20 μm. The difference between both chip designs is the electrode area of the second electrode pair. The electrode area of electrode pair 2 is equal to that of electrode pair 1 in the first design and about 7 times larger in the second chip design. Since the particles are measured between electrode pair 1, it is expected that the increase of the electrode area of electrode pair 2 improves the sensitivity as a result of the decreased measured impedance. In figure 5-1(c) design 2 is shown.

Besides the additional step in the fabrication, one channel in the chip needs to be blocked before experiments can be done. The floating electrode is sputtered on the bottom of the channel, implicating that initially there needs to be a microfluidic channel between both electrode pairs. As already mentioned such liquid connection is not desirable in the final setup, since particles may enter the region between both electrode pairs. Therefore this connecting channel is designed with an additional access hole, such that it can be filled with UV curing glue. A small drop of Loctite 358 was put into the access hole and after several seconds the UV source (ELC-403, Electro-Lite Corporation; 365 nm) was turned on for about 20 s, causing the glue to cure almost instantly.

5.3.2 Measurement setup

For all experiments the chip was put into a chip holder, such that reliable fluidic and electrical connections could be made. The chip holder contains screw threads which are aligned with the access holes of the microfluidic chip. Using a Harvard PHD2000

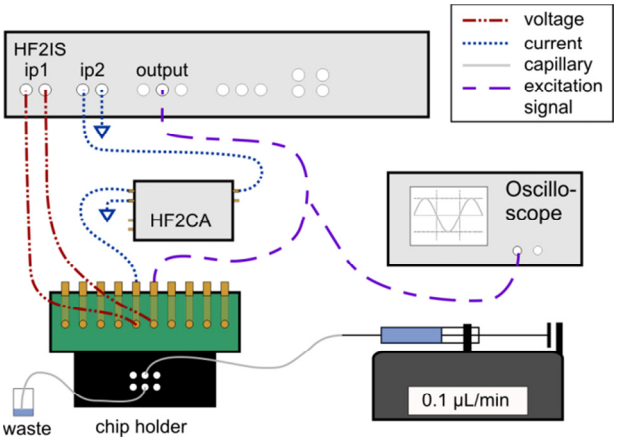

figure 5-3 Schematic diagram of the measurement setup. The chip holder makes fluidic and electrical connections to the chip. In this diagram, the inlet and outlet are located underneath the middle two screw threads and the electrodes of the chip are connected to the middle four electrodes on the chip holder. So each electrode on the microfluidic chip has two electrical connections on the chip holder, making a four point measurement possible. Input 1 (ip1) of the HF2IS measures the voltage across the chip, while input 2 (ip2) measures via the HF2CA the current through the chip.

syringe pump, fluid was pumped through the chip via a glass capillary (inner diameter 148 µm) and connected to the microfluidic chip using Upchurch nuts and ferrules (Upchurch Scientific, Oak Harbor, WA, USA).

Two types of experiments were performed. The first study involves the measurement of the frequency characteristics of both microfluidic chip types. For this purpose the chips were filled with background electrolyte and a bode plot from 100 Hz to 40 MHz was made using a HP impedance/gainphase analyser type HP4194A, controlled by LabVIEW (7 Express, version 7.0, 2003, National Instruments).

In the second study beads suspended in background electrolyte were detected using electrical impedance measurements. From the results of the first study, the optimal measurement frequency was determined. The actual impedance measurements were done using a HF2IS impedance spectroscope in combination with the HF2CA current amplifier (both Zurich Instruments, Zurich, Switzerland). In figure 5-3 a schematic diagram of the electrical impedance measurement setup is shown. The HF2IS impedance spectroscope was used to generate the excitation signal

(2 V_{PP}, 500 kHz) as well as to measure the voltages at two inputs. An oscilloscope (Agilent Technologies, type DSO3062A) was connected to the impedance spectroscope for verifying the excitation signal. The first input measured the excitation voltage across both electrodes in the microchannel, while the other input measured the output signal from the HF2CA current-to-voltage converter and thus indirectly the current through the microfluidic chip. In this way, a four point impedance measurement was performed. Both input signals were captured with a sample rate of 899 Hz and used for analysis on a laptop using Matlab (R2007B, version 7.5.0.342, 2007, the MathWorks Inc). In Matlab the electrical impedance was calculated from both signals. In addition, the program was used for the calculation of the peak heights in the same way as described in chapter 4 [2]. During all measurements, the chip was mounted on an inverted microscope (Leica CTR 6000, Leica Microsystems GmbH, Wetzlar, Germany).

5.3.3 Samples

Polybead Polystyrene Violet dyed beads with a diameter of 3 μm and Polybead Polystyrene Black dyed beads with a diameter of 6 μm, both obtained from Polysciences Inc (Warrington, Pennsylvania USA) were used during the experiments. The beads were suspended in Ferticult™ Flushing medium (chemically balanced salt solution, HEPES buffered with 0.4% HSA, purchased from Fertipro NV (Beernem, Belgium)) with a specific electrical conductivity of 1.4 $S \cdot m^{-1}$.

5.4 Results and discussion

The microfluidic channels in the chip were isotropically etched in the glass substrate, resulting in a channel width approximately twice the depth of the channel plus the actual width of the mask. For this wet etching process a photoresist layer was used as mask. After the isotropic etching of the microfluidic channel, the photoresist layer was not removed, but also used as mask for the sputtering of the floating electrode. As a result of this procedure, the width of the floating electrode is restricted by the size of the photoresist layer. In our designs, the size of the mask at the electrode pair has a width of 6 μm. From measurements on realized chips, the actual width of the floating electrodes amounted to about 15 ± 2 μm. So in the case of isotropically etching, the floating electrode does not entirely span the bottom of the microchannel but is significantly wider than the width of the mask as a result of the inherent widening of sputtering through a shadow mask.

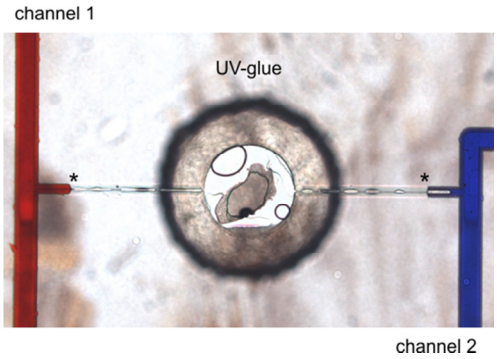

figure 5-4 Blocking of the interconnecting channel that is used as host for the floating electrode, using UV curing glue. The asterisks indicate the crossings between the fluid and the cured UV glue.

In both chip designs, electrode pairs 1 and 2 are located in a different microfluidic channel. One electrode pair is used for detection of particles in the fluid, while the other measures only the electrical impedance of the fluid and acts actually as a connection to the outer world. An interconnecting channel is needed to host the floating electrode and this channel has to be blocked for liquids before experiments can be done which is achieved with UV glue. As an example figure 5-4 shows the blocking mechanism in chip design 1. Both channels containing the red and blue liquid are clearly separated from each other.

5.4.1 Characterization of the chips

In figure 5-5 the results of the impedance measurements of three different chip designs are shown. Parallel designs 1 and 2 and the chip with a planar electrode configuration used in chapter 4 [2] were filled with background electrolyte and the averages of 50 measurements are shown. The influence of the electrical double layer and the parasitic capacitances can be clearly seen for every electrode design at low and high frequencies respectively. The value of the resistive plateau differs for every chip. The planar electrode configuration has a higher resistive plateau than the two parallel electrode configurations. As expected, chip type 2 has a lower resistive plateau compared to chip type 1, since the area of electrode pair 2 is larger in design 2, decreasing the overall impedance. The chosen measurement frequency of 500 kHz used for the detection of particles is appropriate for the three designs, which all have the resistive plateau at this frequency.

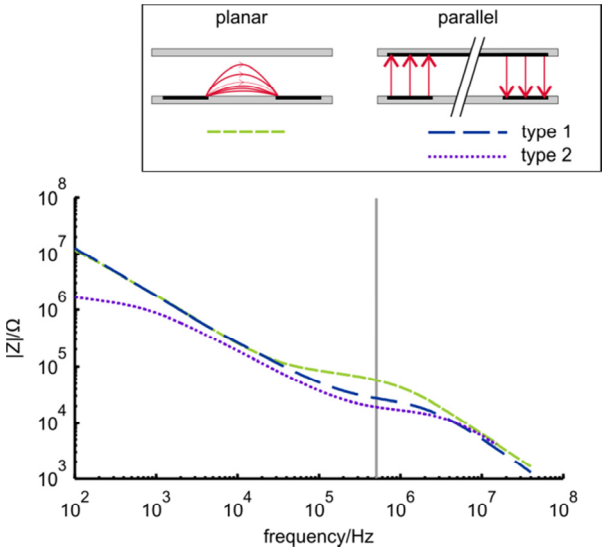

figure 5-5 The measured frequency response of the real electrical impedance signal for three chip designs each with a different electrode configuration. The vertical line indicates the optimal measurement frequency. Parallel electrode configuration type 2 has a 7 times larger electrode area of electrode pair 2, compared to parallel electrode configuration type 1.

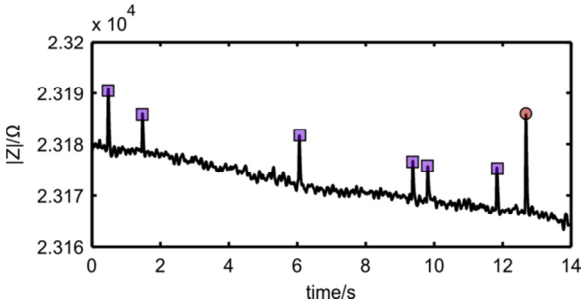

figure 5-6 An example of the raw electrical impedance signal with the new parallel electrode configuration. The peaks with the squares indicate the passage of one 6 µm bead, while the peak with the circle is caused by the passage of two 6 µm beads simultaneously which event was visually observed.

5.4.2 Detection of beads

First electrical impedance measurements with parallel electrode configuration type 1 were performed. By measuring the electrical impedance and simultaneously observing the video images taken by the microscope camera, every 6 µm bead that passed the electrode was visually and electrically detected. A typical example of the measured signal is shown in figure 5-6. The electrical impedance changes of 146 beads have been measured and amounted to 9.3 ± 3.6 Ω.

Subsequently, 6 µm beads have been detected with parallel electrode configuration type 2, resulting in an impedance change of 12.8 ± 5.9 Ω (n = 115). This experiment was also performed with 3 µm beads (3.0 ± 1.4 Ω, n = 264). The impedance changes measured for both 3 and 6 µm beads are shown in figure 5-7. The 6 µm beads generate a significant ($p < 0.01$) larger impedance change than the 3 µm beads, as expected by their size. These results clearly indicate that with the parallel electrode configuration it is possible to distinguish 3 and 6 µm beads from each other.

5.4.3 Influence of electrode configuration

Measurements with electrode configuration type 1 already showed that it is possible to detect 6 µm polystyrene beads in suspension. The same measurements were done with a planar electrode configuration (23.1 ± 12.9 Ω, n = 140) and the parallel electrode configuration type 2 (12.8 ± 5.9 Ω, n = 115). The average value of the electrical impedance change for the planar electrode pair is significantly ($p < 0.01$)

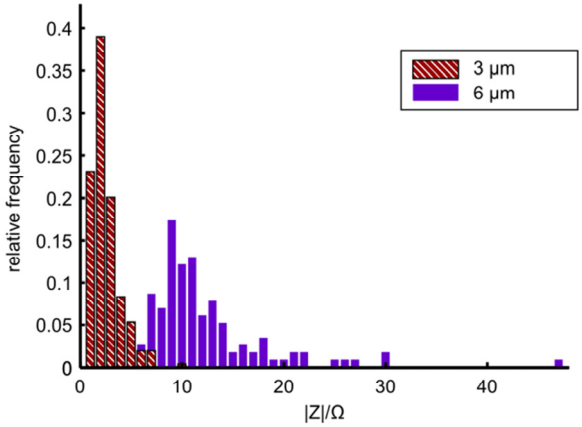

figure 5-7 A histogram of the impedance changes caused by 3 and 6 µm beads.

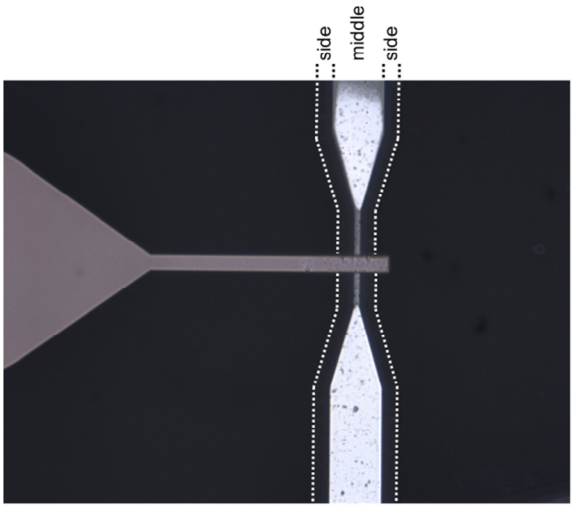

(a)

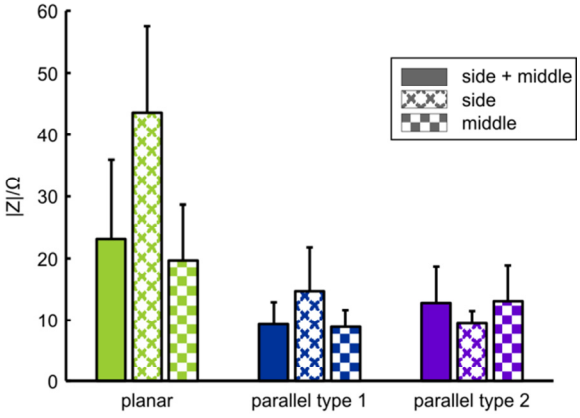

(b)

figure 5-8 (a) A microscope image (differential interference contrast) of the electrode pair 1 of the parallel electrode configuration indicating the side and middle positions of the channel. (b) The influence of the position of the 6 µm bead in the channel. The error bars indicate one standard deviation.

larger than those of the two parallel electrode configurations. This can be explained by the volume fraction of the particle. In the parallel configuration, the measurement volume is about twice that of the planar configuration due to the two electrode pairs in series. Therefore the same particle has a lower volume fraction in the parallel electrode configuration than in the planar one, causing a smaller impedance change (see eqn (5-1)).

To compare the three electrode configurations, the coefficient of variation (standard deviation / mean) was calculated for each electrode configuration, resulting in 0.56, 0.39 and 0.46 for planar, parallel type 1 and parallel type 2 respectively. Part of the spread for each configuration is caused by the variation in bead diameter. However, the larger spread for the electrical impedance change in the planar electrode configuration can be explained by the position of the beads in the channel passing the electrodes. Beads that are at the flexion of the microfluidic channel generate significantly larger electrical impedance changes than beads that flow through the middle of the microfluidic channel (see figure 5-8). At the flexion of the microfluidic channel the electrical field is the strongest, since the depth of the channel is less. So a particle in this part of the microfluidic channel will cause a higher electrical impedance change.

The difference between type 1 and type 2 of the parallel electrode configuration is a result of the different area of electrode pair 2 that only measures the background electrolyte. As mentioned, we expect better sensitivity when the area is larger, since the impedance at that electrode pair is reduced. The results show that the electrical impedance change is indeed somewhat larger for type 2. However, the coefficient of variation was larger for this electrode configuration.

5.5 Conclusions

A new method for the fabrication of parallel electrodes in a microfluidic chip has been developed, which can be used for a microfluidic impedance cytometer. A floating electrode is used in the new method, making electrical connections only to one side of the chip possible. With this method, a floating electrode is positioned at the opposite side of the channel relative to the connecting electrodes, creating a parallel electrode configuration. Due to this floating electrode, the fabrication is easier than previously reported methods for the realization of parallel electrode configurations. With the new electrode configuration it was possible to detect polystyrene beads suspended in a fluid. Furthermore the coefficient of variation in electrical impedance change was less for the new configuration compared to a planar configuration, since the position

of the beads in the channel has less influence on the impedance change. The new floating electrode structure is not solely useful for electrical impedance measurements, but we think other applications like separation based on DEP can also be performed with this floating electrode concept. Future work will be focused on improving the sensitivity of the configuration for instance by using a highly conductive background electrolyte in the additional channel at electrode pair 2.

5.6 Acknowledgements

This research is supported by the Dutch Technology Foundation STW, which is the applied science division of NWO, and the Technology Programme of the Ministry of Economic Affairs, Agriculture and Innovation. The chip fabrication support by Daniel Wijnperlé and the LabVIEW support from Mathieu Odijk are gratefully acknowledged.

5.7 References

1. Valero, A., T. Braschler, and P. Renaud, *A unified approach to dielectric single cell analysis: impedance and dielectrophoretic force spectroscopy.* Lab on a Chip, 2010. **10**(17): p. 2216-2225.
2. Segerink, L.I., et al., *On-chip determination of spermatozoa concentration using electrical impedance measurements.* Lab on a Chip, 2010. **10**: p. 1018-1024.
3. Holmes, D., et al., *Leukocyte analysis and differentiation using high speed microfluidic single cell impedance cytometry.* Lab on a Chip, 2009. **9**: p. 2881-2889.
4. Hua, S.Z. and T. Pennell, *A microfluidic chip for real-time studies of the volume of single cells.* Lab on a Chip, 2009. **9**(2): p. 251-256.
5. Malleo, D., et al., *Continuous differential impedance spectroscopy of single cells.* Microfluidics and Nanofluidics, 2010. **9**(2-3): p. 191-198.
6. Cho, Y.H., et al., *Development of microfluidic device for electrical/physical characterization of single cell.* Journal of Microelectromechanical Systems, 2006. **15**(2): p. 287-295.
7. Jang, L.S. and M.H. Wang, *Microfluidic device for cell capture and impedance measurement.* Biomedical Microdevices, 2007. **9**(5): p. 737-743.
8. Ghenim, L., et al., *Monitoring impedance changes associated with motility and mitosis of a single cell.* Lab on a Chip, 2010. **10**: p. 2546-2550.
9. Benazzi, G., et al., *Discrimination and analysis of phytoplankton using a microfluidic cytometer.* IET Nanobiotechnology, 2007. **1**(6): p. 94-101.
10. Coulter, W.H., *High speed automatic blood cell counter and cell size analyzer.* Proceedings of the National Electronic Conference 1956. **12**: p. 1034-1040.

11. Hoffman, R.A. and W.B. Britt, *Flow-system measurement of cell impedance properties.* Journal of Histochemistry & Cytochemistry, 1979. **27**(1): p. 234-240.
12. Ayliffe, H.E., A.B. Frazie, and R.D. Rabbitt, *Electrical impedance spectroscopy using microchannels with integrated metal electrodes.* IEEE Journal of Microelectromechanical Systems, 1999. **8**(1): p. 50-57.
13. Sun, T. and H. Morgan, *Single-cell microfluidic impedance cytometry: a review* Microfluidics and Nanofluidics, 2010. **8**(4): p. 423-443.
14. Cheung, K., S. Gawad, and P. Renaud, *Impedance spectroscopy flow cytometry: on-chip label-free cell differentiation.* Cytometry part A, 2005. **65A**: p. 124-132.
15. Holmes, D. and H. Morgan, *Single cell impedance cytometry for identification and counting of CD4 T-Cells in human blood using impedance labels.* Analytical Chemistry, 2010. **82**(4): p. 1455-1461.
16. Gawad, S., L. Schild, and P. Renaud, *Micromachined impedance spectroscopy flow cytometer for cell analysis and particle sizing.* Lab on a Chip, 2001. **1**: p. 76-82.
17. Rodriguez-Trujillo, R., et al., *High-speed particle detection in a micro-Coulter counter with two-dimensional adjustable aperture.* Biosensors & Bioelectronics, 2008. **24**(2): p. 290-296.
18. Wood, D.K., M.V. Requa, and A.N. Cleland, *Microfabricated high-throughput electronic particle detector.* Review of Scientific Instruments, 2007. **78**(10): p. 104301.
19. Sun, T., et al., *Analytical electric field and sensitivity analysis for two microfluidic impedance cytometer designs.* IET Nanobiotechnology, 2007. **1**(5): p. 69-79.
20. Morgan, H., et al., *Single cell dielectric spectroscopy.* Journal of Physics D: Applied Physics, 2007. **40**: p. 61-70.
21. Asami, K., *Characterization of biological cells by dielectric spectroscopy.* Journal of Non-Crystalline Solids 2002. **305**: p. 268-277.
22. Maxwell, J., *A treatise on electricity and magnetism*. Vol. 1. 1873, Oxford: Clarendon Press.
23. Langereis, G.R., *An integrated sensor system for monitoring washing processes*, PhD thesis, 1999, University of Twente

chapter 6

On-chip motility determination

For the motility determination of a semen sample a microfluidic chip has been developed that uses the ability of spermatozoa to cross the laminar stream lines of two flows in combination with electrical detection at two electrode pairs. Immotile cells or particles stay in the sample flow and are detected at one electrode pair, while motile cells cross the flow barrier and are counted at the other planar electrode pair. A model for this behaviour is proposed, that defines the apparent mobility as an independent parameter for the motility of a cell. From the ratio of counted cells at both electrode pairs, this value can be determined and can be used as a measure to distinguish between a semen sample with motile spermatozoa and a semen sample containing only dead spermatozoa.

6.1 Introduction

After years of decreasing fertility rates in Europe, the numbers are rising again [1]. Social and behavioural circumstances are major factors that caused the decline, but also biological factors resulting in a decrease in fertility should not be overlooked [2, 3]. A decrease in semen quality is noticed in the twentieth century, due to both a significant decrease in concentration of spermatozoa as well as a reduction of the average semen volume [4]. It is suggested that the decline in semen quality is one of the causes of the lower fertility rate and an increase in the use of assisted reproductive technologies [5]. Before a good choice for a treatment of an involuntary childless couple can be made, the fertility of the couple needs to be investigated and for the man this is accomplished with a semen analysis. Important parameters assessed with a semen analysis are the concentration of spermatozoa in semen and the motility of these cells. Currently the gold standard for the assessment is a labour intensive, manual method, where the semen sample is investigated by placing an aliquot under the microscope [6], making the assessment subjective. A CASA system can replace this, but this is an expensive system that still needs a laboratory technician who does the quality control and operates the system. A better solution for the semen analysis would be an objective, reliable test that can be performed at home, at multiple moments in a certain time interval. Microfluidic systems are very well suited for this, since they tend to be cheap, can be made disposable and various measurements can be done on one single microfluidic chip. We already showed that it is possible to determine the spermatozoa concentration using a microfluidic chip [7]. In this chapter we present a microfluidic chip which can be used for the determination of the motility of spermatozoa.

The motility of spermatozoa is normally expressed in the percentages progressive motile, non-progressive motile and immotile spermatozoa respectively [6]. According to the WHO the lower reference limits for fertile men are 32% for progressive motility and 40% for total motility (progressive + non progressive). A first approach to assess the motility of spermatozoa on chip was performed by Kricka and co-workers at the end of the twentieth century [8]. They found that the time needed for the first spermatozoon to swim through a branched microchannel is correlated with the forward progression score [9]. Disadvantages of this method are that the score depends on the motility of only one or a few cells and still requires the need for visual verification. Another platform makes use of holographic images in combination with digital summation and subtraction of frames to determine the concentration and motility of the spermatozoa up to concentration of $12.5 \cdot 10^6$ mL^{-1} [10]. However, for higher concentrations the sample needs to be diluted, which is not favourable in a

home test system. In still other approaches the concentration of motile spermatozoa is determined. Motile spermatozoa are separated from the semen sample by swimming to another well [11], through hyaluronic acid [12] or upstream a flow [13]. After this separation, the concentration of cells is measured by means of fluorescence intensity [11], appearance of a red stripe on the nitrocellulose strip [12] or using DC-electrical detection of single cells during a certain time interval [13].

Besides these microfluidic systems for the assessment of semen quality, microfluidic systems have been developed for the separation of motile spermatozoa for IVF or ICSI procedures. One example is the MISS and this PDMS device uses the ability of motile spermatozoa to swim out of the characteristic laminar flow in microfluidic channels [14, 15]. Others have adapted the device by the use of a coating [16], another substrate material [17] and by changing the angle under which the spermatozoa enter at the separation part [18, 19]. The MISS device has also been used for other purposes, like the separation of hyperactivated boar spermatozoa using chemotaxis [20] or the prevention of polyspermic penetration in porcine IVF [21].

For the motility determination in a microfluidic chip the motile spermatozoa are firstly separated from the semen and subsequently detected. We use the same principle for the separation of the swimming spermatozoa from semen which method is also used for the separation of spermatozoa for IVF and ICSI procedures as mentioned earlier and used in the MISS device. Furthermore with our microfluidic chip the spermatozoa that cross the barrier between both liquid flows and the ones that do not, are detected using electrical impedance measurements. First we describe the two parts of the microfluidic chip in more detail. Next a model of the spermatozoa behaviour in the chip is proposed. Subsequently the measurement setup, the samples and the experiments are described, followed by the results of these experiments and a discussion. This chapter ends with some conclusions.

6.2 Microfluidic chip

6.2.1 Design

The microfluidic chip that has been developed for the assessment of spermatozoa motility contains two important functions: the separation and the detection (see figure 6-1). The separation part is based on the principle used for the selection of spermatozoa for assisted reproductive technologies [14, 15]. At the separation channel two fluid streams join and due to a low Reynolds number, both streams are in laminar flow. When immotile spermatozoa are placed in one stream, they will stay in

this stream even when they meet the other stream. However, motile spermatozoa are able to swim out of the stream ending up in the other stream. Hyakutake and co-workers did some numerical simulations on the MISS design and found that the depth of the channel has negligible influence on the separation efficiency, which was however largely dependent on the residence time that the spermatozoa are in the separation channel. The separation efficiency can roughly be predicted by the mean liquid velocity in the separation channel. Also the width of the sample inlet has influence on the separation efficiency as a result of a change in the sample flow [22]. The ratio of the sample inlet channel width to medium inlet channel width of the MISS device described by Cho and co-workers is 1:3 and with this ratio about 40% of the motile spermatozoa at the sample inlet ended up in the other outlet 2 [14].

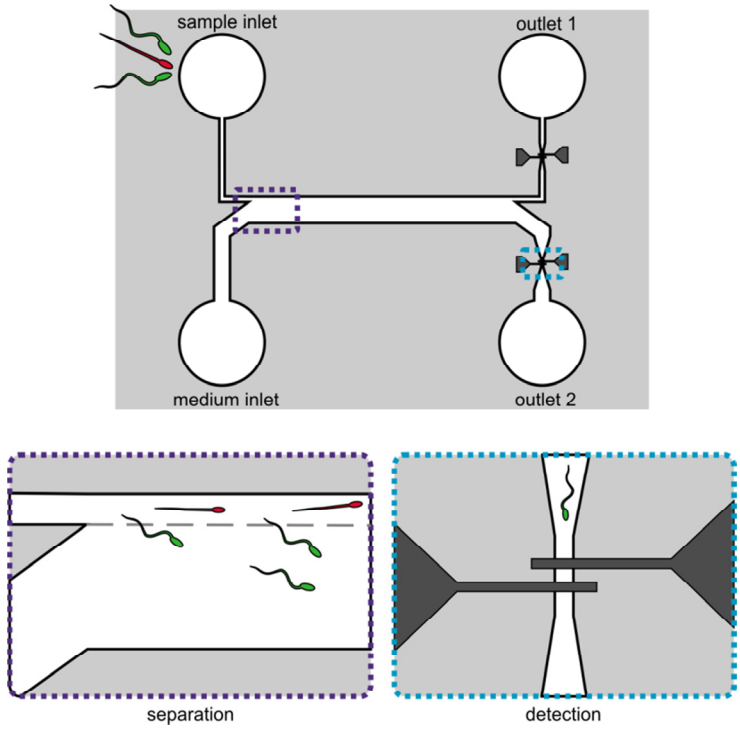

figure 6-1 Schematic overview of the chip design. It has two main parts: the separation channel (left) and two detection regions (right). Motile spermatozoa (green) are able to cross the laminar flow barrier (dashed line) and will end up in outlet 2 while immotile ones (red) will stay in their streamlines and flow to outlet 1.

The detection region of our microfluidic chip consists of a planar electrode pair were the outlet channels taper to a width of 38 µm (see figure 6-1). This electrode configuration is based on earlier work used for the concentration measurements, where each spermatozoon that passes the electrode pair has been detected with impedance measurements [7]. For this the measurement frequency needs to be chosen at a frequency below 1-3 MHz, since then cells behave like insulating spheres [23, 24] but also at a frequency high enough where the influence of the electrical double layer capacitance at the electrodes can be neglected [7].

Except for the depth, our microfluidic chip has the same dimensions as the MISS device reported earlier [14]. The width of the sample and medium inlet channels are 100 µm and 300 µm respectively. The length of the 500 µm wide separation channel is 5 mm and all channels in the glass-glass chip are 18 µm deep. Both electrodes of each electrode pair are 20 µm wide and have an interelectrode distance of 30 µm.

6.2.2 Fabrication

For the fabrication of the microfluidic chip the same process is used as for the chip developed for the determination of the concentration [7] (see paragraph 4.3.1). In short, two 500 µm thick 100 mm Borofloat glass wafers were used as substrates. In one glass wafer the microfluidic channels were isotropically etched with a 25% HF solution using a Cr/Au mask. The inlets and outlets were powderblasted from the other side of the wafer using a photopatternable foil. The other glass wafer contains the Pt electrodes. This wafer was patterned first with photoresist and a recess was made using isotropically etching with HF. Next an adhesion layer of Ta was sputtered followed by the Pt layer, the resist was removed such that embedded electrodes were created. At the end, both glass wafers were bonded together, followed by dicing, resulting in separate microfluidic chips.

6.3 Method

6.3.1 Model

The design of the microfluidic chip has similarities with a Y-mixer. For this mixer an analytical model has been proposed for the determination of the concentration distribution c in the microchannel for an arbitrary mixing ratio between the solute ($c=C_0$) and solvent stream ($c=0$). The dimensionless concentration distribution $c_n=c/C_0$ in the microchannel can be determined with the following equation:

$$c_n(x_n, y_n) = r_s + {}^{2}/_{\pi} \sum_{n=1}^{\infty} {}^{\sin(nr_s\pi)}/_{n} \cdot \cos(n\pi y_n)$$

$$\times \exp\left(\left({}^{-2n^2\pi^2}/_{Pe + \sqrt{Pe^2 + 4n^2\pi^2}}\right) x_n\right) \qquad (6\text{-}1)$$

with x_n=x/w_{ch} and y_n=y/w_{ch} dimensionless coordinates, w_{ch} the channel width, r_s the ratio of the width of the sample stream to the width of the separation channel and Pe the Peclet number defined as:

$$Pe = {}^{Uw_{ch}}/_{D} \qquad (6\text{-}2)$$

with U the velocity in the channel and D the diffusion coefficient [25]. In this model it is assumed that the flow velocity across the channel width is homogeneous, which is valid for our chip since the width of the channel is several times larger than the depth. In general, this model is used to determine the concentration of a specific solute across the channel width. Here this model is used for the theoretical determination of the separation efficiency of motile and immotile spermatozoa in our microfluidic chip. The diffusion coefficient of immotile spermatozoa is $1.5 \cdot 10^{-13}$ $m^2 \cdot s^{-1}$ [14], but it is unknown for motile spermatozoa and needs to be determined. We want to describe the random movement of a spermatozoon in flow with a model analogous to that of the Brownian movement of a small particle (see figure 6-2). The diffusion coefficient D for molecules can be determined as follows:

$$D = {}^{\langle x^2 \rangle}/_{2t} \qquad [m^2 \cdot s^{-1}] \qquad (6\text{-}3)$$

$$\langle x^2 \rangle = {}^{\langle u \rangle^2}/_{b} \qquad [m^2] \qquad (6\text{-}4)$$

with $\langle x^2 \rangle$ the mean-square displacement, t the time, <u> the average velocity of a molecule and b the number of intermolecular collisions it encounters per unit time [26]. Since a diffusion coefficient for motile cells does not exist, we define the apparent mobility D_m, which can be used as measure for the diffusion coefficient. To get the apparent mobility of motile spermatozoa a comparable calculation has been performed. Note that the motile spermatozoa swim more or less at a constant velocity, while molecules having Brownian motion show different velocities during their random walk. For sake of simplicity it is assumed in our model that the difference in velocity distribution hardly influences the calculation of the apparent

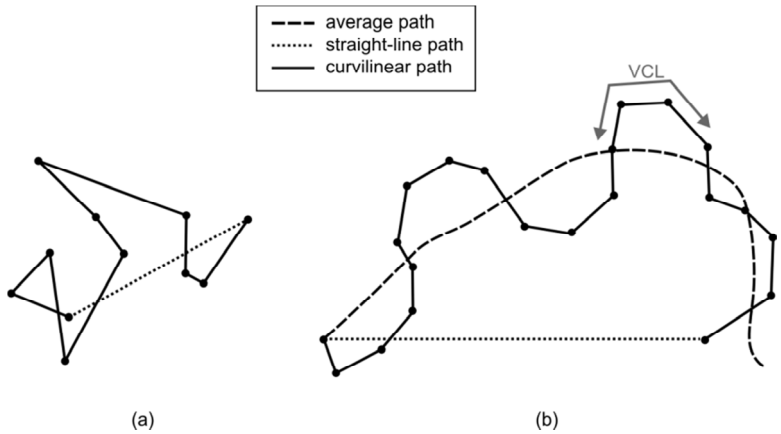

figure 6-2 (a) the Brownian motion of a molecule in a lipid bilayer (modified from [26]); (b) the swimming behaviour of a spermatozoon (modified from [6]).

mobility. From a local pig insemination centre the average results of swimming characteristics of boar spermatozoa are obtained, which are determined with a CASA system. The beat-cross frequency (39.3 Hz) has been used as the number of intermolecular collisions b, since it is defined by the WHO as: "the average rate at which the sperm's curvilinear path crosses its average path" [27]. For the average velocity <u> the curvilinear velocity (175.2 $\mu m \cdot s^{-1}$) has been used, which describes the average velocity of the head of the spermatozoon along its actual curvilinear path [27]. Using these values, the apparent mobility for motile boar spermatozoa is calculated to be $3.9 \cdot 10^{-10}$ $m^2 \cdot s^{-1}$ and this value is used in the model. The diffusion coefficient of a sphere or spherical macromolecule can also modelled using the viscosity of the fluid η, the radius of the particle r_p and the temperature T [26]:

$$D = {}^{kT}/_{6\pi\eta r_p} \qquad [m^2 \cdot s^{-1}] \qquad (6\text{-}5)$$

with k the Boltzmann constant. According to this equation the behaviour of motile spermatozoa at 37 °C can be described by the diffusion of a 1.2 nm spherical particle by Brownian motion. For immotile spermatozoa ($D = 1.5 \cdot 10^{-13}$ $m^2 \cdot s^{-1}$) this is in correspondence with their size, namely 3 μm. A script in Matlab (R2007B, version 7.5.0.342, 2007) has been made to calculate the concentration distribution of immotile and motile spermatozoa for a specific flow ratio and residence time.

6.3.2 Measurement setup

In figure 6-3 a schematic diagram of the measurement setup is shown. During the measurements the chip was placed in a chipholder on an inverted microscope (Leica CTR 6000, Leica Microsystems GmbH, Wetzlar, Germany), such that visual verification is possible. Fluidic connections to the chip were made using Upchurch nuts and ferrules (Upchurch Scientific, Oak Harbor, WA, USA) that were screwed into the chipholder, resulting in reliable connections between the glass capillaries and the inlets and outlets of the chip. With two Harvard PHD2000 syringe pumps the fluid was pumped through the chip. Besides the fluidic connections, the chipholder had also a connection for a printed circuit board, making electrical connections possible.

For the electrical impedance measurements a HF2IS impedance spectroscope in combination with a HF2CA current amplifier (both Zurich Instruments, Zurich, Switzerland) were used. For each electrode pair a sine wave (200 kHz, 2 V_{PP}) was generated by the spectroscope and verified with an oscilloscope (Agilent Technologies, type DSO3062A). A current amplifier was positioned close to the chip and connected to the electrodes on the chip and the input of the spectroscope that captured the two signals simultaneously at a sample frequency of 899 Hz. From the captured signals the electrical impedances at both electrode pairs were calculated using Matlab (R2007B, version 7.5.0.342, 2007, the Mathworks Inc). A Matlab script was used for the calculation of the peak heights in the electrical impedance signals using the same method as in previous work [7] (see paragraph 4.3.2).

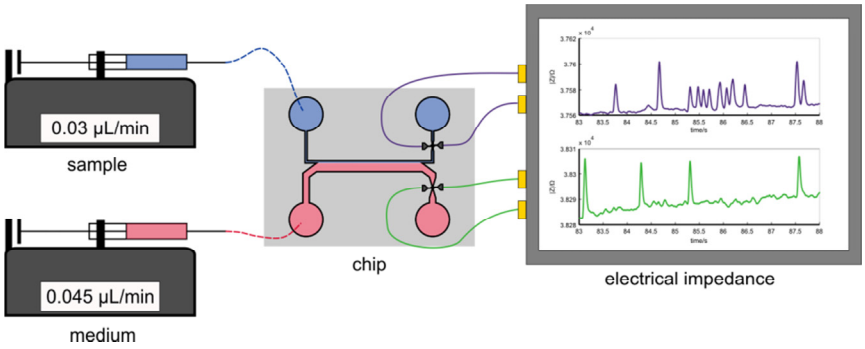

figure 6-3 A schematic diagram of the measurement setup.

6.3.3 Samples

In the first experiments Ferticult™ Flushing medium, a chemically balanced salt solution, HEPES buffered with 0.4% HSA, purchased from Fertipro NV (Beernem, Belgium) was used as background electrolyte, since this washing medium was also used for the concentration determination [7]. For the flow ratio experiments, Brilliant Blue FCF (E133) was used as medium to optically distinguish both liquid streams. Polybead Polystyrene Violet Dyed beads with a diameter of 3 µm were used, obtained from Polysciences Inc (Warrington, Pennsylvania, USA). Instead of human semen, boar semen obtained from a local pig insemination centre was used for the experiments since this is good quality semen that can be stored at 17 °C for several days without losing quality. The boar semen was kept in Solusem®, a modified BTS extender (AIM Worldwide, Vught, the Netherlands) and used as background electrolyte during all the semen experiments. To obtain immotile spermatozoa samples, the semen samples were heated to 56 °C for 30 minutes prior to the experiment [28].

6.3.4 Experiments

With the microfluidic chip a total of four different experiments were performed. First the frequency characteristics of the chip filled with background electrolyte used for the semen samples were determined. Only the frequency behaviour was determined with Solusem® as medium, since in earlier work the frequency behaviour of a chip filled with washing medium was already investigated. Therefore the chip was filled with Solusem® and with the HP impedance/gainphase analyser type HP4194A, controlled by LabVIEW (7 Express, version 7.1, 2004, National Instruments) the frequency behaviour from 100 Hz to 40 MHz was determined

In the second experiment the flow ratio was determined for the two inlets by adding Brilliant Blue FCF into the sample inlet and washing medium into the medium inlet. The optimal flow ratio is defined as the ratio where all the fluid that enters from the sample inlet into the chip flows to outlet 1 and all the fluid from the medium inlet ends up in outlet 2. To minimize the effect of diffusion, the flow rate at the sample inlet was set to 1 $\mu L \cdot min^{-1}$.

With the optimal flow ratio the electrical impedance detection at both electrode pairs was performed simultaneously. For this a suspension of beads ($\sim 1 \cdot 10^8$ mL^{-1}) in washing medium was added in the sample inlet, while the medium inlet was filled with only washing medium. After 30 seconds the flow ratio was changed from the optimal ratio to a ratio where some beads from the sample inlet end up in outlet 2.

In the last experiment a semen sample with only immotile spermatozoa and a highly motile sample were tested with the chip. For both samples the motility ratio M was determined:

$$M = {}^{n_{ep2}}/_{n_{ep1}} \tag{6-6}$$

with n_{ep1} and n_{ep2} the amount of counted spermatozoa at electrode pair 1 and electrode pair 2 respectively.

6.4 Results and discussion

6.4.1 Model

In figure 6-4 the concentration profiles in the separation channel, calculated with the analytical model, are shown for immotile and motile spermatozoa. The concentration profiles at the end of the channels for a residence time of 20 s and a flow ratio of 2:3 are shown in figure 6-5(a). Clearly no immotile spermatozoa cross the laminar flow barrier, while 25% of the spermatozoa swim to outlet 2. Assuming that the diffusion coefficient of motile human spermatozoa is the same as motile boar spermatozoa, the separation efficiency has also been calculated for the MISS chip of Cho and co-workers and amounted to 46%, which is slightly higher than the experimental value (40%) [14]. The separation efficiency of the MISS device is larger than the value obtained with our microfluidic chip, due to differences in flow ratio. The tapering in the outlet channel of our microfluidic chip causes a different flow ratio, making the width of the sample inlet stream larger and lowering the efficiency [22].

In figure 6-5(b) the influence of a different diffusion coefficient for motile spermatozoa is shown, showing that this has a significant effect on the separation efficiency and thus the ratio detected at outlet 2 (see figure 6-5(c)). In figure 6-5(d) the relation between the radius of a spherical particle and the diffusion coefficients is shown. As already mentioned, the diffusion coefficient of a motile spermatozoon determined from swimming characteristics, compares with the diffusion coefficient of a spherical particle with a radius of 0.6 nm.

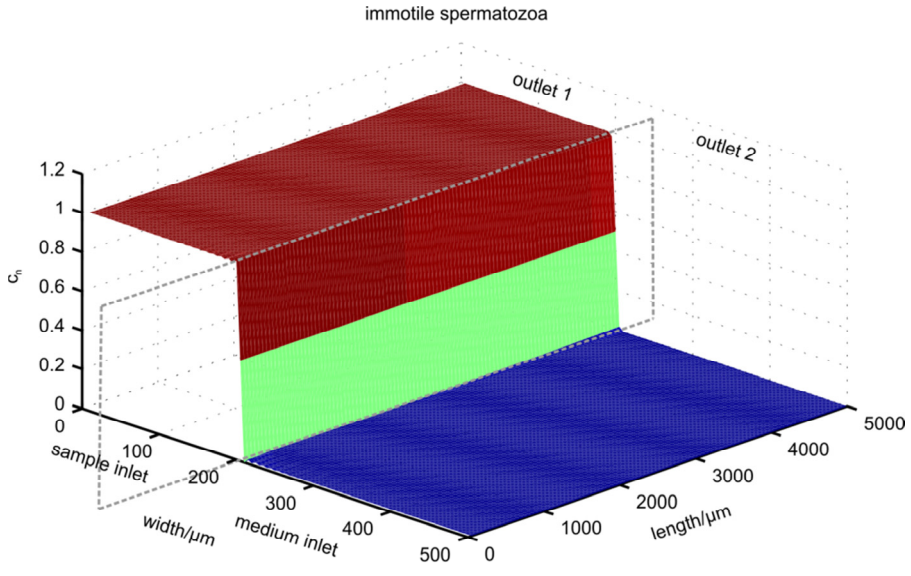

(a)

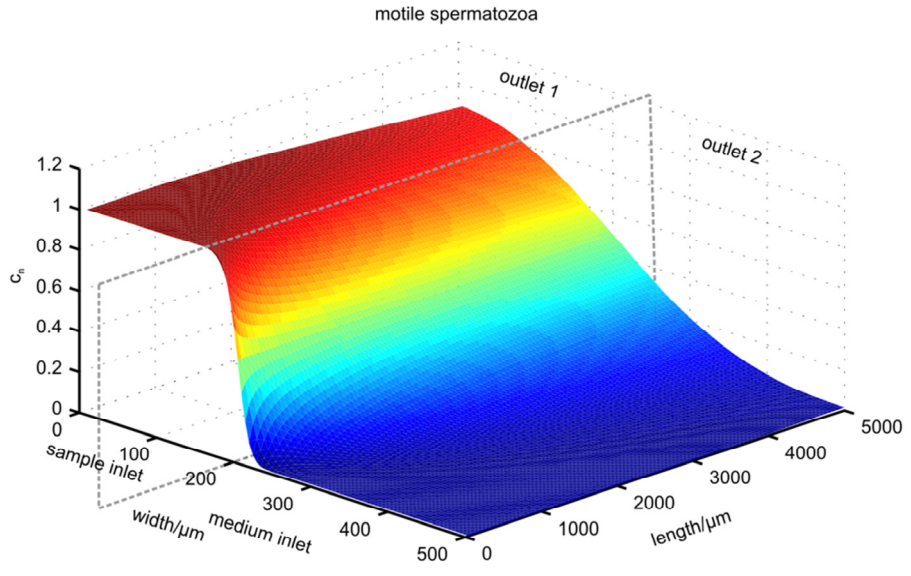

(b)

figure 6-4 The concentration profiles in the separation channel determined with the model for (a) immotile spermatozoa and (b) the motile spermatozoa.

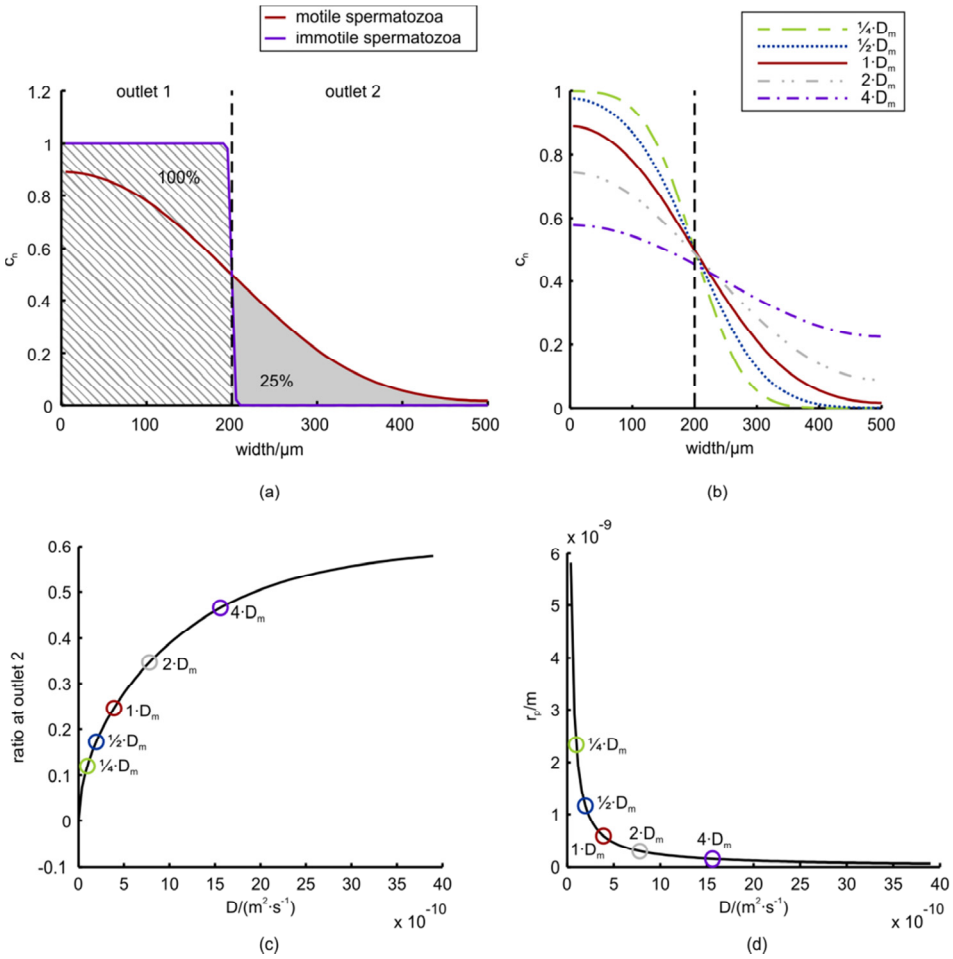

figure 6-5 (a) The concentration profile at the end of the separation channel for a residence time of 20 s; (b) the influence of a different diffusion coefficient on the separation efficiency; (c) the ratio at outlet 2 for different diffusion coefficients (residence time is 20 s, D_m is $3.9 \cdot 10^{-10}$ $m^2 \cdot s^{-1}$) and; (d) the relation between a diffusion coefficient and the radius of a spherical particle.

6.4.2 Frequency behaviour

In the first experiment the frequency behaviour of the microfluidic chip was investigated, such that the optimal measurement frequency for the next experiments could be determined. The optimal measurement frequency is that frequency where the bode plot shows a resistive plateau, indicating that the influence of the double layer capacitance can be neglected, and below 1 MHz to ensure that the cells behave

like isolating spheres [23, 24]. The background electrolyte (Solusem®) has a higher impedance, due to a lower specific conductivity of 0.7 $S \cdot m^{-1}$ than the washing medium (1.4 $S \cdot m^{-1}$) and for these two electrolytes a measurement frequency of 200 kHz fulfils both demands.

6.4.3 Flow ratio

Two fluid streams come together in the separation channel of the microfluidic chip and at this part of the chip motile spermatozoa are able to cross the laminar flow barrier. The flow rates at both inlet channels are important for the functioning of the chip. The fluid from the sample inlet has to arrive exclusively at outlet 1, while outlet 2 should only contain fluid from the medium inlet. To determine the required flow ratio, sample inlet 1 was filled with blue fluid and the medium inlet contained a clear fluid. In figure 6-6 several microscopic images of the microfluidic chip are given for six different flow ratios. Cleary a flow ratio of 2:3 is optimal for measurements with this chip, which is not in correspondence with the width ratio of 1:3 that exists between the channels at the entrance or exit of the separation channel. However, due to the tapering in the outlet channels at the position of the electrode pairs, the fluid resistances are changed in the outlet channels, causing this deviant flow ratio. This has been confirmed with calculations that showed a slightly lower ratio 2:2.3.

Besides the optimal flow ratio, also the residence time of a spermatozoon in the separation channel influences the separation efficiency [22] and in the MISS device the cells stay approximately 20 seconds in this channel [14]. The velocity and the residence time of 3 μm polystyrene beads in the separation channel were determined for different flow rates using the optimal flow ratio. From these results we choose flow rates of 0.030 $\mu L \cdot min^{-1}$ and 0.045 $\mu L \cdot min^{-1}$ for the sample inlet and medium inlet respectively, such that the particles stay about 23 seconds in the separation channel.

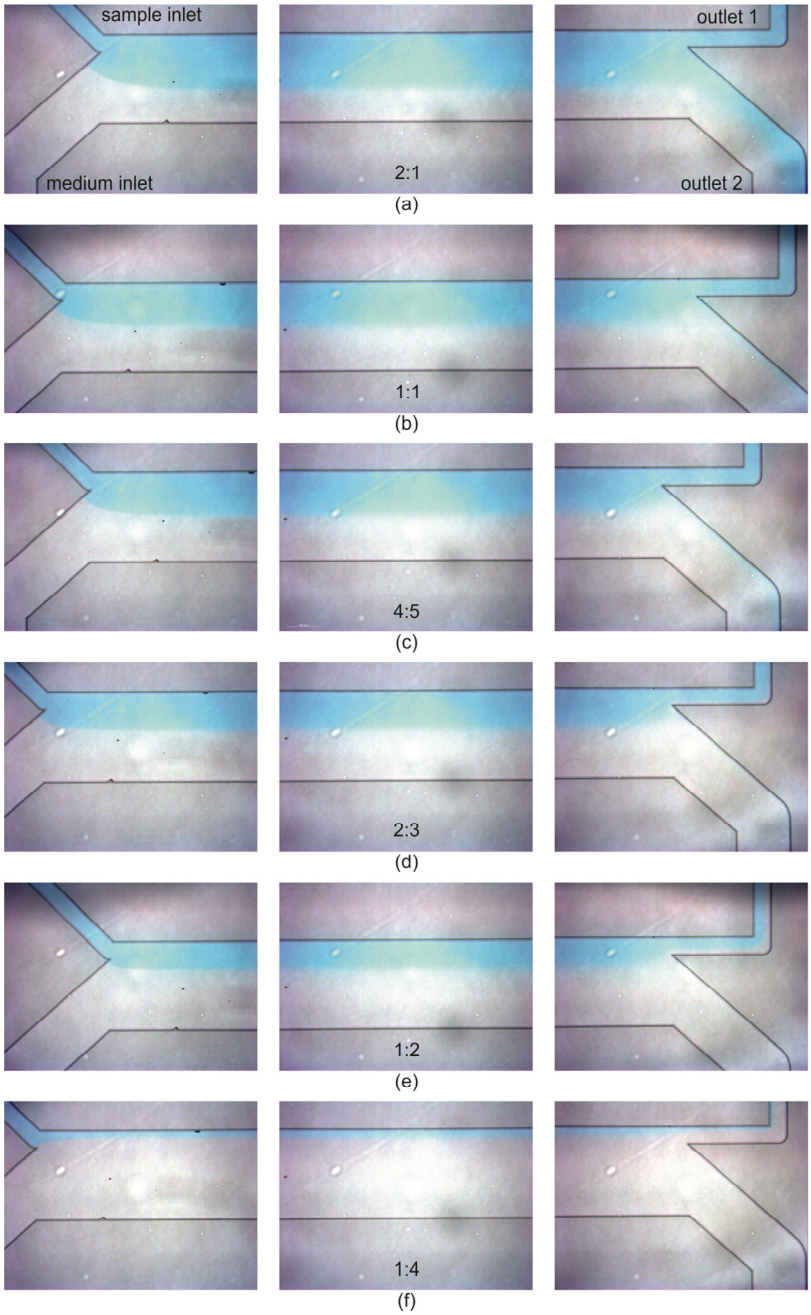

figure 6-6 Microscopic images of the flows in the chip for different flow ratios at both inlets. With a flow ratio 2:3 (d), the fluid from the sample inlet enters exclusively the channel of outlet 1.

6.4.4 Polystyrene beads

The second important function of the microfluidic chip is the detection of the cells in both outlet channels. Therefore a suspension of 3 µm polystyrene beads was put into the chip at the sample inlet and at the medium inlet only the medium (Ferticult™ Flushing medium) was added. After 30 seconds the flow rates were changed from 0.030 µL·min^{-1} and 0.045 µL·min^{-1} (2:3) for the sample inlet and medium inlet respectively, to 0.050 µL·min^{-1} and 0.025 µL·min^{-1} (2:1), such that beads also entered outlet channel 2. Every bead was electrically detected in outlet channel 1 and in outlet channel 2. A typical result of this experiment is shown in figure 6-7. About 35 seconds after changing the flow ratio, the first bead was detected at electrode pair 2. This time lag between changing the flow ratio and the detection is larger than the desired

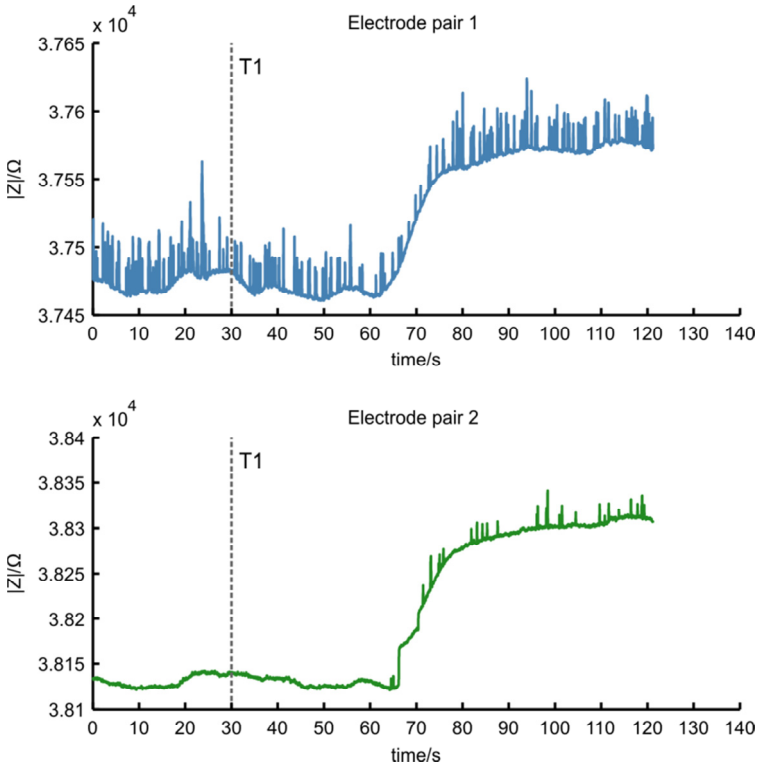

figure 6-7 Raw electrical impedance signals of the detection of 3 µm beads. After 30 seconds (T1) the flow ratio was changed form 2:3 to 2:1, such that the beads also enter the channel containing electrode pair 2. Note that the first bead at electrode pair 2 is detected after 65 seconds and that at the same time there is an increase in the overall impedance of both signals.

residence time in the separation channel, since the distance of a bead travelling to the detection area is larger than the length of the separation channel and the concentration of beads going to outlet channel 2 is low. In every experiment an increase of the impedance (<0.5%) in both signals is observed 35 seconds after changing the flow ratio. This is exactly at the moment the first bead is detected. Although there is obviously a correlation between both events, no clear explanation has been found yet.

6.4.5 Semen samples

Both the functioning of the separation channel and the detection regions were tested with the preceding experiments. In the final experiment the chip was first filled with a semen sample with dead spermatozoa. Subsequently a sample with highly motile spermatozoa containing 91% motile spermatozoa and 82% progressive motile spermatozoa was tested. These semen samples were obtained from a local insemination centre of pigs and checked with a calibrated CASA system. With both samples in total three measurements were performed. In figure 6-8 typical results of measurements with immotile and motile spermatozoa are shown. From the results the motility ratios of a motile and immotile semen sample were calculated and amounted to $2 \cdot 10^{-1}$ and $6 \cdot 10^{-3}$ respectively (see table 6-1), clearly indicating that this ratio is related to the motility. The factor of the apparent mobility is also calculated for the measurements, showing the same correlation. The advantage of this parameter is that it is independent of chip dimensions and experimental setting such as residence time. The measurements with dead spermatozoa gave rise to some problems. Due to the heating necessary to make them immotile, the membrane properties of the spermatozoa were changed [28], such that they tend to stick to each other and to the walls of the channel, resulting in less total detected spermatozoa at the electrode pairs.

In case of the measurements with motile cells, about 18% of these cells ended up in the outlet channel 2, which is lower than the efficiency calculated with our model (26% for residence time of 23 s). Several spermatozoa crossed the flow barrier, but were not detected at electrode pair 2 since a number of cells accumulated at the border of the separation channel, declining the efficiency. However, the ratios obtained with the three measurements were comparable with each other (see table 6-1), indicating that the percentage of cells that crosses the laminar flow barrier and is detected at electrode pair 2 is fixed. Therefore we expect that the ratio obtained with the microfluidic device can be correlated with the percentage of (progressive) motile spermatozoa. In future work the correlation between the spermatozoa motility and

the parameters determined with the microfluidic chip (ratio and factor of apparent mobility) will be further investigated.

With the gold standard of semen analysis at least 200 spermatozoa in replicate need to be evaluated before a reliable result can be obtained [6]. Every measurement with the motile sample lasted about 180 seconds and on average 189 cells were counted in each measurement. Of course the amount of detected cells depends on the concentration of the spermatozoa, but the results show that the motility assessment on-chip can be done within a few minutes, making it suitable for home testing. Besides the motility of spermatozoa, the concentration of spermatozoa is also an important parameter of a semen analysis. We already showed that it is possible to determine the concentration on-chip by the addition of a known concentration of beads to the semen sample [7]. This can easily be integrated on the microfluidic chip that we used for the motility assessment, assuming that the percentage of motile spermatozoa that accumulate at the border of the microfluidic channel is constant.

table 6-1 The motility ratios determined with the microfluidic chip for two semen samples, n = the number of cells counted, $x \cdot D_m$ is the diffusion constant determined with our model where x is the factor of apparent mobility.

Motility ratios of two semen samples with immotile and motile spermatozoa						
	Immotile sample			**Motile sample**		
	ratio	**n**	**x**	**ratio**	**n**	**x**
Measurement 1	0	75	0	0.15	211	0.4
Measurement 2	0.01	70	$5 \cdot 10^{-3}$	0.23	200	0.9
Measurement 3	0	27	0	0.23	156	0.9
Mean + standard deviation	0.005 ± 0.008		$3 \cdot 10^{-3}$	0.21 ± 0.045		0.7
Cumulative	0.006	172	$3 \cdot 10^{-3}$	0.2	567	0.7

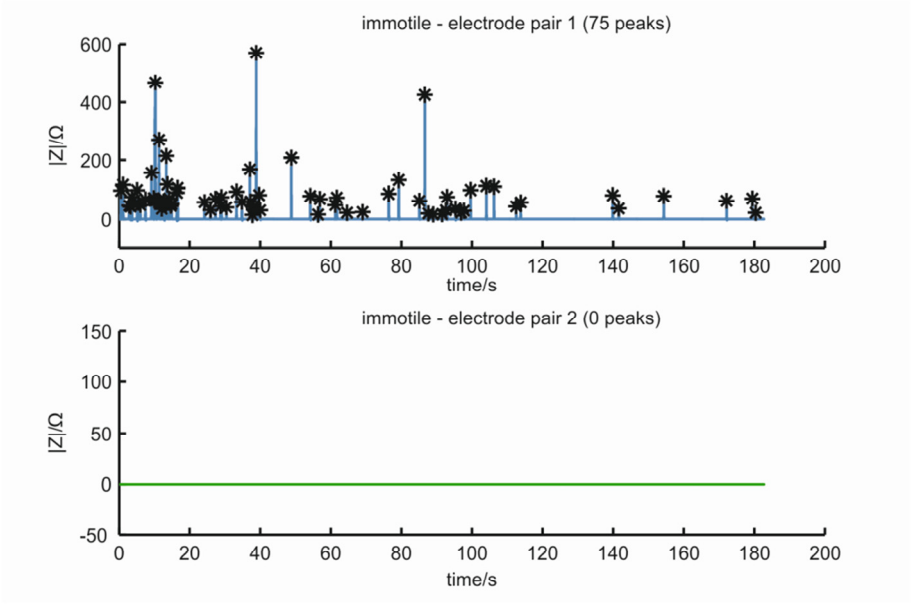

(a)

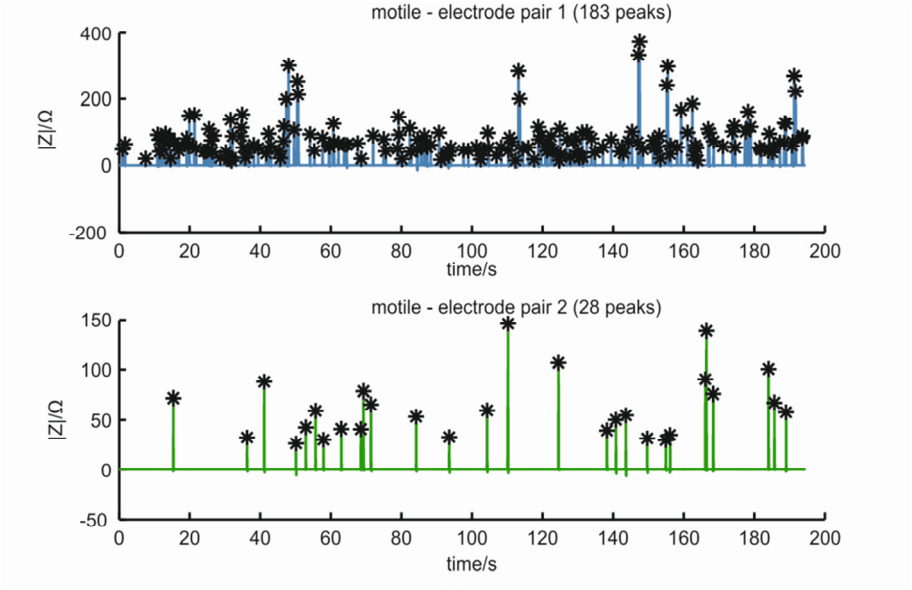

(b)

figure 6-8 Processed electrical impedance signals for (a) a semen sample with only immotile spermatozoa and (b) a sample with 91% motile spermatozoa.

6.5 Conclusions

A microfluidic chip has been developed that is used to determine the motility of spermatozoa in semen samples. The ability of motile spermatozoa to cross a laminar flow barrier was used for on-chip spermatozoa selection for assisted reproductive procedures and we used this in combination with electrical counting to measure the motility of spermatozoa in a semen sample. Based on the ratio detected at two outlet channels, a semen sample with highly motile spermatozoa could be distinguished from a sample containing immotile spermatozoa. A new model has been proposed similar to the model describing the Brownian motion (diffusion) of small particles, for the determination of the separation efficiency that uses the apparent mobility of spermatozoa as a measure for the diffusion constant. Future work will be focused on quantification of the motility of spermatozoa in semen samples and integration of the concentration determination on the same chip.

6.6 Acknowledgements

This research is supported by the Dutch Technology Foundation STW, which is an applied science division of NWO, and the Technology Program of the Ministry of Economic Affairs, Agriculture and Innovation. The chip fabrication by Johan Bomer and Lennart de Vreede are gratefully acknowledged, like the supply of boar semen samples and velocity data by the "KI station Twenthe" and PigGenetics (Hanneke Feitsma and Marleen Broekhuijse) respectively.

6.7 References

1. Eurostat. *Latest figures on the demographic challenges in the EU*. Demography report 2010 (2011) [cited 06/04/2011]; Available from: http://epp.eurostat.ec.europa.eu/portal/page/portal/eurostat/home.
2. Skakkebæk, N.E., et al., *Is human fecundity declining?* International Journal of Andrology, 2006. **29**(1): p. 2-11.
3. Aitken, R.J., P. Koopman, and S.E.M. Lewis, *Seeds of concern.* Nature, 2004. **432**(7013): p. 48-52.
4. Carlsen, E., et al., *Evidence for decreasing quality of semen during past 50 years.* BMJ, 1992. **305**: p. 609-613.
5. Jensen, T.K., et al., *Declining trends in conception rates in recent birth cohorts of native Danish women: a possible role of deteriorating male reproductive health.* International Journal of Andrology, 2008. **31**(2): p. 81-89.

6. WHO, *WHO laboratory manual for the examination and processing of human semen*. 5th ed. 2010, Geneva.
7. Segerink, L.I., et al., *On-chip determination of spermatozoa concentration using electrical impedance measurements.* Lab on a Chip, 2010. **10**: p. 1018-1024.
8. Kricka, L.J., et al., *Applications of a microfabricated device for evaluating sperm function.* Clinical Chemistry, 1993. **39**(9): p. 1944-1947.
9. Kricka, L.J., et al., *Micromachined analytical devices: microchips for semen testing.* Journal of Pharmaceutical and Biomedical Analysis, 1997. **15**(9-10): p. 1443-1447.
10. Su, T.-W., et al., *Compact and light-weight automated semen analysis platform using lensfree on-chip microscopy.* Analytical Chemistry, 2010. **82**(19): p. 8307-8312.
11. McCormack, M.C., S. McCallum, and B. Behr, *A novel microfluidic device for male subfertility screening.* Journal of Urology, 2006. **175**: p. 2223-2227.
12. Björndahl, L., et al., *Development of a novel home sperm test.* Human Reproduction 2006. **21**(1): p. 145-149.
13. Chen, Y.A., et al., *Analysis of sperm concentration and motility in a microfluidic device.* Microfluidics and Nanofluidics, 2011. **10**(1): p. 59-67.
14. Cho, B.S., et al., *Passively driven integrated microfluidic system for separation of motile sperm.* Analytical Chemistry, 2003. **75**: p. 1671-1675.
15. Schuster, T.G., et al., *Isolation of motile spermatozoa from semen samples using microfluidics.* Reproductive BioMedicine Online, 2003. **7**(1): p. 75-81.
16. Wu, J.M., et al., *A surface-modified sperm sorting device with long-term stability.* Biomedical Microdevices, 2006. **8**: p. 99-107.
17. Shibata, D., et al., *Analysis of the sperm motility and fertilization rates after the separation by microfluidic sperm sorter made of quartz.* Fertility and Sterility, 2007. **88**(Suppl. 1): p. S110.
18. Wu, T.-L., et al., *High efficient sperm motility sorting based on encoutered surve-straight micro streaming flow*. in *Microtas*. 2008. San Diego, USA.
19. Huang, H.Y., et al., *Improved quantity and quality of recovered motile spermatozoa with modified microfluidic system device with curve-straight channel.* Reproductive Sciences, 2010. **17**(3): p. 931.
20. Holt, W., et al., *Microfluidic sorting of boar spermatozoa*. in *16th International congress on animal reproduction* 2008. Budapest, Hungary.
21. Sano, H., et al., *Application of a microfluidic sperm sorter to the in-vitro fertilization of porcine oocytes reduced the incidence op polyspermic penetration.* Theriogenology, 2010. **74**: p. 863-870.
22. Hyakutake, T., et al., *Application of a numerical simulation to improve the separation efficiency of a sperm sorter* Biomedical Microdevices, 2009. **11**(1): p. 25-33.
23. Asami, K., *Characterization of biological cells by dielectric spectroscopy.* Journal of Non-Crystalline Solids 2002. **305**: p. 268-277.
24. Gawad, S., L. Schild, and P. Renaud, *Micromachined impedance spectroscopy flow cytometer for cell analysis and particle sizing.* Lab on a Chip, 2001. **1**: p. 76-82.

25. Nguyen, N.T. and Z.G. Wu, *Micromixers - a review.* Journal of Micromechanics and Microengineering, 2005. **15**(2): p. R1-R16.
26. Tinoco, I., et al., *Physical chemistry, principles and application in biological sciences*. Vol. 4th. 2002, New Jersey: Pearson education international.
27. WHO, *WHO Laboratory manual for the examination of human semen and sperm-cervical mucus interaction*. 4th ed. 1999, Cambridge: Cambridge University Press.
28. Jeyendran, R.S., et al., *Development of an assay to assess the functional integrity of the human-sperm membrane and its relationship to other semen characteristics.* Journal of Reproduction & Fertility, 1984. **70**(1): p. 219-228.

chapter 7

2D Fluorescence detection system*

In this chapter we describe a compact fluorescence detection system for on-chip analysis of beads, comprising a low-cost optical HD-DVD pickup. The complete system consists of a fluorescence detection unit, a control unit and a microfluidic chip containing microchannels and optical markers. With these markers the laser beam of the optical pickup can be automatically focused at the centre of the microchannel. With the complete system a two dimensional fluorescent profile across the channel width can be obtained, such that there is no need to dynamically focus the particles in a specific part of the channel. Fluorescent µm-sized beads suspended in medium have been detected with the system. Since on both sides of the main beam two additional laser beams at a known distance are generated, also the velocity of individual beads has been determined.

* Modified from: L.I. Segerink, M.J. Koster, A.J. Sprenkels and A. van den Berg. *A compact 2D fluorescence detection system for µm-sized beads on-chip*. Submitted.

7.1 Introduction

One of the first steps in the evaluation of the fertility of a man is a semen analysis. Based on several distinctive parameters of the semen, such as the concentration and motility of the spermatozoa, the quality of the semen is determined. Next to this standard semen analysis, evaluating other functional properties of spermatozoa can give additional information [1, 2]. Several specialized semen tests have been developed, such as the membrane vitality assessment and the DNA damage test. For both flow cytometry can be used to asses these [1]. Flow cytometry is widely used for the measurement of cell characteristics and it can also be used for the analysis of semen [3]. This is not only restricted to assessment of spermatozoa characteristics, such as the detection of apoptosis [4, 5], diploidy of the spermatozoon [6] or chromatin integrity [7], but also parameters assessed with a conventional semen analysis can be determined, such as the motility based on measuring the mitochondrial membrane potential [8] and the concentration of spermatozoa [4, 9]. Flow cytometry has also been used for sexing of spermatozoa based on DNA content [10]. In conclusion with flow cytometry reliable fast analysis of multiple parameters of cells can be performed, which is not possible with other techniques.

However, for flow cytometry an expensive, complex system is needed and operation of the system has to be performed by trained technicians [11]. Furthermore relative large sample and reagent volumes are required for the analysis [11]. To overcome these disadvantages and to make it applicable for microfluidic chips, we have developed a compact fluorescence detection system for on-chip analysis, which comprises a cheap HD-DVD pickup. The use of an optical detection system in combination with a microfluidic chip for the detection of particles or cells has already been reported [12-19], but most examples need hydrodynamic [12-15, 17] or electrokinetic [16, 18] focusing to position the particles or cells properly in the laser beam. In some of these examples optical components are integrated in the microfluidic chip, such as a (leaky) wave guide [13, 16] or an optical lens [15]. In another example cells are both fluorescently as electrically detected, enabling to distinguish between fluorescent and non-fluorescent cells [19]. Kostner and co-workers used a conventional DVD pickup in combination with a microfluidic chip for the detection of hydrodynamically focused cells by measuring the extinction using a mirror [12]. Besides the detection of cells, the DVD pickup has also been used for other applications, such as the detection of fluorescence in a DNA chip [20] and the investigation of microfluidic properties and microsurfaces [21]. In these two examples the scan function of the pickup was used, such that two-dimensional information about the position of painted fluorescent dye on a cover slip [20] and

surface profiles of silicon microstructures [21] were obtained. In yet another system only the lenses of the pickup in combination with an external laser source are used to detect different concentrations of a fluorescent dye [22]. Unlike these studies we used a HD-DVD pickup to measure the fluorescence in a microfluidic channel in two dimensions for the detection of fluorescent particles or cells, by using in advantage various of the existing functionalities of the pickup. Since a two-dimensional fluorescent profile across the channel is obtained, dynamic focusing of the sample is not needed.

In this chapter the development of the two-dimensional fluorescence detection system, the μflow, is described. First the complete system and the microfluidic chip are described in more detail, followed by a description of the samples and experiments. Subsequently the results of the experiments are shown and discussed. Finally some conclusions are given.

7.2 μFlow

With the μflow the fluorescence of a suspension in a microchannel of a microfluidic chip can be measured. The complete system comprises a fluorescence detection part, a microfluidic chip and a control part as shown in figure 7-1.

7.2.1 Fluorescence detection system

For the fluorescence detection an optical pickup is used, since it is cheap and has already a lot of built-in functionality, thereby reducing complexity and costs. There are different optical pickup formats and their standards are shown in table 7-1. The highest resolution is achieved with the HD-DVD format and therefore the widely available PHR-803T pickup is used, that contains a 405 nm ultraviolet laser. Since the PHR-803T is backwards compatible with CD and DVD formats, it contains also a dual emitting laser diode with 660 nm and 780 nm wavelengths respectively.

Parts of the optical pickup are used in the fluorescence detection system, such as the focusing system, laser diodes and lenses (see figure 7-2). For the fluorescent detection a semiconductor photomultiplier (Hamamatsu S10362-11-100U, Hamamatsu Photonics GmbH, Herrsching am Ammersee, Germany) has been used, which is smaller in size, more sensitive and cheaper than conventional photomultipliers. In front of this photomultiplier some additional optical components are placed that are not integrated in the optical pickup as shown in figure 7-2. The fluorescent light from the pickup first encounters the first beamsplitter (Thorlabs MD416, Thorlabs GmbH, Dachau/Munich, Germany), followed by the second

beamsplitter (Thorlabs 480, Thorlabs GmbH, Dachau/Munich, Germany) that transmits light with a wavelength larger than 480 nm. After this beamsplitter both the transmitted as well as the reflected light pass each a bandpassfilter, are converged by a Plano-Convex lens (NT47-872-INK, Edmund Optics Ltd, York, UK) and finally the intensity of the light is measured by the semiconductor photomultiplier. The bandpassfilters used for the transmitted and the reflected light are the Thorlabs MF525-39 and the Thorlabs FB450-40 (both Thorlabs GmbH, Dachau/Munich, Germany) respectively.

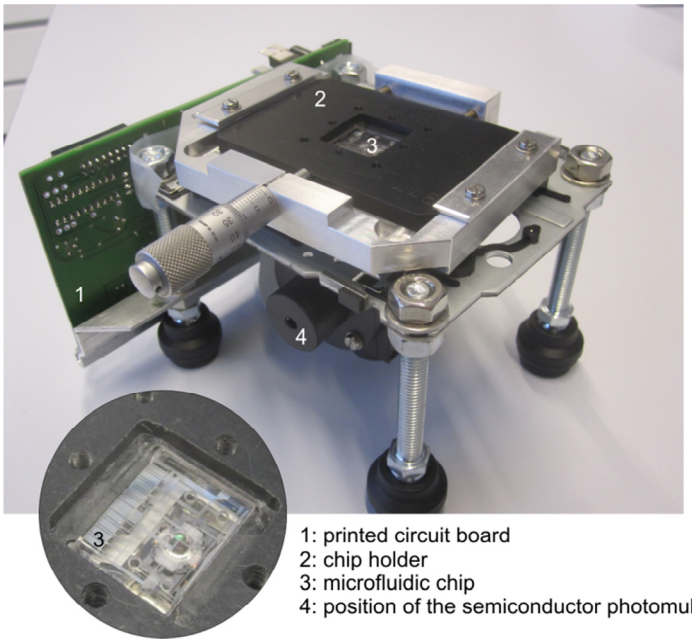

figure 7-1 A photograph of the home-built fluorescence detection system containing the microfluidic chip. The top of the chip holder (2) is removed to show the microfluidic chip.

table 7-1 Specification of optical formats used in pickups (λ is the wavelength and NA is the numerical aperture).

The standards of the CD, DVD and HD-DVD format			
	CD	**DVD**	**HD-DVD**
λ [nm]	780	660	405
NA	0.45	0.60	0.65
Resolution [µm]	1.06	0.67	0.38

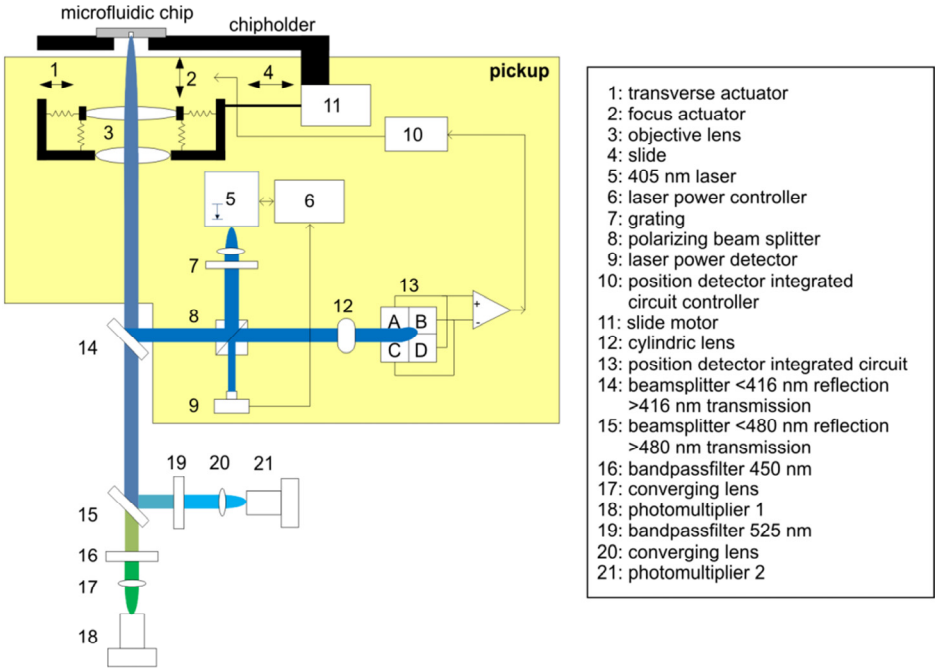

figure 7-2 Schematic overview of the fluorescence detection system built around the PHR-803T HD-DVD pickup.

Due to the high resolution of the HD-DVD pickup, the depth of focus is small, meaning that focusing the laser light on the microfluidic chip is critical. In the PHR-803T an autofocus function is incorporated that uses the astigmatic principle. The beam profile that is projected on the Position Detector Integrated Circuit (PDIC) by the cylindric lens with two focal points, is circular when it is in focus and elliptic when it is out of focus (see figure 7-3(a)). This can be measured by the focus error signal (FES) given by:

$$FES = A_{PDIC} + D_{PDIC} - B_{PDIC} - C_{PDIC} \qquad [V] \qquad (7\text{-}1)$$

with A_{PDIC}, B_{PDIC}, C_{PDIC} and D_{PDIC} the voltages corresponding to the projected beam on the photodetectors of the PDIC (see 13 in figure 7-2) [12, 20]. When the FES signal is minimal, the laser beam is below the marker, while at its maximum value it is above. By adjusting the vertical position of the lenses by the focus voice coil actuator, the focus point is changed.

Not only the vertical position of the lens can be changed with the voice coil actuator, but also the horizontal position. With horizontal positioning it is possible to position the laser beam at the correct spot on the microfluidic chip as long as the horizontal displacement is smaller than 1 mm. For larger and coarser displacements the slide motor of the optical pickup may be used. With the voice coil actuator a scan in the horizontal plane can be made, such that the fluorescence profile in two-dimensions can be obtained.

A LabVIEW interface (2010 SP1, National Instruments) is used to manage the microcontroller and data acquisition card which are used to control the complete system. Together with a microcontroller program this interface is used to configure the settings, automatically find the position of the channels on the chip and perform the measurements in real-time.

7.2.2 Microfluidic chip

The sample that needs to be investigated is located in a microfluidic channel of a glass-glass chip. The microfluidic chip contains three microchannels that are all 18 μm deep and 100 μm wide. Optical reflective markers are integrated on the chip and are used by the implemented autofocus and channel-find algorithms. In figure 7-3(a) the working principle of the autofocus and positioning of the laser beam in the centre of a microchannel is shown. The intensities on the four photodetectors (A - D) of the PDIC are used as input for the autofocus and the channel-find algorithms.

The microfluidic chip was made from two 500 μm 100 mm Borofloat glass substrates and the same fabrication process is used as described in chapter 4. The transmission of Borofloat glass for the used wavelengths is 90%. On one glass substrate the microchannels were isotropically etched with HF after patterning the substrate with a Cr/Au mask. The inlets and outlets of the microchannels were powder blasted from the backside of the substrate. On the other substrate the optical markers were realized, embedded in the substrate by a lift-off technique. After making a recess in the glass substrate using a photoresist mask, Pt was sputtered with Ta as adhesion layer. Subsequently the photoresist was removed, leaving the markers behind. The two glass substrates were bonded together and finally diced forming the microfluidic chips.

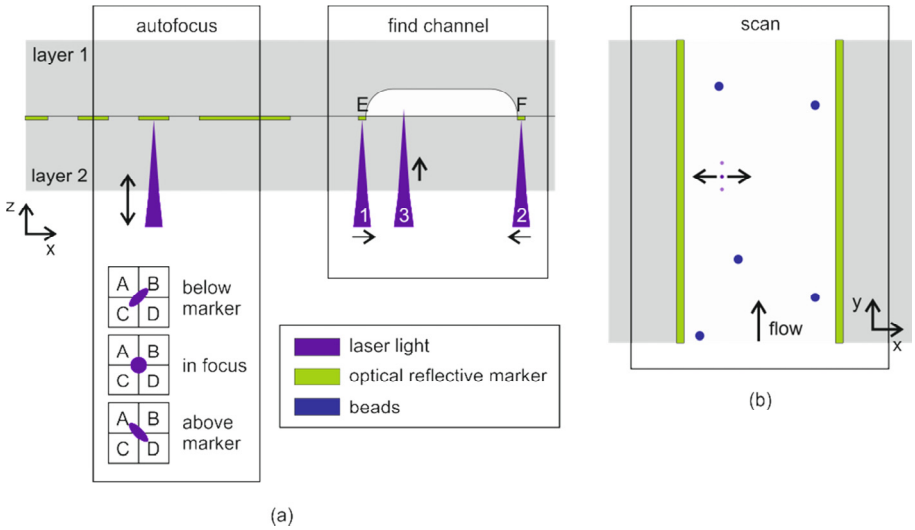

figure 7-3 Schematic picture of the microfluidic chip with the optical reflective markers. (a) Cross section of the microfluidic chip. First the laser light of the optical pick up is focused on reflective markers. When a circular light spot on the PDIC is measured, the laser light is in focus. Subsequently the microfluidic channel is found by moving the chip horizontally and detecting markers E and F on the chip. (b) The two-dimensional scan of the laser light in the microchannel shown in a view from above.

7.3 Experimental setup

7.3.1 Samples

As medium Ferticult™ Flushing medium, which is a chemically balanced salt solution, HEPES buffered with 0.4% HSA was used, purchased from Fertipro NV (Beernem, Belgium). Two sizes of fluorescent beads were used: PeakFlow™ Blue flow cytometry beads (P-14826) with a diameter of 6 µm and PeakFlow™ Blue flow cytometry beads (P-14825) with a diameter of 2.5 µm, which were obtained from Invitrogen (Paisley, UK). Both beads have an excitation wavelength between 350-370 nm and an emission wavelength of 450 nm. As non-fluorescent beads Polybead Polystyrene Blue Dyed beads were used, obtained from Polysciences Inc (Warrington, Pennsylvania, USA), having a diameter of 6 µm.

7.3.2 µFlow testing

Before experiments with beads in a suspension were performed, some of the functionalities of the µflow were tested. First the frequency responses of the focus and transverse voice coil actuators of the optical pickup were determined with a laser Doppler vibrometer, from which the resonance frequencies of both voice coil actuators could be determined. The resonance frequency of the transverse voice coil actuator is used for all two-dimensional scans in the microchannel (see figure 7-3(b)).

Subsequently both the autofocus and channel detection algorithms were tested. In this test a microfluidic chip was placed in the chip holder with the top of the chip holder in place, preventing interfering light disturbing the measurement.

7.3.3 Detection of beads

After testing the correct functioning of the µflow and both algorithms, experiments with fluorescent beads in suspension were performed. The 6 µm fluorescent beads were diluted in the medium to a concentration of $3.4 \cdot 10^6$ mL^{-1} and a sample of this suspension was introduced in the chip. Difference in the heights of the fluid columns on the inlet and outlet of the microchannel were used to generate a proper fluid flow. With the laser a two dimensional scan is made perpendicular to the flow direction (see figure 7-3(b)) which was performed at the resonance frequency of the voice coil actuator for optimal response. During each scan period 100 sample points are collected, meaning that 50 samples are collected for the area of interest since during one period the area of interest is scanned twice. The same experiment was performed with a suspension of 2.5 µm fluorescent beads in medium which has a concentration of $2.4 \cdot 10^6$ mL^{-1}. Finally, an experiment with 6 µm non fluorescent beads was performed.

7.4 Results and discussion

A compact fluorescence detection system, the µflow, has been developed which is 20 x 15 x 15 cm^3 in size. For the autofocus and channel-find algorithms the original PDIC of the optical pickup is used, while for measuring the fluorescence in the microchannel the added semiconductor photomultiplier has been used.

7.4.1 µFlow testing

With a laser Doppler vibrometer, the frequency responses of the focus and transversal voice coil actuators were measured. From these responses the resonance frequencies

were calculated and amounted to 64 Hz and 68 Hz for the focus and transverse voice coil actuators respectively.

The FES value obtained from the PDIC is used for the autofocus algorithm. To test this algorithm the laser beam was positioned under an optical marker and subsequently the focus was varied 50 µm in vertical direction starting out of focus above the marker. As shown in figure 7-4 the FES response of the PDIC changes during the measurement in vertical direction as expected. A maximum in the FES response corresponds to the situation where the focus of the laser light is above the marker, while a minimum in the response occurred when the focus of the light is below the marker. Between the maximum and minimum the FES response has a linear range and this is used in the autofocus algorithm. First the position of the maximum of the FES response is determined and subsequently the laser is moved to the position where the optical marker is in focus.

For the detection of markers on the microfluidic chip the beam intensity on the PDIC is used. In figure 7-4 it is clearly seen that the intensity of the PDIC is dependent on the vertical position of the laser light. The intensity gets smaller when the optical marker is out of focus. The value of the PDIC is compared with a threshold voltage, eliminating the influence of the PDIC noise. For a laser illumination power of 1.5 mW the marker is still detected when the focus of the laser is 17 µm below or 13 µm above

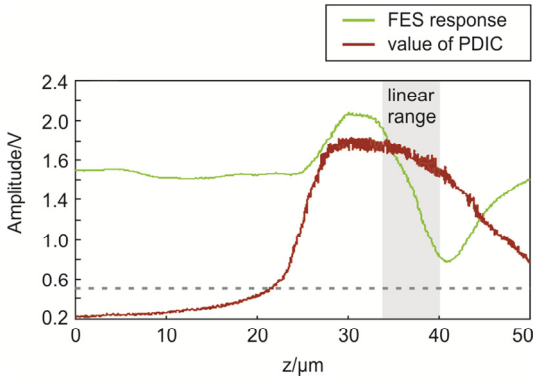

figure 7-4 The measured FES response with an offset of about 1.5 V and PDIC value when the focus of the laser light (1.5 mW) was varied 50 µm in vertical direction starting out of focus above the marker. The grey area is the linear range of the FES response (slope 0.27 V·µm^{-1}, range 6.8 µm). The dashed line indicates the threshold used for marker detection.

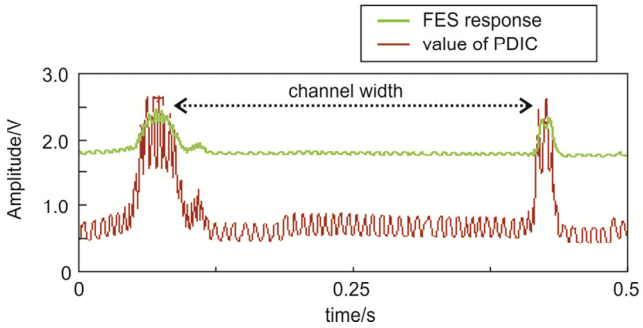

figure 7-5 Results of the channel detection. Next to the border of the channel are reflective makers which are detected (the peaks in the signals). The distance between the peaks corresponds to the channel width.

the marker, which is the practical focusing range of the system. However, when the chip is placed in the chipholder, the chip may be tilted somewhere between 50 and 100 µm, more than the tolerance used for the marker detection. To compensate for this tilt, the position of the focus is determined at both sides of the chip and these results are used in the channel-find algorithm.

The channel-find algorithm makes use of the different optical markers on the chip to locate one of the three microchannels. With the LabVIEW interface the channel of interest could be selected and after determining the focus point with the autofocus algorithm, the laser light is automatically positioned in the middle of the channel of interest within a minute. In figure 7-5 a horizontal scan of a microfluidic channel containing no fluid is made starting at the left side of the channel. Clearly the markers at each side of the channel are detected which can be seen in the value of the PDIC signal.

7.4.2 Detection of beads

For the detection of fluorescent particles in the microchannel, the lens of the optical pickup scans perpendicular to the flow direction at a frequency of 65 Hz driven by the transverse voice coil actuator. The scan width could be chosen with the software and a total of 50 fluorescent intensity samples are taken per period in this area of interest. Due to the scanning, there is no need to dynamically focus the particles in the microchannel, making the system far less complex. In figure 7-6 the detection results of 6 µm fluorescent beads are given. The scan width was chosen to be 100 µm, resulting in a resolution of 2 µm per pixel. Note that the diameter of the beads in the fluorescent scan is larger than the actual size. This broadening can be explained by

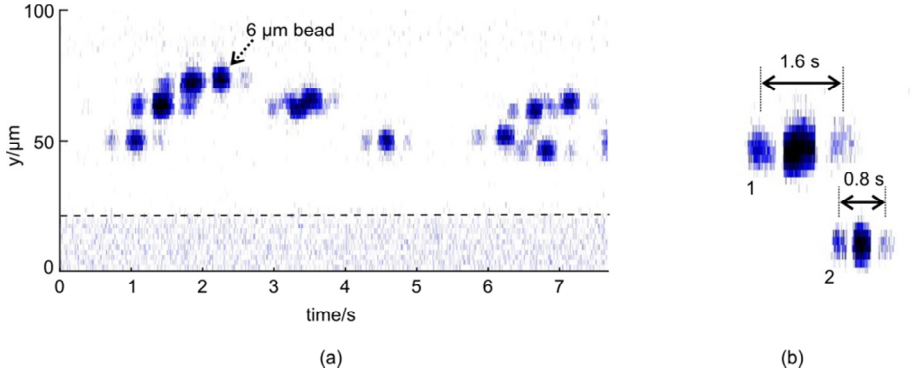

figure 7-6 (a) A two-dimensional image of cross-section of the microchannel containing multiple 6 µm fluorescent beads. The dashed line indicates the channel wall. (b) The detection of two 2.5 µm beads in the microchannel. Note that every bead is also detected by the two side beams of the laser light and the time between the detection of the bead is determined.

the shape of the laser light and the vertical position of the bead in the microchannel. The laser beam in the optical pick up has a Gaussian light intensity distribution. When a bead is scanned, the bead is already detected when the border of the laser beam touches the bead, causing a fluorescence detection signal at that position. Since the laser beam has also a certain diameter, this is added twice to the actual bead diameter, making the detected size of the bead larger. In case the bead is out of focus, thus in a lower or higher position in the channel than the focus point of the laser beam, the diameter of the laser light is even larger, increasing the measured size of the bead even more.

Besides the main laser light, also two additional side beams are generated by the optical pickup (see figure 7-3(b)), so every bead is detected three times. In figure 7-6(b) two 2.5 µm fluorescent beads are shown. Clearly the detection of the beads by the side beams can be seen. The time delay between the side beams can be derived from the two-dimensional image and since the distance between the side beams is fixed (17.5 µm at focus position), the velocity of each individual bead can be determined. For example bead 1 and bead 2 in figure 7-6(b) have a velocity of 11 $\mu m \cdot s^{-1}$ and 22 $\mu m \cdot s^{-1}$ respectively. With the current setup, the limit of detection of 2.5 µm fluorescent beads is about 400 $\mu m \cdot s^{-1}$ are not always detected. By increasing the scan rate, this can be improved. Another improvement consists of combining the horizontal scan that is perpendicular to the flow direction with a vertical scan, resulting in a three-dimensional image of the fluorescence in the channel. Another

interesting possibility is to derive the vertical position of the beads in the microchannel from the three-dimensional image.

To verify that the two-dimensional images are the result of fluorescence and not caused by scattering of the light, non-fluorescent beads were also tested with the setup. The non-fluorescent beads could not be detected at all, indicating that only the fluorescence of the particles in the microchannel is measured.

7.5 Conclusions

A low-cost HD-DVD pickup can be used for real-time fluorescence measurements on chip, without the need for dynamic focusing the particles or cells in the microchannel. A two-dimensional image of the cross section of the microchannel is generated with the fluorescence detection system and it was possible to visualize fluorescent µm-sized beads in the microchannel, indicating that also fluorescently labelled cells can be detected. Due to the presence of two beams on both sides the main laser beam, also the velocity of each individual bead in the microchannel could be derived. Furthermore, electrodes can easily be integrated in the microchannel, such that electrical impedance measurements can be performed simultaneously, which may provide additional information about the particle or cell properties. Future investigation is focused on measurements of cell properties by incorporating electrical impedance measurements.

7.6 Acknowledgements

This research is supported by the Dutch Technology Foundation STW, which is an applied science division of NWO, and the Technology Program of the Ministry of Economic Affairs, Agriculture and Innovation. The fabrication of the framework of the µFlow by Hans de Boer and chip fabrication by Johan Bomer and Lennart de Vreede are gratefully acknowledged. We also thank Dr. H. Woelders of the Animal Sciences of Wageningen UR, the Netherlands.

7.7 References

1. Samplaski, M.K., et al., *New generation of diagnostic tests for infertility: Review of specialized semen tests.* International Journal of Urology, 2010. **17**(10): p. 839-847.

2. WHO, *WHO laboratory manual for the examination and processing of human semen*. 5th ed. 2010, Geneva.
3. Cordelli, E., et al., *Flow cytometry applications in the evaluation of sperm quality: semen analysis, sperm function and DNA integrity.* Contraception, 2005. **72**(4): p. 273-279.
4. Perticarari, S., et al., *A new multiparameter flow cytometric method for human semen analysis.* Human Reproduction, 2007. **22**(2): p. 485-494.
5. Oosterhuis, G.J.E., et al., *Measuring apoptosis in human spermatozoa: a biological assay for semen quality?* Fertility and Sterility, 2000. **74**(2): p. 245-250.
6. Kovács, T., et al., *DNA flow cytometry of human spermatozoa: consistent stoichiometric staining of sperm DNA using a novel decondensation protocol.* Cytometry part A, 2008. **73**: p. 965-970.
7. Evenson, D.P., et al., *Utility of the sperm chromatin structure assay as a diagnostic and prognostic tool in the human fertility clinic.* Human Reproduction, 1999. **14**(4): p. 1039-1049.
8. Evenson, D.P., Z. Darzynkiewicz, and M.R. Melamed, *Simultaneous measurement by flow-cytometry of sperm cell viability and mitochondrial-membrane potential related to cell motility.* Journal of Histochemistry & Cytochemistry, 1982. **30**(3): p. 279-280.
9. Eustache, F., P. Jouannet, and J. Auger, *Evaluation of flow cytometric methods to measure human sperm concentration.* Journal of Andrology, 2001. **22**(4): p. 558-567.
10. Seidel, G.E. and D.L. Garner, *Current status of sexing mammalian spermatozoa.* Reproduction, 2002. **124**: p. 733-743.
11. Huh, D., et al., *Microfluidics for flow cytometric analysis of cells and particles.* Physiological Measurement, 2005. **26**(3): p. R73-R98.
12. Kostner, S. and M.J. Vellekoop, *Cell analysis in a microfluidic cytometer applying a DVD pickup head.* Sensors and Actuators B: Chemical, 2008. **132**(2): p. 512-517.
13. Krüger, J., et al., *Development of a microfluidic device for fluorescence activated cell sorting.* Journal of Micromechanics and Microengineering, 2002. **12**: p. 486-494.
14. Yang, S.-Y., et al., *A cell counting/sorting system incorporated with a microfabricated flow cytometer chip.* Measurement Science and Technology, 2006. **17**: p. 2001-2009.
15. Rosenauer, M., et al., *Miniaturized flow cytometer with 3D hydrodynamic particle focusing and integrated optical elements applying silicon photodiodes.* Microfluidics and Nanofluidics, 2011. **10**(4): p. 761-771.
16. Fu, L.-M., et al., *Electrokinetically driven micro flow cytometers with integrated fiber optics for on-line cell/particle detection.* Analytica Chimica Acta, 2004. **507**(1): p. 163-169.
17. Wolff, A., et al., *Integrating advanced functionality in a microfabricated high-throughput fluorescent-activated cell sorter.* Lab on a Chip, 2003. **3**(1): p. 22-27.

18. Holmes, D., H. Morgan, and N.G. Green, *High throughput particle analysis: combining dielectrophoretic particle focussing with confocal optical detection.* Biosensors and Bioelectronics, 2006. **21**(8): p. 1621-1630.
19. Joo, S., et al., *A portable microfluidic flow cytometer based on simultaneous detection of impedance and fluorescence.* Biosensors and Bioelectronics, 2010. **25**(6): p. 1509-1515.
20. Kim, K.-H., et al., *A new DNA chip detection mechanism using optical pick-up actuators.* Microsystem Technologies, 2007. **13**: p. 1359-1369.
21. Yim, V., et al., *Multipurpose DVD pick-up scanner for analysis of microfluidics and micromechanical structures*. in *30th Annual International IEEE EMBS conference*. 2008. Vancouver, British Columbia, Canada.
22. Shimomura, T., C. Izawa, and T. Matsui, *A highly sensitive, highly reproducible laser-induced fluorescence detection system with optical pickup.* Measurement Science and Technology, 2008. **19**: p. 1-10.

chapter 8

Summary and outlook

In this chapter the main results and conclusions of this thesis are summarized. Subsequently some recommendations regarding the further development and validation of the fertility chip are given. In addition other use of the chip for instance in the veterinary sector may also be advantageously. As an example some promising preliminary results of the detection of leukocytes suspended in whole milk for the detection of mastitis are given.

8.1 Summary

Before assistive reproductive treatment will be started for a couple that is childless by default, the cause of the fertility disorder needs to be investigated for both the man as well as the woman. For the man this implies that the quality of his semen needs to be known. Currently, at the hospital laboratories the semen analysis is performed manually using a microscope or a CASA system, making it time-consuming and subjective or expensive. To overcome these disadvantages and make it applicable for testing in the private environment of the man, a start has been made towards the development of a fertility chip for semen analysis, which is described in this thesis.

Microfluidic chips offer several advantages for diagnostic purposes compared to the conventional laboratory systems. As stated in chapter 2 microfluidic chips have recently been developed for both the analysis of semen and spermatozoa as well as a tool to separate and select the 'best' spermatozoon/spermatozoa for IVF or ICSI procedures. Although some of these devices are already commercially available, they give only qualitative information about the semen which is unusable for treatment decisions by a gynaecologist. Therefore we have developed a microfluidic chip to quantitatively asses the semen quality.

With microfluidic impedance cytometry, the dielectric properties of cells flowing separately in a microchannel along an integrated electrode pair can be determined in a label-free, non-invasive way (chapter 3). The impedance is measured between an electrode pair and the passage of a single cell results in an impedance change. This change contains information about the cell size, membrane and the cytoplasm, but is also dependent on the electrode configuration in the microchannel, the electrolyte properties and the measurement frequency used. Due to the influence of the electrical double layer at the electrode-liquid interface and the parasitic capacitances at respectively low and high frequencies, the measurement should be preferably performed at intermediate frequencies such that the actual resistance of the electrolyte is measured. To determine the influence of the microfluidic chip design and the cell properties on the frequency behaviour, several models are discussed.

We use microfluidic impedance cytometry to determine the concentration of spermatozoa on-chip (chapter 4). For this a glass-glass chip has been developed consisting of a microchannel comprising a planar electrode pair. Spermatozoa are not the only cells that could be present in semen. In case of infection, semen will also contain leukocytes, making it necessary to distinguish these cell types from each other. It was shown that the change in impedance measured at 96 kHz with our microfluidic chip was related to the cell or particle size, allowing to distinguish between spermatozoa, leukocytes and 6 μm polystyrene beads suspended in washing

medium. By the addition of a known concentration of beads, the spermatozoa concentration could be determined on-chip without knowing the actual flow rate. In total 7 boar semen samples with concentrations in the subfertile and fertile range have been tested. The results show a good correlation with the actual concentration determined with a counting chamber, which is currently the gold standard.

The use of a planar electrode pair for microfluidic impedance cytometry has the advantage of an easy fabrication process. However, the electrical field distribution is inhomogeneous, such that the position of the cell in the microchannel has influence on the measured impedance change. For the concentration measurement this was not a problem, since the differences between spermatozoa, polystyrene beads and HL-60 cells were larger than the variation in impedance caused by the cell or particle position in the channel. However, if one will look at small differences in size or shape within one cell type, an electrode configuration with a more homogeneous electrical field should be used. A parallel electrode configuration has a more homogeneous field than a planar configuration, but it involves difficulties with the fabrication process and electrical connections to the outer world. Therefore a new parallel electrode configuration has been developed that does not suffer from these disadvantages (chapter 5). Compared to the fabrication process of planar electrodes, only one additional step is needed. The new parallel configuration consists of a floating electrode at the bottom of the channel, opposite of two planar electrodes in the channel, thereby creating two parallel electrode pairs. With this configuration polystyrene beads suspended in fluid were detected and the coefficient of variation of the impedance change was less compared to impedance changes measured with a planar electrode configuration, mainly due to a less dependency of the position of the beads in the channel.

Besides the concentration, the motility of the spermatozoa in a semen sample is also an important parameter for the semen analysis (chapter 6). A glass-glass chip consisting of a separation and a detection part has been used to determine this parameter. In the separation part, only motile spermatozoa are able to cross the barrier between two laminar liquid flow and these are counted at another electrode pair than the immotile spermatozoa and particles which stay in the main flow. A model has been proposed for the distribution of motile and immotile spermatozoa in the separation channel using the equivalent diffusion coefficients for both samples. For motile spermatozoa the apparent mobility has been calculated and used to calculate the concentration profile of motile spermatozoa in the separation channel for a specific flow ratio and residence time. Two samples, one containing immotile spermatozoa and the other highly motile spermatozoa, were tested with this chip. The ratio detected at the two outlet channels for these samples not only correlated with

the motility, but also with the calculated factor of the apparent mobility, which is a measure independent of dimensions of the microchannel and residence time of the cells in the chip.

Using electrical impedance detection, two important parameters of the semen analysis can be determined on-chip. However, additional information can be obtained when the functional properties of the spermatozoa are evaluated, which is not done with a conventional semen analysis. Fluorescent staining of the spermatozoa gives this additional information, which is normally assessed using a flow cytometer. Since this expensive, complex system is not suited for at home testing, we developed a compact fluorescence detection system for on-chip analysis (chapter 7). This system consists of two parts: the fluorescence detection system comprising a low-cost optical pickup and a microfluidic chip containing a microchannel and optical markers. With the complete system a scan parallel to the channel width can be performed, resulting in a fluorescent profile across the channel width. Therefore it is not necessary to dynamically focus the particles or cells in the microchannel. Using this system, fluorescent beads suspended in medium have been detected and since two additional side beams are generated at a fixed distance from the main laser beam, also the velocity of individual beads could be determined.

8.2 Outlook

In this thesis the proof of principle for the determination of the concentration and motility of spermatozoa on-chip has been demonstrated. Both chip designs include a detection part, where each spermatozoon passing the planar electrode pair is detected and counted. In theory every cell or particle that passes the electrode pair can be detected if the dielectric properties of the cell or particle are different from those of the surrounding electrolyte. Therefore the microfluidic chip that was used for the concentration determination can also be used for other applications. One example is for instance mastitis detection. Mastitis is the inflammation of the udder of cows, resulting in leukocytes in milk and the concentration of these cells can be used as an indicator of inflammation [1]. Two forms of mastitis consist: the clinical and the subclinical form, which is not visible by eye. The economic losses of mastitis for each cow in the Netherlands is estimated to be € 140,- per year, of which subclinical mastitis has the largest contribution [2]. Annually the total losses of mastitis are estimated to be larger than 100 million euro in the Netherlands [3]. To test the usability of the microfluidic chip used for the concentration measurements for counting cells in milk, leukocytes (HL-60 cells) are suspended in whole milk and this

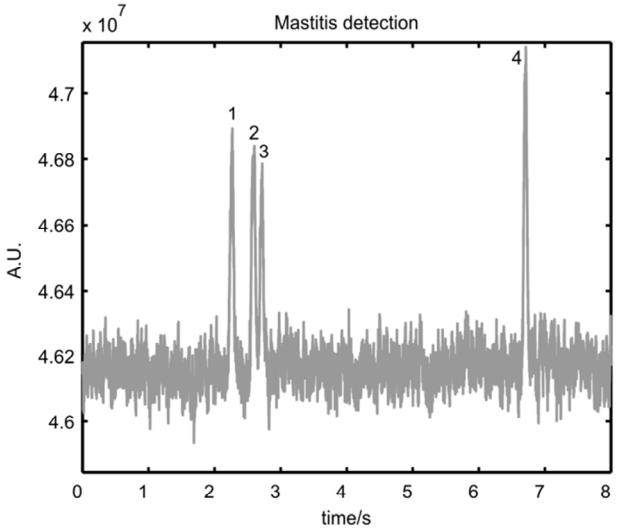

figure 8-1 The detection of four leukocytes (HL-60 cells) suspended in whole milk.

suspension was tested. In figure 8-1 the result of a preliminary measurement is shown and clearly indicates that the leukocytes could be easily detected. The noise level of the baseline is relatively large, which may be caused by the fat drops of the whole milk. This example unambiguously shows that our microfluidic chip can also be used for other purposes.

Boar semen samples were used in all experiments for the motility and concentration determination on-chip, since these samples have always guaranteed good quality, no diseases and can be stored for a longer time period. However, the main goal is to use it for determining the semen quality of men. We already showed that human spermatozoa could be detected using electrical impedance measurements [4], but before it can be used for diagnostic purposes, the determination of both parameters on-chip needs to be validated with semen samples of infertile, subfertile and fertile men. Before this validation can be performed, a complete measurement system needs to be developed. At this moment the experimental setup is large and not suited for measurements at other locations than the laboratory. Furthermore, with the current setup the operation needs trained persons, experienced with the electronics and fluidics in the chip to avoid problems such as air bubbles or leakage. Finally, the software for the analysis still needs some control and manual input, before the concentration and motility ratio can be determined. All these different parts need to be improved and integrated in a measurement system in combination with a disposable chip. Not before that has been achieved, the fertility chip and the

accompanying measurement system are suitable for testing the semen of men by the men themselves.

For the motility chip a model has been proposed where a new measure apparent mobility is introduced. This parameter is independent of the channel dimensions and residence time of the cells in the separation channel and can be objectively determined with our microfluidic chip. Both the curvilinear velocity as well as the beat frequency of the head of the spermatozoon can be expressed using this parameter. This value can possibly be used to qualify the semen quality irrespective of experimental circumstances. Supplementary research to this has to be performed with good and bad quality semen samples.

In summary the concentration of spermatozoa could be determined on-chip and statements about the motility of spermatozoa in a semen sample could be made. However, complementary research is necessary before the fertility chip will be a diagnostic tool in the fertility treatment of an involuntary childless couple.

8.3 References

1. Pyorala, S., *Indicators of inflammation in the diagnosis of mastitis.* Veterinary Research, 2003. **34**(5): p. 565-578.
2. Huijps, K., T. Lam, and H. Hogeveen, *Costs of mastitis: facts and perception.* Journal of Dairy Research, 2008. **75**(1): p. 113-120.
3. GDD. *Mastitis (uierontsteking)*. (2009) [cited 28 June 2011]; Available from: http://www.gddeventer.com.
4. Segerink, L.I., et al., *Spermatozoa count on chip.* Nederlands Tijdschrift voor Klinische Chemie en Labgeneeskunde, 2009. **34**(2): p. 61-61.

Appendix

A.1 Cover

The cover of this thesis shows on the background a selection of the media attention that was received during this PhD project. In figure A1-1 the background is shown with each single article numbered. The numbered items have been published in the following magazines, internet sites et cetera and are shown on the cover with permission:

1. Screenshot of Tube your future site, 2010. Available from: http://www.tubeyourfuture.nl/filmpjes/central-sperm-investigation-ut Ray van Ravensberg, Tim Anemaet, Liset Vliegen, Marijn Groen, Marc Jan Eijkholt, *Central Sperm Investigation UT*. Tube your future 2010, 2nd price ("de zilveren walvis").
2. Jennifer Newton, *Male fertility exam at home.* Highlights in Chemical Technology 2010. **3.**

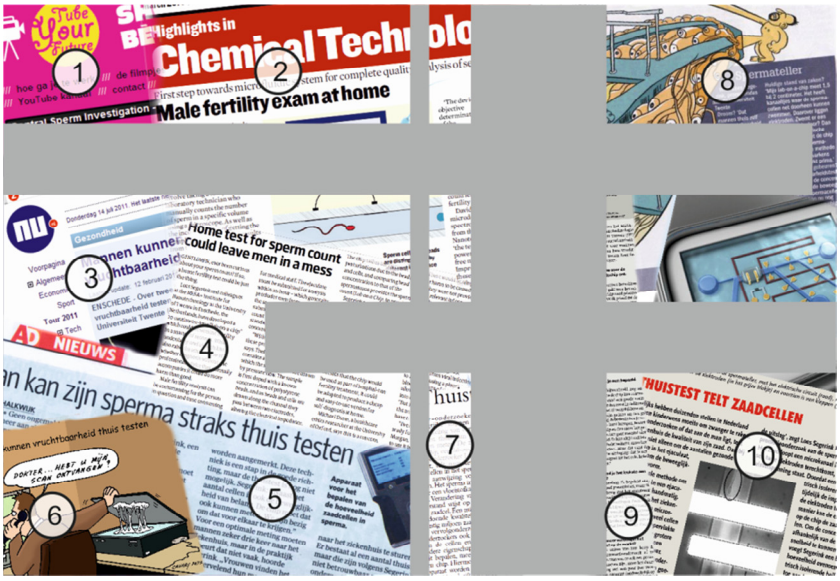

figure A1-1 The background of the thesis showing a selection of the media attention.

3. Nu.nl, *Mannen kunnen thuis vruchtbaarheid testen.* 11 February 2010. Available from: http://www.nu.nl/gezondheid/2182529/mannen-kunnen-thuis-vruchtbaarheid-testen.html.
4. Colin Barras, *Home test for sperm count could leave men in a mess.* New Scientist 2010. **2746:** p. 10.
5. Laura Schalkwijk, *Man kan zijn sperma straks thuis testen.* Algemeen Dagblad of 17 February 2010. P. 4.
6. Canary Pete, *Mannen kunnen thuis vruchtbaarheid testen.* Medisch contact 2010. **7.**
7. Utnieuws, *Thuistest*. Utnieuws of 18 February 2010
8. Tonie Mudde, *Spermateller.* Quest, bijlage Quest Extra Klein, kleiner, kleinst of July 2010. P. 45.
9. Nienke Hoek, *Vraag en antwoord.* Telegraaf, bijlage Wetenschap & Innovatie 2010. **1**: p. 7.
10. Jim Heirbaut, *Dossier microsystemen.* De ingenieur 2010. **17**: p. 24.

Samenvatting

Voordat er bij een ongewenst kinderloos stel met een passende vruchtbaarheidsbehandeling behandeling gestart kan worden, zal de oorzaak van het vruchtbaarheidsprobleem zowel bij de man als bij de vrouw onderzocht moeten worden. Bij de man wordt hiervoor de kwaliteit van het semen bepaald, wat momenteel op handmatige wijze met een microscoop of met behulp van een CASA systeem in een klinisch laboratorium van een ziekenhuis wordt uitgevoerd. Deze analyse is arbeidsintensief, subjectief en duur. Een test waarmee de man zelf zijn semen thuis zou kunnen testen, heeft deze nadelen niet. Daarom is 4 jaar geleden gestart met de ontwikkeling van een 'fertility chip' waarmee thuis de kwaliteit van semen bepaald kan worden. De resultaten van dit onderzoek worden in dit proefschrift beschreven.

Vergeleken met conventionele analysesystemen in ziekenhuislaboratoria, heeft het gebruik van microfluïdische chips voor diagnostische doeleinden verschillende voordelen. Zoals in hoofdstuk 2 vermeld wordt, zijn er recent een aantal microfluïdische chips ontwikkeld die gebruikt kunnen worden voor de analyse van semen en spermatozoa. Daarnaast zijn er chips ontwikkeld die als hulpmiddel gebruikt kunnen worden voor de scheiding en selectie van de 'beste' spermatozoön/spermatozoa voor IVF en ICSI behandelingen. Hoewel sommige van deze chips al commercieel verkrijgbaar zijn, geven ze alleen kwalitatieve informatie over het semen, waardoor ze niet door een gynaecoloog gebruikt kunnen worden bij de keuze van een juiste vruchtbaarheidsbehandeling. Om die redenen hebben wij een microfluïdische chip ontwikkeld die kwantitatieve resultaten over de semenkwaliteit geeft.

Met behulp van impedantiecytometrie kunnen de diëlektrische eigenschappen van afzonderlijke, ongelabelde cellen op een niet-invasieve wijze bepaald worden door ze één voor één langs een geïntegreerd elektrodepaar in een microkanaal te laten stromen (hoofdstuk 3). De passage van een cel langs het elektrodepaar resulteert in een impedantieverandering, die informatie over grootte, het membraan en het cytoplasma van de cel bevat, maar is ook afhankelijk van de elektrodeconfiguratie in het microkanaal, de eigenschappen van de elektrolyt en de meetfrequentie. Door de invloed van de elektrische dubbellaag bij de overgang van elektrode naar vloeistof en de parasitaire capaciteiten bij respectievelijk lage en hoge meetfrequenties, wordt de meting bij voorkeur op tussenliggende frequenties uitgevoerd zodat daadwerkelijke de elektrolytweerstand gemeten wordt. Er kunnen verschillende modellen gebruikt

worden om de invloed van het ontwerp van de microfluïdische chip en de eigenschappen van de cel op het frequentiegedrag te bepalen.

Wij gebruiken impedantiecytometrie om de concentratie van spermatozoa met behulp van een chip te bepalen (hoofdstuk 4). Hiervoor is een chip ontworpen met een microkanaal waarin zich aan één zijde een planair elektrodepaar bevindt. Naast spermatozoa kan semen ook andere cellen bevatten. Bij een ontsteking bijvoorbeeld bevat semen ook leukocyten en is het daarom noodzakelijk om deze verschillende celsoorten van elkaar te kunnen onderscheiden. Uit metingen met onze chips is een relatie aangetoond tussen celgrootte en de grootte van de impedantieveranderingen. Op deze manier kunnen spermatozoa, leukocyten en 6 µm polystyreen bolletjes met behulp van impedantieverandering onderscheiden worden. Door toevoegen van een bekende concentratie van deze bolletjes aan een semenmonster, kan ook de spermatozoa concentratie bepaald worden zonder dat de daadwerkelijke stroomsnelheid bekend hoeft te zijn. In totaal zijn er 7 semenmonsters van varkens getest met concentraties in het subfertiele en fertiele gebied. De resultaten laten een duidelijke correlatie zien met de daadwerkelijke concentratie die bepaald is met een telkamer, de huidige gouden standaard.

Het gebruik van een chip met een planair elektrodepaar voor impedantiecytometrie heeft als voordeel dat deze eenvoudig in een cleanroom is te realiseren. Een nadeel van planaire elektroden is echter het niet-homogene elektrische veld, waardoor de positie van een cel of deeltje in het microkanaal invloed heeft op de gemeten impedantieverandering. In het geval van de bepaling van de concentratie is dit geen probleem, omdat de verschillen in de impedantieverandering tussen die van spermatozoa, leukocyten en polystyreen bolletjes aanzienlijk groter zijn dan de variaties veroorzaakt door de positie in het kanaal. Echter wanneer er naar kleine veranderingen in celgrootte of celvorm gekeken wordt, zou een andere elektrodeconfiguratie met een homogener elektrische veld beter zijn. Een parallelle elektrodeconfiguratie heeft zo'n homogener elektrisch veld, maar het fabricageproces hiervan is complexer en de elektrische verbindingen van en naar de chip zijn lastiger te realiseren. In hoofdstuk 5 wordt een nieuwe parallelle elektrodeconfiguratie beschreven die deze nadelen niet heeft. Vergeleken met het eenvoudige fabricageproces van een planair elektrodepaar is er maar één extra processtap nodig. Deze nieuwe parallelle elektrodeconfiguratie bestaat uit een zwevende elektrode die op de bodem van het microkanaal ligt, tegenover twee vlakke elektroden aan de bovenkant van het kanaal, zodat twee parallelle elektrodeparen gevormd worden. Met deze configuratie zijn polystyreen bolletjes gedetecteerd en de spreiding in de impedantieverandering was kleiner dan die gemeten met een planair elektrodepaar. Dit was vooral het gevolg van het homogenere elektrische veld waardoor de positie

van de bolletjes in het kanaal minder invloed had op de gemeten impedantieveranderingen.

Bij een semenanalyse is niet alleen de concentratie maar ook de motiliteit van spermatozoa in semen een belangrijke parameter (hoofdstuk 6). Hiervoor is een chip ontwikkeld met een scheidings- en een detectiegedeelte om de motiliteit te bepalen. In het scheidingsgedeelte zijn alleen de beweeglijke spermatozoa in staat om uit de laminaire vloeistofstroom te zwemmen en deze cellen worden bij een ander elektrodepaar gedetecteerd dan de niet-beweeglijke cellen die in de stroom blijven. Er is een model opgesteld dat de verdeling van motiele en niet-motiele spermatozoa in het scheidingskanaal beschrijft met behulp van een equivalente diffusieconstante. Voor motiele spermatozoa is bovendien de schijnbare mobiliteit berekend waarmee het concentratieprofiel van zwemmende spermatozoa in het scheidingskanaal, bij een specifieke stromingsratio en tijd, bepaald kan worden. Twee monsters, waarvan één niet zwemmende spermatozoa bevat en de andere progressief zwemmende spermatozoa zijn met deze chip getest. De ratio die bij beide uitgangskanalen is gedetecteerd, is gerelateerd aan de motiliteit, net zoals de berekende factor van ogenschijnlijke mobiliteit; een factor die onafhankelijk is van de kanaaldimensies en tijd.

Met behulp van detectie van cellen door middel van het meten van veranderingen in de elektrische impedantie in een chip zijn twee belangrijke parameters van de semenanalyse bepaald. Er kan echter nog extra informatie verkregen worden wanneer ook functionele eigenschappen van spermatozoa bepaald worden, hetgeen bij de huidige semenanalyse nog niet wordt gedaan. Bijvoorbeeld het fluorescent labellen van spermatozoa kan extra informatie geven die nu nog bepaald wordt met een flow cytometer. Omdat een flow cytometer een duur en complex systeem is, is het ongeschikt voor thuistesten. Om die reden en daarom hebben wij een compact, fluorescentie detectiesysteem ontwikkeld dat gebruikt kan worden met onze chips (hoofdstuk 7). Dit systeem bestaat uit twee delen: een fluorescentie detectiesysteem dat bestaat uit een goedkope optische pick-up en een microfluïdische chip die een microkanaal en optische markers bevat. Met het complete systeem kan een scan loodrecht op de stroomrichting van de cellen in het kanaal worden gemaakt, zodat een fluorescentieprofiel van de deeltjes in het kanaal verkregen wordt. Hierdoor is het niet meer noodzakelijk om het deeltje of de cel dynamisch te focussen in het microkanaal. Met dit systeem zijn fluorescente bolletjes in een medium gedetecteerd en omdat er zich op een vaste afstand van de centrale laserstraal nog twee extra zijstralen bevinden, kon bovendien de snelheid van afzonderlijke bolletjes worden bepaald.

Nomenclature

Abbreviations

AC	alternating current
ALH	amplitude of lateral head displacement
BTS	Beltsville Thawning solution
CASA	computer assisted semen analysis
CCD	charge coupled device
CD	compact disc
CPE	constant phase element
DC	direct current
DEP	dielectrophoresis
DNA	deoxyribonucleic acid
DVD	digital versatile disc
FES	focus error signal
HD-DVD	high density DVD
HIV	human immunodeficiency virus
HAS	human serum albumin
ICSI	intracytoplasmic sperm injection
IUI	intrauterine insemination
IVF	in vitro fertilization
MAD	mean angular displacement
MAR	mixed antiglobulin reaction
MISS	microscale integrated sperm sorter
NA	numerical aperture
PAP	Papanicolaou staining
PC	personal computer
PDIC	position detector integrated circuit
PDMS	polydimethylsiloxane
ROS	reactive oxygen species
SCSA	sperm chromatine structure array
TAC	total antioxidant capacity

TUNEL	deoxynucleotidyl transferase-mediated dUTP nick end labelling
UV	ultraviolet
VAP	average path velocity
VCL	curvilinear velocity
VSL	straight line velocity
WHO	world health organization

Parameters

$\|Z_{high}\|$	[Ω]	Impedance at high frequency
$\|Z_{low}\|$	[Ω]	Impedance at low frequency
$<u>$	$[m \cdot s^{-1}]$	Average velocity of a molecule
$<x^2>$	$[m^2]$	Mean-square displacement of a molecule
A	$[m^2]$	Surface area of the electrode
a	-	Fractional exponent of constant phase element
A_{PDIC}	[V]	Voltage on the photodetector A of the PDIC
A_{wire}	$[m^2]$	Cross sectional area of the wire
b	$[s^{-1}]$	Number of intermolecular collisions the molecule encounters per unit time
B_{PDIC}	[V]	Voltage on the photodetector B of the PDIC
c	$[mol \cdot L^{-1}]$	Concentration distribution
C_0	$[mol \cdot L^{-1}]$	Concentration of the solute
c_b	$[mL^{-1}]$	Concentration of polystyrene beads
C_d	$[F \cdot m^{-2}]$	Double layer capacitance per unit area
C_D	$[F \cdot m^{-2}]$	Capacitance diffuse layer per unit area
C_{DL}	[F]	Double layer capacitance
C_H	$[F \cdot m^{-2}]$	Capacitance Helmholtz layer per unit area
C_i	[F]	Capacitance of cytoplasm of the cell
C_m	[F]	Capacitance of the cell membrane
$C_{m,0}$	$[F \cdot m^{-2}]$	Membrane capacitance at low frequency
c_n	-	Dimensionless concentration distribution
C_{par}	[F]	Parasitic capacitance
C_{PDIC}	[V]	Voltage on the photodetector C of the PDIC
c_s	$[mL^{-1}]$	Concentration of spermatozoa
d	[m]	Diameter particle
D	$[m^2 \cdot s^{-1}]$	Diffusion coefficient
d_m	[m]	Thickness of cell membrane

D_m	[$m^2 \cdot s^{-1}$]	Apparent mobility
D_{PDIC}	[V]	Voltage on the photodetector D of the PDIC
D_t	[m]	Diameter tube
e	[C]	The charge of an electron
f_1	[Hz]	Lower frequency limit of resistive plateau
f_2	[Hz]	Higher frequency limit of resistive plateau
$G_{m,0}$	[$S \cdot m^{-2}$]	Membrane conductance at low frequency
f_{CM}^*	-	Clausius-Mossoti factor
j	-	$j = \sqrt{-1}$, imaginary unit
k	[$J \cdot K^{-1}$]	Boltzmann constant
K_{cell}	[m^{-1}]	Cell constant
L	[m]	Length of the electrode
L_{wire}	[m]	Length of the wire
M	-	Motility ratio
N	-	Amount of fingers for interdigitated electrodes
n^0	[m^{-3}]	The number concentration of each ion in the bulk
N_b	-	Number of counted polystyrene beads
n_{ep1}	-	Number of counted spermatozoa at electrode pair 1
n_{ep2}	-	Number of counted spermatozoa at electrode pair 2
N_s	-	Number of counted spermatozoa
Pe	-	Peclet number
Q_a	[$s^{\alpha} \cdot \Omega^{-1}$]	Coefficient of constant phase element
r	[m]	Inner radius of the cell
R_{el}	[Ω]	Electrolyte resistance
R_i	[Ω]	Resistance of the cytoplasm of the cell
R_{lead}	[Ω]	Lead resistance
R_m	[Ω]	Resistance of the cell membrane
r_p	[m]	Radius of the particle
r_s	-	Ratio of the width of the sample stream to the width of the separation channel
s	[m]	Interelectrode distance
T	[K]	Absolute temperature
t	[s]	Time
U	[$m \cdot s^{-1}$]	Flow velocity in the channel
w	[m]	Width of the electrode
w_{ch}	[m]	Width of the microchannel
x_n	-	Dimensionless x-coordinate
x_{OHZ}	[m]	Position of the outer Helmholtz layer

y_n	-	Dimensionless y-coordinate
Z	[Ω]	Impedance
z	-	The magnitude of the charge on the ions
z^*	[Ω·m]	Complex impedance of the material
Z_{CPE}	[$\Omega \cdot s^{-a}$]	Impedance of the constant phase element
$Z_{eq,ECM}$	[Ω]	Equivalent impedance of the suspension calculated with equivalent circuit model of the cell
$Z_{eq,MWT}$	[Ω]	Equivalent impedance of the suspension calculated with Maxwell-Wagner theory
α	-	Correction factor for the spreading of current lines
γ_s	-	Shape factor for non-spherical particles
ΔR	[Ω]	Resistance difference
$\Delta\varepsilon_1$	[$F \cdot m^{-1}$]	Magnitude of the dielectric dispersion with relaxation time constant τ_1
$\Delta\varepsilon_2$	[$F \cdot m^{-1}$]	Magnitude of the dielectric dispersion with relaxation time constant τ_2
ε	-	Relative permittivity
ε^*	-	Complex relative permittivity
ε_0	[$F \cdot m^{-1}$]	Permittivity of free space
ε_∞	[$F \cdot m^{-1}$]	Permittivity at infinite frequency
ε_{el}	-	Relative permittivity of the electrolyte
ε_{el}^*	-	Complex relative permittivity of the electrolyte
ε_{eq}	-	Equivalent relative permittivity of the suspension
ε_{eq}^*	-	Equivalent complex relative permittivity of the suspension
ε_i	-	Relative permittivity of the cytoplasm of the cell
ε_i^*	-	Complex relative permittivity of the cytoplasm of the cell
ε_m	-	Relative permittivity of the cell membrane
ε_m^*	-	Complex relative permittivity of the cell membrane
ε_p^*	-	Complex relative permittivity of the particle
η	[Pa·s]	Viscosity of the fluid
λ	[nm]	Wavelength
ρ_{el}	[Ω·m]	Resistivity of the background electrolyte
ρ_{eq}	[Ω·m]	Equivalent resistivity of the electrolyte with a particle in it
ρ_{wire}	[Ω·m]	Resistivity of the material of the wire
σ	[$S \cdot m^{-1}$]	Conductivity
σ^*	[$S \cdot m^{-1}$]	Complex conductivity
σ_0	[$S \cdot m^{-1}$]	Limiting low frequency conductivity

σ_{el}	[S·m^{-1}]	Conductivity of the electrolyte
σ_{el}^{*}	[S·m^{-1}]	Complex conductivity of the electrolyte
σ_{eq}	[S·m^{-1}]	Equivalent conductivity of the suspension
σ_{eq}^{*}	[S·m^{-1}]	Complex equivalent conductivity of the suspension
σ_{i}	[S·m^{-1}]	Conductivity of the cytoplasm of the cell
σ_{m}	[S·m^{-1}]	Conductivity of the membrane
σ_{p}^{*}	[S·m^{-1}]	Complex conductivity of the particle
τ_1	[s]	Relaxation constant of the cell membrane
τ_2	[s]	Relaxation constant of the polarization of the cytoplasm with medium
Φ	-	Volume fraction
φ_{OHZ}	[V]	Potential at the outer Helmholtz layer
ω	[rad·s^{-1}]	Angular frequency

List of publications

Journal articles

Segerink, L.I., Koster, M.J., Sprenkels, A.J. and van den Berg, A. *A compact 2D fluorescence detection system for μm-sized beads on-chip*. Submitted.

Segerink, L.I., Sprenkels, A.J., Bomer, J.G., Vermes, I. and van den Berg, A. *A new floating electrode structure for generating homogeneous electrical fields in microfluidic channels*. Lab on a Chip, 2011, **11**: p 1995-2001.

Segerink, L.I., Sprenkels, A.J., ter Braak, P.M., Vermes, I. and van den Berg, A. *On-chip determination of spermatozoa concentration using electrical impedance measurements*. Lab on a Chip, 2010, **10**: p 1018-1024.

Segerink, L.I., Raterink, R.J., Sprenkels, A.J., Vermes, I. and van den Berg, A. *Spermatozoa detection and counting on chip*. Nederlands Tijdschrift voor Klinische Chemie en Labgeneeskunde, 2009. **34**: p 254-255.

Patents

Segerink, L.I., Koster, M.J., Sprenkels, A.J. and van den Berg, A. *Compact 2D fluorescence detection system for on-chip analysis.* EP11165337.4, submitted 9 May 2011.

Segerink, L.I., Sprenkels, A.J., Bomer, J.G. and van den Berg, A. *Lab-on-a-chip device, for instance for use of the analysis of semen*. EP10170399.9, submitted 22 July 2010.

Conference contributions

Segerink, L.I., Sprenkels, A.J., Vermes, I and van den Berg, A. *Motility determination of spermatozoa on-chip*, at NanoBioTech 2011, Montreux, Switzerland.

Segerink, L.I., Koster, M.J., Sprenkels, A.J. and van den Berg, A. *A cheap 2D fluorescence detection system for μm-sized beads on-chip*, at MicroTAS 2011, Seattle, USA.

Kemna, E.W.M., Segerink, L.I., Schoeman, R.M., Wolbers, F., Vermes, I. and van den Berg, A. *Towards a high-throughput electrofusion platform using droplets: cell detection and deterministic encapsulation*, at MicroTAS 2011, Seattle, USA.

Segerink, L.I., Sprenkels, A.J., Bomer, J.G. and van den Berg, A. *On-chip detection of beads with a new electrical impedance sensor*, at IEEE Sensors 2010, Waikoloa, USA.

Segerink, L.I., Sprenkels, A.J., Vermes, I. and van den Berg, A. *On-chip spermatozoa and leucocytes counter*, at MicroTAS 2009, Jeju, South-Korea.

Segerink, L.I., Raterink, R.J., Sprenkels, A.J., Vermes, I. and van den Berg, A. *Spermatozoa count on chip*, 2009 at Voorjaarscongres NVKC, Veldhoven, the Netherlands.

Lectures

Segerink, L.I. and de Moor, A.G.J., *Cell analyser.* 11 October 2011, invited talk at Bètapostdoc retreat, Kapellerput, Heeze, the Netherlands.

Segerink, L.I., *Lab-on-a-chip, patiëntvriendelijke thuistests?!* 6 February 2011, Paradiso, Amsterdam, the Netherlands.

Segerink, L.I., *Fertility chip.* 13 September 2010, invited talk at kickoff meeting of "Docentonwikkelteams", Enschede, the Netherlands.

Segerink, L.I., *On-chip determination of spermatozoa concentration*. 9 June 2010, invited talk at chair of Joel Voldman, MIT, Boston, USA.

Segerink, L.I., *Hoe kleiner, hoe beter?* 20 November 2009, invited talk for "jaarlijks co-schapcongres VUMC", VUMC, Amsterdam, the Netherlands.

Segerink, L.I., *Fertiliteits chip. Point-of-care semen analyse met behulp van lab-on-a-chip.* 19 January 2009, invited talk for meeting "Twentse gynaecologen vereniging", Medisch Spectrum Twente, Enschede, the Netherlands.

Dankwoord

Naar dit deel van het proefschrift wordt toch vaak het eerst gebladerd en waarschijnlijk is dit ook het eerste wat jij nu leest. Dit werd bevestigd, toen het concept van dit proefschrift bij mij thuis lag en er opmerkingen werden gemaakt over mijn toen nog lege dankwoord; over de rest werd niets gezegd. Op zich te begrijpen, want er zijn velen die ervoor gezorgd hebben dat ik me vier jaar lang kon storten op dit project. Bedankt hiervoor!

Daarnaast zijn er enkele personen die ik toch nog even extra wil bedanken. Allereerst Albert, mijn promotor. Zo'n vier jaar geleden kwam ik via Erik Staijen in contact met jouw BIOS groep. Een promotieonderzoek daar zou wel wat voor mij zijn, aldus Erik. Op de dag dat jij Abraham zag, was de eerste kennismaking en jouw enthousiasme was (en is nog steeds) erg motiverend. Jouw kritische blik, brede kijk en de vrijheid die jij mij gaf, waardeer ik enorm. De BIOS-werkweken, uitjes, BBQ's, mountainbiketochten en weet ik al niet meer hebben daarnaast erg bijgedragen aan een fantastische periode, dank hiervoor!

Mijn dagelijks begeleider, Ad, verdient ook zeker heel veel dank! In de vier jaren stond jij altijd voor mij klaar. Dit was niet alleen beperkt tot elektrotechnische zaken, maar ook op andere gebieden heb je me veel geleerd. Hoe vaak je uiteindelijk niet mijn proefschrift van voor naar achter hebt doorgelezen, weet ik niet meer, maar ik ben echt ontzettend blij met het werk wat jij hierin verzet hebt. Ik kon me geen betere begeleider wensen.

Ook Floor wil ik bedanken voor het kritisch doorlezen van dit boekwerk, maar bovenal voor de gezelligheid die je hebt gebracht. Altijd betrokken en geïnteresseerd, top gewoon. Met mijn andere paranimf Evelien heb ik veel tijd doorgebracht in het lab en zij was mijn 'zaadkoerier'. Wat een lol, wat een gezang en bovenal wat een vrolijkheid. Bedankt!

Gelukkig zat ik de afgelopen jaren niet alleen. Egbert, als kamergenoot heb ik veel aan je gehad, hoewel het altijd een verrassing was wanneer je er was. Altijd bereid om mee te denken, hulp te geven en altijd de rust zelve, dankjewel. Zonder de altijd-lachende Paul was het werken met cellen veel lastiger (en ook veel saaier) geworden, dankjewel voor jouw hulp. Mathieu, Wouter S. en Justyna bedankt voor de vele leuke

gesprekken en de gezellige conferenties samen. Aan het eind van de werkdag waren er altijd twee heren, Maarten v.M. en Wouter O., die ervoor zorgden dat ik de tijd niet uit het oog verloor en op tijd naar huis fietste. Hopelijk kunnen we dit nog een tijdje blijven doen! Als er wat geregeld moest worden, dan kon je op Hermine rekenen, erg bedankt hiervoor. Tevens wil ik Lonneke, Bjorn en Andries danken voor het nodige vermaak en gelach in het cellab. Vele handen maken licht werk, in mijn geval gold dit zeker voor de vele technici die mij geholpen hebben. Hans, Johan, Lennart, Jan v.N. en Daniël jullie hebben echt fantastisch werk geleverd. Hartstikke bedankt. Overigens wil ik de overige (ex-)BIOSers erg bedanken voor de gezelligheid en hulp die ik heb mogen ontvangen. Edwin, Séverine, Jan E. , Jean-Philippe, Susan, Rogier V., Rogier S., Verena, Pavel, Lingling, Mingliang, Adithya, Natalia, Iris, Eddy, Dietrich, Bianca, Erik K., Ganesh, Georgette, Erik F., Songyue, Arpita, Rerngchai, Floris, Trieu, Allison, Henriette, Fleur, Guillaume, Loan, Muhammad, Yanbo, Kirsten, Jochem en Claudi, thanks a lot! Er zijn talrijke studenten geweest die ook een steentje hebben bijgedragen aan dit onderzoek. Robert-Jan, Mark, Maarten v.M., Erik, Maarten K. en Karel, dankjewel!

Naast mijn collega's hebben ook anderen bijgedragen aan mijn onderzoek. Zo wil ik Istvan Vermes voor zijn inbreng bedanken. Hanneke Feitsma en Jan Nijland, bedankt voor het leveren van de tubes en jullie expertise. Ook Jur Oosterhuis wil ik erg bedanken voor zijn betrokkenheid en enthousiasme. Hopelijk mogen we nog veel samenwerken in de toekomst. Tevens wil ik de heren van B4G bedanken, door jullie zal dit werk gelukkig niet alleen in de boekenkast belanden.

Velen hebben ervoor gezorgd dat er meer is dan werken. Onder deze velen, hoewel we de naam niet echt meer eer aan doen, de Wilde Wiefkes (jullie zijn nog steeds te bewonderen op mijn bureaublad), de hockeydames en –heren van PW (goed om je hoofd helemaal leeg te krijgen) en de mensen die voor de nodige gezelligheid in en om Twente zorgen.

Vanuit de gehele (schoon)familie was er veel interesse in dit onderzoek en werd de hele omgeving trots verteld wat ik toch weer aan het doen was. Erg leuk! Lieve papsie en mamsie, jullie hebben me altijd gestimuleerd en dit resultaat is dan ook wel aan jullie te danken! Theo en Stieneke, al wonen jullie niet om de hoek, de betrokkenheid was er niet minder om. Erg fijn om zulke schoonouders te hebben. Ook dank aan mijn lieve broertje, Anouk, Emiel en Olga. De laatste regels van dit dankwoord zijn bestemd voor mijn lieve Casper. Bedankt voor jouw steun, je bent geweldig!

Liefs Loes